



Universiteit
Leiden
The Netherlands

MRI evaluation of end-organ damage in diabetes and hypertension

Elderen, S.G.C. van

Citation

Elderen, S. G. C. van. (2010, December 21). *MRI evaluation of end-organ damage in diabetes and hypertension*. Retrieved from <https://hdl.handle.net/1887/16265>

Version: Corrected Publisher's Version

License: [Licence agreement concerning inclusion of doctoral thesis in the Institutional Repository of the University of Leiden](#)

Downloaded from: <https://hdl.handle.net/1887/16265>

Note: To cite this publication please use the final published version (if applicable).

MRI evaluation of end-organ damage, in Diabetes and Hypertension

Saskia Gerdina Cornelia van Elderen
2010



Printed by: Optima Grafische Communicatie, Rotterdam

ISBN/EAN: 978-90-9025758-7

© 2010, S.G.C. van Elderen, Leiden, The Netherlands. All rights reserved. No part of this thesis may be reproduced or transmitted in any form, by any means, without prior written permission of the author.

MRI evaluation of end-organ damage, in Diabetes and Hypertension

PROEFSCHRIFT

ter verkrijging van
de graad van Doctor aan de Universiteit Leiden,
op gezag van de Rector Magnificus Prof. mr. P.F. van der Heijden,
volgens besluit van het College voor Promoties
te verdedigen op dinsdag 21 december 2010

klokke 15.00 uur

door

Saskia Gerdina Cornelia van Elderen

geboren te Eindhoven
in 1982

PROMOTIECOMMISSIE

Promotores

Prof. Dr. A. de Roos

Prof. Dr. J.W.A. Smit

Co-promotores

Dr. ir. J.J.M. Westenberg

Dr. J. van der Grond

Overige commissieleden

Prof. Dr. M.A. van Buchem

Prof. Dr. A.G. Webb

Dr. L.J.M. Kroft

The research described in this thesis was carried out at the department of Radiology (head: Prof. dr. J.L. Bloem) and Endocrinology (head: Prof. dr. J.W.A. Smit) of the Leiden University Medical Center.

Financial support by the Netherlands Heart Foundation and the Dutch Diabetes Foundation for the publication of this thesis is gratefully acknowledged. Additional financial support is provided by The J.E. Jurriaanse Foundation, Foundation Imago Oegstgeest, Foundation of Image Processing, Philips Healthcare Benelux, Novo Nordisk BV, Boehringer Ingelheim BV, Toshiba Medical Systems Nederland, Guerbet Nederland BV, Philips Healthcare Nederland, Eli Lilly Nederland BV, and Servier Nederland Farma BV.

Aan mijn ouders

Contents

Chapter 1	General introduction and outline	9
Part I:	Evaluation of end-organ damage by standardized MR imaging tests, in Diabetes and Hypertension	
Chapter 2	The effect of hypertension on aortic pulse wave velocity in type 1 diabetes mellitus patients: assessment by MR imaging <i>Submitted</i>	19
Chapter 3	Association of aortic arch pulse wave velocity with left ventricular mass and lacunar brain infarcts in hypertensive patients: assessment by MR imaging <i>Radiology 2009;253(3):681-688</i>	31
Chapter 4	Aortic stiffness is associated with cardiac function and cerebral small vessel disease in patients with type 1 diabetes mellitus: assessment by MR imaging <i>European Radiology 2010;20(5):1132-1138</i>	47
Chapter 5	Increased aortic stiffness measured by MR imaging in type 1 diabetes mellitus patients and the relationship with renal function <i>American Journal of Roentgenology, accepted 2010</i>	61
Chapter 6	Cerebral perfusion and aortic stiffness are independent predictors of white matter brain atrophy in type 1 diabetes mellitus patients: assessment by MR imaging <i>Submitted</i>	73
Chapter 7	Progression of brain atrophy and cognitive decline in diabetes mellitus, a 3 year follow-up <i>Neurology 2010;75(11):997-1002</i>	85

Part II: Innovative MR techniques

Chapter 8	Phosphorus-31 MR spectroscopy of skeletal muscle in maternally inherited diabetes and deafness A3243G mitochondrial mutation carriers <i>Journal of Magnetic Resonance Imaging 2009;29(1):127-131</i>	99
Chapter 9	Initial results on in vivo human coronary MR angiography at 7 Tesla <i>Magnetic Resonance in Medicine 2009;62(6):1379-1384</i>	111
Chapter 10	Right coronary MR angiography at 7 Tesla: a direct quantitative comparison with 3 Tesla in young healthy volunteers <i>Radiology 2010;257(1):254-259</i>	125
	Summary and conclusions	137
	Samenvatting en conclusies	143
	List of publications	151
	Dankwoord	157
	Curriculum vitae	161

Chapter 1

General introduction and outline

INTRODUCTION

Diabetes mellitus and hypertension disease are important public health problems with a worldwide increasing prevalence. The global prevalence of diabetes rises from 2.8% in 2000 to 4.4% in 2010 (1). Diabetes and hypertensive patients have a significantly increased risk of cardiovascular disease like myocardial infarction, stroke and of cardiovascular death due to not totally unraveled pathophysiological mechanisms. Recent advances in knowledge have contributed to the understanding of the increased cardiovascular disease risk in these high risk populations by assigning a role for changes in the wall of the aorta (2,3).

The aorta is a complex organ originating from the heart and passing blood to all end-organs. Importantly the aorta is an elastic tube with a capacity to distend and recoil in response to high pulsatile flow resulting from cardiac contraction. Herewith, the aorta has the capacity to reduce cardiac afterload and to facilitate continuous perfusion of the end-organs.

Intrinsic aortic wall abnormalities have been described in diabetes due to high glucose levels resulting in formation of advanced glycation end products which crosslink to collagen in the aortic vessel wall (4). In patients with hypertension, continuous hemodynamic stress at the aortic wall leads to structural and functional changes in the arterial wall (5). Possibly, arterial stiffness and endothelial dysfunction precede the presence of clinical hypertension (6). Inflammatory mechanisms and formation of atherosclerosis also play an important role in aortic wall changes in diabetes and hypertension (2). These complex heterogeneous mechanisms result in degeneration of the aortic vessel wall, leading to reduced aortic elasticity.

Stiffening of the aorta may initiate a negative cascade affecting the heart and all other end-organs. As a consequence of aortic stiffness, cardiac remodeling, compromised perfusion of the coronary arteries, and subsequently diastolic and systolic cardiac dysfunction may occur, which may ultimately lead to heart failure and cardiac death (7). Furthermore, stiffness of the central large arteries results in a deficient absorption of the pulse wave and an increase in central pulse pressure. This high pulsatile flow is transmitted from the aorta to all end-organs like the brain and kidneys causing damage to the endothelial and smooth muscle cells, disrupting the cerebral and renal arterioles. Also, aortic stiffness may represent systemic endothelial dysfunction or wall thickening caused by shared underlying mechanisms. Numerous recent reports emphasize the importance of aortic stiffness as a prognostic indicator for future cardiovascular disease and mortality in diabetes (8,9) and hypertensive patients (10).

Aortic stiffness can be assessed by means of pulse wave velocity (PWV) measurements (11). PWV is defined as the velocity of the systolic pulse wave front propagating through the aorta, reflecting the elastic properties of the aortic vessel wall. During the last decades, Magnetic Resonance Imaging (MRI) has emerged as a reliable, accurate, ionizing radiation-free modality for a general evaluation of anatomy and function of the heart, brain and vessels. MRI has

also been established as a non-invasive accurate tool for assessment of aortic stiffness by measuring aortic PWV (12).

In this thesis, subclinical end-organ damage of the heart, brain and kidneys and their relationship with aortic stiffness will be assessed using a comprehensive MRI evaluation in diabetes mellitus and hypertensive patients.

Furthermore, new developments in high magnetic field MRI, with the introduction of human 7 Tesla MRI scanners, potentially contribute to imaging of end-organ damage at early stages of disease. In the final two chapters of this thesis, development of coronary magnetic resonance angiography (MRA) at high field 7 Tesla MRI is described, relevant for studying coronary artery disease with subsequent myocardial ischemic and functional end-organ damage. Coronary artery disease remains the leading cause of death for men and women in the Western world (13). The technique of coronary MRA, most commonly applied at 1.5 Tesla MRI, remains challenging due to the small diameter of the coronary arteries and cardiac and respiratory motion, and is not yet routinely applicable as a clinical diagnostic tool.

The current gold standard for the diagnosis of hemodynamically significant coronary artery disease is x-ray coronary angiography. X-ray coronary angiography, however, has a few disadvantages. A small but significant risk of complications has been reported and these are related to the invasive nature of the procedure, radiation exposure and the use of iodinated contrast agents (14). In addition, up to 40% of patients who undergo invasive x-ray coronary angiography are found to have no significant coronary artery lumen stenosis (15). For these reasons, there is a strong need for an alternative technique that is noninvasive, more cost effective, and which can provide not only information about the vessel lumen but also about the vessel wall and myocardial condition, without the need for ionizing radiation and nephrotoxic contrast agents.

MRI systems with higher field strengths enable imaging with increased signal-to-noise ratio, allowing improved spatial resolution, improved temporal resolution and/or reduced scanning times (16-18). Individually or in combination, these improvements are likely to result in improved image quality, and ultimately better access to small diameter and branching vessels. High field coronary MRA is therefore a promising tool for the non-invasive identification of significant proximal coronary artery disease without the use of ionizing radiation (19,20).

Because of the large resonance frequency increase going from low 1.5 and 3 Tesla to high 7 Tesla magnetic field strength MR, considerable technical challenges are expected for cardiovascular studies at 7 Tesla to account for the increased magnetic field inhomogeneities. In the studies performed for this thesis, we show the implementation and the benefits of imaging coronary MRA at 7 Tesla.

OUTLINE OF THIS THESIS

This thesis evaluates MRI assessed end-organ damage, and the role of aortic pulse wave velocity in diabetes and hypertensive patients. In addition, the application and implementation of innovative MR techniques will be discussed.

Chapter 2 studies the independent and contributive effect of diabetes mellitus and hypertension on aortic pulse wave velocity. In **chapter 3** the influence of aortic pulse wave velocity on cardiac and cerebral MR findings is evaluated in hypertensive patients. In **chapter 4** a similar evaluation regarding the effect of aortic pulse wave velocity on cardiac and cerebral MR findings is assessed in type 1 diabetes mellitus patients. **Chapter 5** describes a role of aortic pulse wave velocity in renal function of type 1 diabetes mellitus. **Chapter 6** shows two separate vascular mechanisms; cerebral perfusion and aortic pulse wave velocity, being related to white matter brain atrophy in type 1 diabetes mellitus. **Chapter 7** reports accelerated progression of brain atrophy with cognitive consequences in elderly type 2 diabetes mellitus patients. **Chapter 8** evaluates the metabolic effect of diabetes mellitus on the skeletal muscle in patients carrying a mitochondrial mutation, present in approximately 1% of all diabetes patients, using the MR Phosphorus-Spectroscopy technique. **Chapter 9** shows feasibility of imaging techniques to perform coronary imaging at 7 Tesla MR field strength. In **chapter 10** a first comparison study of coronary MR angiography at 7 Tesla in healthy volunteers is assessed showing the benefits of imaging at high magnetic field strength.

REFERENCES

1. Wild S, Roglic G, Green A, Sicree R, King H. Global prevalence of diabetes: estimates for the year 2000 and projections for 2030. *Diabetes Care* 2004; 27:1047-1053.
2. Roes SD, Alizadeh DR, Westenberg JJ, et al. Assessment of aortic pulse wave velocity and cardiac diastolic function in subjects with and without the metabolic syndrome: HDL cholesterol is independently associated with cardiovascular function. *Diabetes Care* 2008; 31:1442-1444.
3. van der Meer RW, Diamant M, Westenberg JJ, et al. Magnetic resonance assessment of aortic pulse wave velocity, aortic distensibility, and cardiac function in uncomplicated type 2 diabetes mellitus. *J Cardiovasc Magn Reson* 2007; 9:645-651.
4. Aronson D. Cross-linking of glycated collagen in the pathogenesis of arterial and myocardial stiffening of aging and diabetes. *J Hypertens* 2003; 21:3-12.
5. Safar ME, Levy BI, Struijker-Boudier H. Current perspectives on arterial stiffness and pulse pressure in hypertension and cardiovascular diseases. *Circulation* 2003; 107:2864-2869.
6. Duprez DA. Cardiac autonomic imbalance in pre-hypertension and in a family history of hypertension. *J Am Coll Cardiol* 2008; 51:1902-1903.
7. O'Rourke MF, Hashimoto J. Mechanical factors in arterial aging: a clinical perspective. *J Am Coll Cardiol* 2007; 50:1-13.
8. Cruickshank K, Riste L, Anderson SG, Wright JS, Dunn G, Gosling RG. Aortic pulse-wave velocity and its relationship to mortality in diabetes and glucose intolerance: an integrated index of vascular function? *Circulation* 2002; 106:2085-2090.
9. Schram MT, Chaturvedi N, Fuller JH, Stehouwer CD. Pulse pressure is associated with age and cardiovascular disease in type 1 diabetes: the Eurodiab Prospective Complications Study. *J Hypertens* 2003; 21:2035-2044.
10. Laurent S, Katsahian S, Fassot C, et al. Aortic stiffness is an independent predictor of fatal stroke in essential hypertension. *Stroke* 2003; 34:1203-1206.
11. Stevanov M, Baruthio J, Gounot D, Grucker D. In vitro validation of MR measurements of arterial pulse-wave velocity in the presence of reflected waves. *J Magn Reson Imaging* 2001; 14:120-127.
12. Groenink M, de Roos A, Mulder BJ, Spaan JA, van der Wall EE. Changes in aortic distensibility and pulse wave velocity assessed with magnetic resonance imaging following beta-blocker therapy in the Marfan syndrome. *Am J Cardiol* 1998; 82:203-208.
13. Rosamond W, Flegal K, Furie K, et al. Heart disease and stroke statistics--2008 update: a report from the American Heart Association Statistics Committee and Stroke Statistics Subcommittee. *Circulation* 2008; 117:e25-146.
14. Davidson CJ, Mark DB, Pieper KS, et al. Thrombotic and cardiovascular complications related to nonionic contrast media during cardiac catheterization: analysis of 8,517 patients. *Am J Cardiol* 1990; 65:1481-1484.
15. Ditsmann W, de Ridder M. The soft science of German cardiology. *Lancet* 2002; 359:2027-2029.
16. Bi X, Deshpande V, Simonetti O, Laub G, Li D. Three-dimensional breathhold SSFP coronary MRA: a comparison between 1.5T and 3.0T. *J Magn Reson Imaging* 2005; 22:206-212.

17. Liu X, Bi X, Huang J, Jerecic R, Carr J, Li D. Contrast-enhanced whole-heart coronary magnetic resonance angiography at 3.0 T: comparison with steady-state free precession technique at 1.5 T. *Invest Radiol* 2008; 43:663-668.
18. Sommer T, Hackenbroch M, Hofer U, et al. Coronary MR angiography at 3.0 T versus that at 1.5 T: initial results in patients suspected of having coronary artery disease. *Radiology* 2005; 234:718-725.
19. Kim WY, Danias PG, Stuber M, et al. Coronary magnetic resonance angiography for the detection of coronary stenoses. *N Engl J Med* 2001; 345:1863-1869.
20. Sakuma H, Ichikawa Y, Chino S, Hirano T, Makino K, Takeda K. Detection of coronary artery stenosis with whole-heart coronary magnetic resonance angiography. *J Am Coll Cardiol* 2006; 48:1946-1950.

Part I:

**Evaluation of end-organ damage
by standardized MR imaging tests,
in Diabetes and Hypertension**

Chapter 2

The effect of hypertension on aortic pulse wave velocity in type 1 diabetes mellitus patients: assessment by MR imaging

SGC van Elderen, A Brandts, JT Tamsma, JWA Smit, LJM Kroft,
HJ Lamb, RW van der Meer, JJM Westenberg, A de Roos

Submitted

ABSTRACT

Purpose

The aim of our study was to investigate in type 1 diabetes mellitus (DM) patients the role of hypertension and of type 1 DM itself on aortic stiffness by using magnetic resonance (MR) imaging.

Materials and Methods

Consecutive patients from the diabetes and hypertension outpatient clinic and healthy volunteers were included in our study. Subjects were divided into four groups: 32 healthy volunteers (mean age: 54.5 ± 6.8 years), 20 type 1 DM patients (mean age: 48.3 ± 5.9 years), 31 hypertensive patients (mean age: 59.9 ± 7.2 years) and 28 patients with both type 1 DM and hypertension (mean age: 50.1 ± 6.2 years). Aortic stiffness was measured by means of pulse wave velocity (PWV) using velocity-encoded MR imaging. Analysis of variance (ANOVA), uni- and multivariable regression models and the Bonferroni-test for multiple testing, were used for statistical analyses.

Results

Mean aortic PWV was 5.7 ± 1.2 m/s in healthy volunteers, 5.9 ± 1.2 m/s in type 1 DM patients without hypertension, 7.3 ± 1.2 m/s in hypertensive patients and 7.3 ± 1.3 m/s in type 1 DM patients with hypertension. Compared to healthy control subjects, aortic PWV was significantly higher in patients with hypertension ($p < 0.001$) and in type 1 DM patients with hypertension ($p < 0.001$), whereas aortic PWV was not increased in patients having type 1 DM alone. Furthermore, aortic PWV was significantly higher in type 1 DM patients with hypertension than in patients with type 1 DM alone ($p = 0.002$). These findings remained after adjustment for confounding factors.

Conclusion

Hypertension has a predominant contributive effect on aortic stiffness in type 1 DM patients whereas the direct diabetic effect on aortic stiffness is small.

INTRODUCTION

Increased aortic stiffness is an important risk factor for adverse cardiovascular outcome in various disease states including diabetes mellitus (DM) (1-3). Studies have demonstrated that aortic stiffness is increased in patients with particularly type 2 DM (1,4). However, type 2 DM is commonly associated with other classical risk factors such as obesity, abnormal lipid status and hypertension that also may affect aortic stiffness (1,5-7).

Cardiovascular risk profiles in patients with type 1 DM usually differ from that in patients with type 2 DM, but similar findings with respect to increased aortic stiffness have been found (3,8-13). A magnetic resonance (MR) imaging study has recently shown that aortic stiffness is associated with cerebrovascular and cardiovascular end-organ damage in type 1 DM patients (3). In these type 1 DM patient studies, the increase in aortic stiffness was relatively minor as compared to other patient groups, such as in patients with type 2 DM and in patients with hypertension (2,3,14,15). Also, in type 1 DM patients increased aortic stiffness has been measured in young type 1 DM patients or in type 1 DM patients with microvascular complications (2,8-13). Therefore, it is conceivable that like in type 2 DM patients, confounding factors may play a dominant role in aortic stiffness of type 1 DM patients as well.

A recent systematic review on aortic stiffness risk factors has demonstrated that age and hypertension are major and independent risk factors for aortic stiffness, while the association between DM (particularly type 2 DM), obesity and abnormal lipid profiles with aortic stiffness were found moderate (16). The hypothesis of our study is that hypertension also has a predominant effect on aortic stiffness in type 1 DM patients. To what extent type 1 DM itself independently adds to aortic stiffness remains to be established. Having knowledge of dominant factors affecting aortic stiffness in type 1 DM patients may be of value in guiding therapy, which is relevant considering the increased cardiovascular risk status in type 1 DM patients with increased aortic stiffness.

A widely used parameter expressing aortic stiffness is the pulse wave velocity (PWV), which is defined as the propagation speed of the pressure or flow wave front traveling along the aorta (17). PWV is estimated by dividing the distance between anatomical locations in the aorta by the time difference between the flow waves at the two locations that can be accurately measured with MR imaging (18).

The purpose of our study was to investigate in type 1 DM patients the role of hypertension and of type 1 DM itself on aortic PWV by using MR imaging.

MATERIALS AND METHODS

Study participants

This study was approved by the local medical ethics committee and all subjects gave informed consent to participate in the study. Consecutive patients, diagnosed with type 1 DM and essential hypertension, from the diabetes and hypertension outpatient clinic were eligible in our study. Healthy volunteers were also eligible and recruited by advertisement in local newspapers. All subjects were within the age range of 40-70 years and underwent MR imaging of the aorta between January 2005 and October 2009.

Subjects were divided into 4 subgroups based on the following criteria: group 1, healthy volunteers (n=32); group 2, patients with type 1 DM (n=20); group 3, patients with hypertension (n=27); group 4, patients with both type 1 DM and hypertension (n=28). The effect of type 1 DM and hypertension on aortic stiffness was investigated by comparing aortic PWV measurements between the groups.

Type 1 DM was defined as fasting blood glucose ≥ 7.0 mmol/l according to WHO criteria (19). Hypertension was defined as: systolic blood pressure > 140 mmHg and/or diastolic blood pressure > 90 mmHg, on repeated physical examination before antihypertensive therapy was instituted and according to criteria of the European Society of Hypertension (ESH) (20), or blood pressure above 140/90 mmHg at time of MR imaging. All diabetic patients were on treatment with insulin and all hypertensive patients were on treatment with antihypertensive medication. Blood pressure was measured at the time of MR imaging using a semi-automated sphygmomanometer (Dinamap, Critikon, Tampa, Florida, USA). Pulse pressure was defined as: systolic blood pressure–diastolic blood pressure. Furthermore, smoking status (i.e. non-smoker or current smoker), body mass index (BMI), glycated hemoglobin (HbA1c), total cholesterol, the cholesterol to high-density lipoprotein (Cholesterol/HDL) ratio, triglycerides and C-reactive protein were determined. Blood was drawn in the morning after an overnight fast within two weeks before MR imaging. The albumin excretion ratio was calculated using the microalbumin and creatinin concentrations in the urine.

Healthy volunteers underwent similar work-up as type 1 DM or hypertensive patients. Healthy volunteers did not comprise subjects with type 1 DM, hypertension, cardiovascular disease, left ventricular hypertrophy as evaluated by means of electrocardiography or MR imaging or any systemic disease.

Exclusion criteria comprised of known history of cardiovascular disease, evidence of aortic valve stenosis or insufficiency, as evaluated by means of physical examination and velocity-encoded MR imaging, Marfan syndrome, aortic coarctation or any aortic disease, known history of other systemic diseases than type 1 DM or hypertension and general contraindications to MR imaging.

MR imaging protocol

Aortic PWV was assessed using a 1.5-T MR imaging scanner (NT 15 Gyroscan Intera; Philips Medical Systems, Best, the Netherlands) as previously described (18). In short, first a longitudinal image of the aorta was acquired during a breath-hold using a segmented gradient-echo sequence. Scan parameters were: repetition time (TR) 4.0ms, echo time (TE) 1.05ms, flip angle (FA) 30°, field-of-view (FOV) 450mm, 128×128 acquisition matrix, reconstructed to 256×256, slice thickness 15mm and 2 number of signal averaged (NSA) using a five-element phased array cardiac surface coil. Then, a retrospectively electrocardiographic-gated gradient-echo sequence with velocity encoding perpendicular to the aorta was applied to measure through-plane flow at two predefined levels: 1) at the level of the ascending aorta 2) at the level of the distal abdominal aorta. Scan parameters were: TR 5.0 ms, TE 2.9 ms, FA 20°, FOV 300 mm, 128×115 acquisition matrix, reconstructed to 256×256, slice thickness 8mm with maximal number of phases reconstructed ensuring high (6-10 ms) temporal resolution. Maximum velocity encoding (Venc) was set to 150 cm/s at the ascending aorta level and 100 cm/s at the abdominal aorta level, respectively.

Image analysis

PWV was calculated using the following formula: $\Delta x/\Delta t$ (m/s), where Δx describes the distance between the ascending aorta and the distal abdominal aorta and Δt describes the transit time between the arrival of the pulse wave at these respective sites. The aortic path length between the measurements sites was determined from a centerline manually positioned along the aorta using the software package MASS (Medis) (21). Aortic velocity maps were analyzed using the in-house developed software package FLOW (Medis) (21). The onset of the systolic wave front was automatically determined from the resulting flow graph by the intersection point of the constant diastolic flow and upslope of the systolic wave front, modeled by linear regression along the steepest part of the upslope.

Manual contour drawing in the aorta velocity maps was performed by two researchers (A.B. and S.v.E, both 3 year experience in cardiac MR imaging) and supervised by a senior researcher (J.W. 15 years experience in cardiac MR imaging), all unaware of the subjects' conditions.

Statistical analysis

Statistical analysis was performed using SPSS for Windows (version 17.0; SPSS, Chicago, Illinois, USA). Data are expressed as mean \pm standard deviation (sd) unless stated otherwise. Aortic PWV data were non-normally distributed and further analyses were performed using the log-transformed PWV data. Analyses of variance (ANOVA) were used to calculate the differences between the groups concerning aortic PWV and continuous variables. The chi-square test was used to calculate the difference in dichotomous variables between groups. Pearson and Spearman correlation analyses were performed to analyze the association

between aortic PWV and continuous and dichotomous variables, respectively. Pearson or Spearman correlation coefficients (r) and p -values are reported.

Univariable and multivariable regression models were used to correct for possible confounding factors. Age and sex were considered as standard confounding factors. Furthermore, clinical and laboratory variables that were statistically significantly different between groups (i.e. with ANOVA) and were related to outcome (i.e. with aortic PWV in Pearson or Spearman correlation analyses) were considered as confounding factors.

To estimate the effect of type 1 DM, hypertension, and type 1 DM with hypertension on aortic PWV, healthy volunteers were used as the reference category. To estimate the additional effect of type 1 DM or hypertension on aortic PWV, type 1 DM patients with hypertension were used as the reference category. Overall p -values and mean \pm standard errors (se) are reported. The Bonferroni-test was used to correct for multiple testing. A $p < 0.05$ was considered statistically significant.

RESULTS

Clinical characteristics

Table 1 describes the clinical characteristics of the study population per subgroup. Age was significantly higher in healthy volunteers and in patients with hypertension as compared to

Table 1. Clinical characteristics of the study population per subgroup

	Healthy volunteers ($n=32$)	DM1 ($n=20$)	Hypertension ($n=27$)	DM1 and hypertension ($n=28$)	p -value
Age (years)	54.5 \pm 6.8	48.3 \pm 5.9	59.9 \pm 7.2	50.1 \pm 6.2	<0.001
Male gender, n (%)	24 (75)	8 (40)	10 (37)	15 (54)	ns
Systolic blood pressure (mmHg)	118 \pm 11	120 \pm 10	165 \pm 18	141 \pm 19	<0.001
Diastolic blood pressure (mmHg)	76 \pm 9	69 \pm 7	96 \pm 13	76 \pm 10	<0.001
Pulse pressure (mmHg)	42 \pm 12	51 \pm 9	69 \pm 19	64 \pm 15	<0.001
Smoking yes, n (%)	4 (13)	2 (10)	5 (19)	5 (18)	ns
Body mass index (kg/m ²)	26.9 \pm 3.0	24.4 \pm 2.1	26.0 \pm 4.7	26.5 \pm 3.4	ns
HbA1c (%)	5.4 \pm 0.2	7.0 \pm 1.0	5.2 \pm 0.3	7.8 \pm 1.0	<0.001
Cholesterol (mmol/l)	5.3 \pm 0.9	4.5 \pm 0.7	5.6 \pm 1.0	4.9 \pm 1.0	0.001
Cholesterol/HDL ratio (mmol/l)	3.7 \pm 1.0	2.8 \pm 0.6	3.7 \pm 1.1	3.2 \pm 1.0	0.003
Triglycerides (mmol/l)	1.1 \pm 0.5	0.9 \pm 0.3	1.4 \pm 0.4	1.6 \pm 1.0	<0.001
C-reactive protein (mg/l)	1.9 \pm 1.8	1.6 \pm 1.5	2.4 \pm 2.7	2.7 \pm 3.7	ns
Microalbuminuria (mg/l)	1.5 \pm 2.1	1.0 \pm 1.5	2.3 \pm 4.4	1.8 \pm 3.2	ns

Values are mean \pm SD or n (%) or data are numbers of patients and numbers in parentheses are percentages. DM1: type-1 diabetes mellitus patients; HbA1c: Glycated hemoglobin; HDL: high density lipoprotein. ns: non-significant.

type 1 DM patients with and without hypertension. The group of healthy volunteers comprised of a higher male/female ratio than the other groups. Systolic blood pressure, diastolic blood pressure and pulse pressure were inherently increased in the hypertensive groups. HbA1c was inherently higher in the groups including type 1 DM patients. Furthermore, lipid profiles were different between groups.

Association between aortic PWV and clinical and laboratory parameters

Aortic PWV was significantly associated with age ($r=0.4$, $p<0.001$), systolic blood pressure ($r=0.5$, $p<0.001$), diastolic blood pressure ($r=0.3$, $p=0.002$), pulse pressure ($r=0.4$, $p<0.001$) and triglycerides ($r=0.2$, $p=0.012$). As pulse pressure is a resultant of systolic blood pressure minus diastolic blood pressure, pulse pressure was considered as a confounding factor, whereas systolic and diastolic blood pressure were not. Sex, smoking status, BMI, HbA1c, lipid status, C-reactive protein and microalbuminuria did not correlate with aortic PWV.

Independent and combined effect of type 1 DM and hypertension on aortic PWV

Mean aortic PWV was 5.7 ± 1.2 m/s in healthy subjects, 5.9 ± 1.2 m/s in type 1 DM patients, 7.3 ± 1.2 m/s in hypertensive patients without DM and 7.3 ± 1.3 m/s in type 1 DM patients with hypertension. Table 2 describes the uni- and multivariable regression models for assessment of the independent and combined effect of type 1 DM and hypertension on aortic stiffness, before and after correction for confounding factors.

Table 2. Difference in aortic PWV between subgroups before and after correction for confounding factors

		<i>Uncorrected model</i>	<i>Model corrected for age and sex</i>	<i>Model corrected for age, sex, pulse pressure and triglycerides</i>
<i>Reference category</i>	<i>Subgroup</i>	<i>p-value</i>	<i>p-value</i>	<i>p-value</i>
a. Healthy volunteers	DM1 patients	0.528	0.058	0.198
	Hypertensive patients	< 0.001*	< 0.001*	<0.001*
	DM1 patients with hypertension	< 0.001*	< 0.001*	<0.001*
b. DM1 patients with hypertension	Hypertensive patients	0.665	0.668	0.668
	DM1 patients	0.002*	0.030*	0.228

a. healthy volunteers serve as the reference category b. DM1 patients with hypertension serve as the reference category. DM1: type-1 diabetes mellitus patients. * p-value < 0.05.

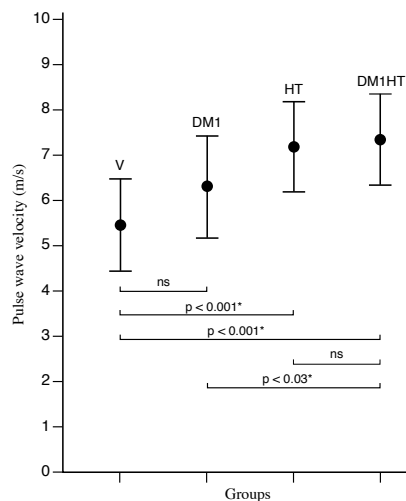
Without correction for confounding factors, aortic PWV was statistically significant higher in patients with hypertension ($p<0.001$) and in patients with both type 1 DM and hypertension ($p<0.001$), but not in patients having only type 1 DM ($p=0.528$) as compared to healthy

volunteers (Table 2a). Furthermore, aortic PWV was statistically significantly higher in type 1 DM patients with hypertension as compared to type 1 DM patients ($p=0.002$), whereas aortic PWV was not statistically significantly different between type 1 DM patients with hypertension and hypertensive patients (Table 2b).

After correction for standard confounding factors age and sex, the differences in aortic PWV remained comparable between groups (Table 2). Mean aortic PWV was 5.4 ± 1.0 m/s in healthy subjects, 6.3 ± 1.1 m/s in type 1 DM patients, 7.2 ± 1.0 m/s in hypertensive patients and 7.3 ± 1.0 m/s in type 1 DM patients with hypertension. Figure 1 shows the difference between the groups regarding aortic PWV corrected for age and sex; having type 1 DM alone does not statistically significant affect aortic PWV as compared to healthy volunteers, although a slight trend for increased aortic PWV in type 1 DM patients as compared to healthy volunteers can be observed. Conversely, hypertension has a major effect in increasing aortic PWV (Figure 1).

After correction for age, gender, pulse pressure and triglycerides mean aortic PWV was 5.6 ± 1.1 m/s in healthy subjects, 6.4 ± 1.1 m/s in type 1 DM patients, 7.1 ± 1.0 m/s in hypertensive patients without diabetes and 7.2 ± 1.0 m/s in type 1 DM patients with hypertension. Additionally correcting for pulse pressure and triglycerides as confounding factors, had effect on the difference in aortic PWV between type 1 DM patients with hypertension and patients having only type 1 DM, which was no longer statistically significant different from each other (Table 2b). This was expected because pulse pressure and triglycerides are inherently increased in subgroups with type 1 DM and hypertension; by correcting for these confounders group outcomes were equalized.

Figure 1. Difference in aortic PWV between subgroups corrected for age and sex



Abbreviations: V : Healthy volunteers; DM1: type-1 diabetes mellitus patients; HT: hypertensive patients; DM1HT: type-1 diabetes mellitus patients with hypertension. Means \pm se per subgroup are given and p-values between subgroups are presented below. ns: non-significant.

DISCUSSION

We investigated the independent and combined effect of type 1 DM and hypertension on aortic stiffness by comparing four subgroups including type 1 DM patients with and without hypertension, hypertensive patients and healthy volunteers by using MR imaging. The main finding was that the independent effect of type 1 DM on aortic PWV was minor; aortic PWV was not significantly different between healthy volunteers and type 1 DM patients. In addition, no differences were found in aortic PWV between type 1 DM patients with hypertension and hypertensive patients that remained after correction for confounding factors age, gender, pulse pressure and triglycerides. Secondly, the independent effect of hypertension on aortic PWV was major; aortic PWV was significantly higher in hypertensive patients than in healthy volunteers. In addition, the combination of type 1 DM and hypertension resulted in increased aortic stiffness, and was significantly higher than in patients having type 1 DM alone, that remained after correction for age and sex.

Previous studies have demonstrated increased aortic stiffness in type 1 DM patients with microvascular complications including microalbuminuria or hypertension as compared to healthy volunteers (2,8-13). Age and hypertension are well-established risk factors of aortic stiffness and hypertension is often present in type 1 DM. It is therefore conceivable that multiple factors may contribute to aortic stiffness in type 1 DM patients. We investigated the effect of type 1 DM itself on aortic PWV by evaluating a fairly well-controlled, uncomplicated type 1 DM patient group with an age range between 40-70 years old. In type 1 DM patients, aortic stiffness was not significantly different from healthy volunteers although a trend towards increased aortic stiffness was observed after correction for age and sex. When comparing subgroups, triglycerides and pulse pressure were inherently increased in patients with hypertension. Therefore, after additional correction for triglycerides and pulse pressure, differences between type 1 DM patients with hypertension and patients having type 1 DM alone became non-significant, that was explained by equalizing subgroups.

Hypertension is a well-known major and independent risk factor for aortic stiffness (16,22), that was also found in our study. Investigating the hypertensive contribution on aortic stiffness in patients with type 1 DM is relevant for cardiovascular risk assessment, as type 1 DM is often associated with hypertension, especially in the elderly (2,16). Age and blood pressure have consistently been shown to be independently associated with PWV (16). The impact of hypertension on aortic stiffening may be twofold: 1. mechanistic stretching of the arterial wall may result in aortic stiffening; 2. structural changes of the arterial wall due to cyclic stress, resulting in stress fracturing of elastin and consequent stiffening (16,23). In contrast to the predominant effect of hypertension on aortic stiffening, only weak correlations have been shown with diabetes, accounting for a mean of 5% of the variation in PWV (16). It is generally believed that increased aortic stiffness plays an important role in the pathway linking various diseases, including type 1 DM, with their increased cardiovascular risk (1,2). We

have now demonstrated that aortic stiffness in type 1 DM patients mainly depends on having additional hypertension, and not on type 1 DM alone. Thus, identification of hypertension in patients with type 1 DM is of importance for risk stratification and may be used for stratifying therapy as to improve cardiovascular outcome.

Some study limitations are addressed. This study has a cross-sectional design. Therefore, direct causative mechanisms of the effect of type 1 DM itself and of hypertension cannot be determined. Follow-up studies are required for further evaluation of the role of type 1 DM and hypertension on aortic stiffness. From our study design with four subgroups it was difficult to exactly age- and gender match all patients and volunteers. Therefore, multivariable regression models were used to account for possible confounding factors, including age. After correction for age and sex the differences in aortic PWV remained comparable between subgroups.

In conclusion, hypertension has a predominant contributive effect on aortic stiffness in type 1 DM patients whereas the direct diabetic effect on aortic stiffness is small. As aortic stiffness and type 1 DM are highly associated with adverse cardiovascular outcome, identifying hypertension in type 1 DM patients seems highly relevant for risk stratification.

REFERENCES

1. Cruickshank K, Riste L, Anderson SG, Wright JS, Dunn G, Gosling RG. Aortic pulse-wave velocity and its relationship to mortality in diabetes and glucose intolerance: an integrated index of vascular function? *Circulation* 2002;106(16):2085-2090.
2. Stehouwer CD, Henry RM, Ferreira I. Arterial stiffness in diabetes and the metabolic syndrome: a pathway to cardiovascular disease. *Diabetologia* 2008;51(4):527-539.
3. van Elderen SG, Brandts A, Westenberg JJ, et al. Aortic stiffness is associated with cardiac function and cerebral small vessel disease in patients with type 1 diabetes mellitus: assessment by magnetic resonance imaging. *Eur Radiol* 2010;20(5):1132-1138.
4. Henry RM, Kostense PJ, Spijkerman AM, et al. Arterial stiffness increases with deteriorating glucose tolerance status: the Hoorn Study. *Circulation* 2003;107(16):2089-2095.
5. Asmar R, Benetos A, London G, et al. Aortic distensibility in normotensive, untreated and treated hypertensive patients. *Blood Press* 1995;4(1):48-54.
6. Sutton-Tyrrell K, Newman A, Simonsick EM, et al. Aortic stiffness is associated with visceral adiposity in older adults enrolled in the study of health, aging, and body composition. *Hypertension* 2001;38(3):429-433.
7. Zebekakis PE, Nawrot T, Thijs L, et al. Obesity is associated with increased arterial stiffness from adolescence until old age. *J Hypertens* 2005;23(10):1839-1846.
8. Brooks B, Molyneaux L, Yue DK. Augmentation of central arterial pressure in type 1 diabetes. *Diabetes Care* 1999;22(10):1722-1727.
9. Giannattasio C, Failla M, Piperno A, et al. Early impairment of large artery structure and function in type I diabetes mellitus. *Diabetologia* 1999;42(8):987-994.
10. Giannattasio C, Failla M, Grappiolo A, Gamba PL, Paleari F, Mancia G. Progression of large artery structural and functional alterations in Type I diabetes. *Diabetologia* 2001;44(2):203-208.
11. Haller MJ, Samyn M, Nichols WW, et al. Radial artery tonometry demonstrates arterial stiffness in children with type 1 diabetes. *Diabetes Care* 2004;27(12):2911-2917.
12. Lacy PS, O'Brien DG, Stanley AG, Dewar MM, Swales PP, Williams B. Increased pulse wave velocity is not associated with elevated augmentation index in patients with diabetes. *J Hypertens* 2004;22(10):1937-1944.
13. Parikh A, Sochett EB, McCrindle BW, Dipchand A, Daneman A, Daneman D. Carotid artery distensibility and cardiac function in adolescents with type 1 diabetes. *J Pediatr* 2000;137(4):465-469.
14. Brandts A, van Elderen SG, Westenberg JJ, et al. Association of aortic arch pulse wave velocity with left ventricular mass and lacunar brain infarcts in hypertensive patients: assessment with MR imaging. *Radiology* 2009;253(3):681-688.
15. van der Meer RW, Diamant M, Westenberg JJ, et al. Magnetic resonance assessment of aortic pulse wave velocity, aortic distensibility, and cardiac function in uncomplicated type 2 diabetes mellitus. *J Cardiovasc Magn Reson* 2007;9(4):645-651.
16. Cecelja M, Chowienzyk P. Dissociation of aortic pulse wave velocity with risk factors for cardiovascular disease other than hypertension: a systematic review. *Hypertension* 2009;54(6):1328-1336.

17. Laurent S, Cockcroft J, van Bortel L, et al. Expert consensus document on arterial stiffness: methodological issues and clinical applications. *Eur Heart J* 2006;27(21):2588-2605.
18. Grotenhuis HB, Westenberg JJ, Steendijk P, et al. Validation and reproducibility of aortic pulse wave velocity as assessed with velocity-encoded MRI. *J Magn Reson Imaging* 2009;30(3):521-526.
19. Alberti KG, Zimmet PZ. Definition, diagnosis and classification of diabetes mellitus and its complications. Part 1: diagnosis and classification of diabetes mellitus provisional report of a WHO consultation. *Diabet Med* 1998;15(7):539-553.
20. Mancia G, de Backer G, Dominiczak A, et al. 2007 Guidelines for the management of arterial hypertension: The task force for the management of arterial hypertension of the European Society of Hypertension (ESH) and of the European Society of Cardiology (ESC). *J Hypertens* 2007;25(6):1105-1187.
21. van der Geest RJ, de Roos A, van der Wall EE, Reiber JH. Quantitative analysis of cardiovascular MR images. *Int J Card Imaging* 1997;13(3):247-258.
22. Safar ME, Levy BI, Struijker-Boudier H. Current perspectives on arterial stiffness and pulse pressure in hypertension and cardiovascular diseases. *Circulation* 2003;107(22):2864-2869.
23. Cecelja M, Chowienczyk P. Arterial stiffening: cause and prevention. *Hypertension* 2010;56(1):29-30.

Chapter 3

Association of aortic arch pulse wave velocity with left ventricular mass and lacunar brain infarcts in hypertensive patients: assessment by MR imaging

A Brandts, SGC van Elderen, JJM Westenberg, J van der Grond, MA van Buchem, MV Huisman, LJM Kroft, JT Tamsma, A de Roos

Radiology 2009;253(3):681-688

ABSTRACT

Purpose

To assess the possible association between aortic arch stiffness, which may cause hypertensive cardiovascular disease, and cardiac and cerebral end-organ damage in patients with hypertension by using magnetic resonance (MR) imaging.

Materials and Methods

Approval from the local institutional review board was obtained, and patients gave informed consent. Fifty patients with hypertension (31 women and 19 men; mean age \pm standard deviation, 49.2 ± 12.7 years; mean systolic blood pressure, 152.1 ± 22.3 mmHg; mean diastolic blood pressure, 88.0 ± 13.1 mmHg), compliant for treatment with antihypertensive medication, were prospectively enrolled for MR examinations of the aorta, heart, and brain with standard pulse sequences. Aortic arch pulse wave velocity (PWV), left ventricular (LV) mass, LV systolic and diastolic function, lacunar brain infarcts, and periventricular and deep white matter hyperintensities (WMHs) were assessed. Univariable and multiple linear and logistic regression analyses were used for statistical analyses.

Results

Mean aortic arch PWV was 7.3 ± 2.5 m/s. Aortic arch PWV was statistically significantly associated with LV mass ($r = 0.30$, $p = .03$, $\beta = 1.73$); indexes of systolic function, including ejection fraction ($r = -0.38$, $p = .01$, $\beta = -1.12$); indexes of diastolic function, including the ratio of early diastolic to atrial contraction peak filling rates ($r = -0.44$, $p < .01$, $\beta = -0.11$); lacunar brain infarcts (odds ratio [OR] = 1.8, $p < .01$); and periventricular (OR = 1.5, $p = .01$) and deep (OR = 1.6, $p = .01$) WMHs. Aortic arch PWV was statistically significantly associated with LV mass ($r = 0.37$, $p = .03$, $\beta = 2.11$) and lacunar brain infarcts (OR = 1.8, $p = .04$), independent of age, sex and hypertension duration, but not with indexes of diastolic and systolic function and WMHs.

Conclusion

Aortic arch stiffness is associated with LV mass and lacunar brain infarcts in hypertensive patients, independent of age, sex, and hypertension duration; these manifestations of end-organ damage may help to risk stratify hypertensive patients.

INTRODUCTION

Hypertension has a high prevalence in the general population and is one of the major risk factors for cardiovascular disease that may affect both the heart and the brain (1,2). The elastic properties of the aortic wall play an important role in the pathogenesis of hypertensive cardiovascular disease (3,4). Owing to continuous stress at the aortic wall, structural and functional changes in the arterial wall may occur, leading to increased aortic stiffness (3–8). Aortic stiffness, as measured by means of ultrasonography (US), is an independent predictor of adverse cardiovascular outcome in hypertensive patients (9,10). Increased aortic stiffness may affect the heart by producing an extra workload on the left ventricle (LV) (11). As a consequence, LV hypertrophy, compromised coronary perfusion, and subsequently diastolic and systolic dysfunction may occur, which may ultimately lead to heart failure and cardiac death (11,12).

Aortic stiffness may also lead to impaired absorption of the pulse wave and an increase in central pulse pressure, which may augment small vessel disease in the brain (13). Lacunar brain infarcts and white matter hyperintensities (WMHs) have been described as early manifestations of cerebral small vessel disease by using magnetic resonance (MR) imaging (14). Both lacunar brain infarcts and WMHs are associated with dementia (15,16) and stroke (17).

The proximal part of the aorta and its first branches (i.e., the more elastic part of the aorta) act as a conduit delivering blood from the LV, primarily to the myocardium and the cerebrum (3,11,13). The hypothesis is that stiffness of the aortic arch is involved in cardiac and cerebral damage in patients with hypertension.

Aortic stiffness can be assessed by means of pulse wave velocity (PWV) measurements (18,19). A number of studies have shown that MR imaging is well suited to accurately assess PWV (18–22), LV function (23,24) and brain abnormalities (25,26). Furthermore, MR imaging allows for assessment of local PWV, also in the aortic arch (3,18), whereas US measurements estimate the stiffness of the entire aorta (7,11).

However, to our knowledge, the association between aortic arch stiffness and cardiac and cerebral damage in hypertensive patients has not been comprehensively studied by using MR imaging.

Accordingly, the purpose of the present study was to assess the possible association between aortic arch stiffness and cardiac and cerebral end-organ damage in hypertensive patients by using MR imaging.

MATERIALS AND METHODS

Study participants

This study was approved by the local institutional review board. Consecutive patients from the hypertension outpatient clinic in whom there was a diagnosis of essential hypertension were prospectively included for the study. Between October 2007 and May 2008, 69 patients were considered for participation in our study. All patients were older than 18 years and were undergoing treatment with antihypertensive medication. Treatment compliance was verified. Exclusion criteria were evidence of aortic valve stenosis or insufficiency, as evaluated by means of physical examination and velocity-encoded MR imaging, and general contraindications to MR imaging. In total, 50 hypertensive patients (19 men and 31 women; mean age \pm standard deviation, 47.1 ± 14.6 years and 50.5 ± 11.5 years, respectively; overall mean age, 49.2 ± 12.7 years) gave written informed consent to participate in the study, and 19 patients were excluded for this study (six patients had general contraindications for MR, six did not fulfill the selection criteria, five were claustrophobic, and two had a diagnosis of aortic valvular disease).

Hypertension was defined as systolic and/or diastolic blood pressure of greater than or equal to 140 mmHg and/or greater than 90 mmHg, respectively, at repeated physical examination before antihypertensive therapy was instituted and according to criteria of the European Society of Hypertension (2). Blood pressure was measured by using a semiautomated sphygmomanometer (Dinamap, Critikon, Tampa, Fla). The duration of hypertension was estimated as the time (in years) passed since the reported age of diagnosis until MR examination. Pulse pressure was defined as systolic minus diastolic blood pressure. Body mass index (i.e., the patient's body weight in kilograms during MR imaging divided by the square root of the height of the patient in centimeters), smoking status (nonsmoker, current smoker, or former smoker), diabetes mellitus (i.e., fasting blood glucose ≥ 7.0 mmol/L or current use of oral antidiabetic agents) and lipid profiles (total cholesterol, high-density lipoprotein, and triglycerides) were determined. Blood was drawn in the morning after an overnight fast within 2 weeks before MR imaging.

Table 1 describes the characteristics of the 50 hypertensive patients. Mean systolic blood pressure was 152.1 ± 22.3 mmHg and mean diastolic blood pressure was 88.0 ± 13.1 mmHg, despite antihypertensive medication. Fourteen patients were current smokers, six patients were former smokers, and nine patients had a diagnosis of diabetes mellitus.

MR imaging protocol

Aortic arch PWV imaging and cardiac imaging were performed by using a 1.5-T MR imager (NT 15 Gyroscan Intera; Philips Medical Systems, Best, the Netherlands) (25 patients) or a 3.0-T MR imager (Achieva; Philips Medical Systems) (25 patients) with similar protocols (27). All brain examinations were performed with the 3.0-T system. Diastolic function findings were

not obtained in nine patients owing to technical problems with valvular flow measurements at 3.0-T MR during the start of the study. Total study duration, to complete all examinations and including the time between cardiovascular and brain examination, was 60 minutes.

Table 1. Characteristics of the study population

<i>Characteristics</i>	<i>Patients with essential hypertension (n=50)</i>
Male gender, n (%)	19 (38)
Age (years)	49.2 ± 12.7
Hypertension duration (years)	7.9 ± 8.3
Systolic blood pressure (mmHg)	152.1 ± 22.3
Diastolic blood pressure (mmHg)	88.0 ± 13.1
Pulse pressure (mmHg)	64.1 ± 19.0
Heart rate (beats per minute)	68.2 ± 11.3
BMI (kg/m ²)	25.5 ± 3.0
Smoking	
No, n (%)	30 (60)
Yes, n (%)	14 (28)
Former smoker, n (%)	6 (12)
Diabetes yes, n (%)	9 (18)
Total cholesterol (mmol/l)	5.2 ± 1.3
HDL (mmol/l)	1.5 ± 0.5
Triglycerides (mmol/l)	1.6 ± 1.2

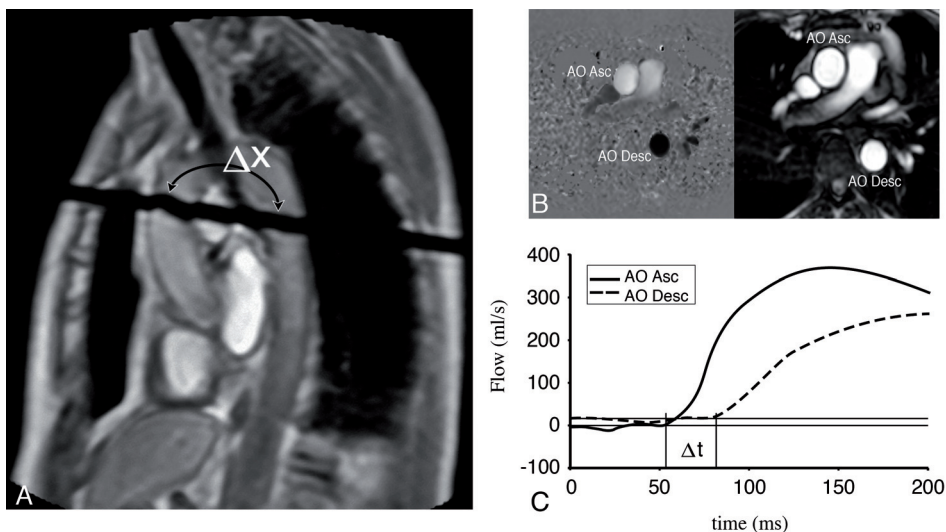
Data are presented as mean and standard deviations or n (%). BMI: body mass index; HDL: high-density lipoprotein.

Aortic arch PWV

Aortic arch PWV was determined as described in the literature (18–22). Figure 1 demonstrates assessment of aortic arch PWV between the ascending and the proximal descending aorta. A retrospectively electrocardiographically gated gradient-echo sequence with maximum velocity encoding perpendicular to the ascending aorta was performed to assess the flow in the ascending and proximal descending aorta. This imaging plane (Figure 1a) was determined from coronal and oblique sagittal views of the aortic arch. Examination parameters for both 1.5- and 3-T MR imaging are included in Table 2. For both 1.5- and 3-T MR, a maximal number of phases was reconstructed ensuring high (6–10 msec) temporal resolution. Maximum velocity encoding was set to 150 cm/sec. The aortic arch PWV sequence took 3–4 minutes when measured for a mean heart rate of 65 beats per minute and was acquired during free breathing. A five-element phased-array cardiac coil was used for data acquisition.

Aortic arch velocity maps were analyzed by using the previously validated in-house developed software package FLOW (Figure 1c) (28). Aortic arch PWV was calculated as $\Delta x / \Delta t$ (in meters per second), where Δx is the distance between the ascending and proximal descending aorta (measured along the centerline in the oblique sagittal view of the aortic arch by using the previously validated in-house developed software package MASS) (Figure

Figure 1. Aortic arch PWV determination with MR imaging. (a) Sagittal gradient-echo image of aorta in 41-year-old woman. Black line represents the acquisition plane for velocity-encoded MR and is perpendicular to the aorta at the level of the pulmonary trunk. Δx = path length of aortic arch along centerline of the aortic arch. (b) Phase (left) and magnitude (right) images acquired with an electrocardiographically gated gradient-echo sequence with velocity encoding at the acquisition sites in the ascending aorta (AO Asc) and proximal descending aorta (AO Desc). (c) Flow curves of ascending and proximal descending aorta. Δt = transit time of arrival of proximal flow wave. Aortic PWV is defined as $\Delta x/\Delta t$ (in meters per second).



1a) (28) and Δt is the transit time between the arrival of the pulse wave at the ascending and the proximal descending aorta, respectively (19). Manual contour drawing in the aorta velocity maps was performed by one researcher (A.B., with 1 year of experience in cardiac MR imaging) and was supervised by a senior researcher (J.J.M.W., with 13 years of experience in cardiac MR imaging).

LV function and mass

For assessment of LV systolic function and LV mass, the entire heart was imaged in short-axis orientation by using electrocardiographically gated breath-hold segmented gradient-echo imaging with steady-state free-precession, as described previously (23,29). Examination parameters for both 1.5- and 3-T MR imaging are described in Table 2. Ten to 12 consecutive sections without gap were imaged with one signal acquired and a minimum of 30 reconstructed phases. Arrhythmia rejection was used with an acceptance window of 10%.

To determine LV volumes, end-systolic and end-diastolic endocardial and epicardial borders were manually traced on short-axis cine images by using the software package MASS (28). Papillary muscles were considered to be part of the myocardium and excluded from the blood pool. LV end-systolic volume, LV end-diastolic volume, ejection fraction, and LV mass were assessed. The LV end-diastolic mass was obtained from the volume of the LV muscle

Table 2. MR imaging parameters for assessment of aortic arch PWV and LV systolic and diastolic function

	1.5 T MRI	3 T MRI
<i>Aortic arch PWV</i>		
TR (ms)	5.0	4.9
TE (ms)	2.9	3.0
FA (°)	20	10
Acquisition matrix	128 x 115	128 x 104
Acquired voxel size (mm ³)	2.3 x 2.3 x 8.0	2.5 x 2.5 x 8.0
Reconstructed number of phases	maximum	maximum
Venc (cm/s)	150	150
<i>LV systolic function</i>		
TR (ms)	3.3	4.4
TE (ms)	1.7	2.2
FA (°)	50	45
Acquisition matrix	256 x 194	128 x 104
Acquired voxel size (mm ³)	1.7 x 1.7 x 10.0	1.3 x 1.7 x 10.0
NSA	1	1
Reconstructed number of phases	40	30
<i>LV diastolic function</i>		
TR (ms)	14	5.2
TE (ms)	4.8	3.2
FA (°)	20	10
Acquisition matrix	128 x 104	128 x 104
Acquired voxel size (mm ³)	2.7 x 3.4 x 8.0	2.5 x 2.5 x 8.0
Reconstructed number of phases	40	40
Venc (cm/s)	150	150

Aortic arch PWV: aortic arch pulse wave velocity; LV systolic function: left ventricular systolic function; LV diastolic function: left ventricular diastolic function; TR: repetition time; TE: echo time; FA: flip angle; Venc: maximum velocity encoding; NSA: number of signal averaged.

tissue including the interventricular septum, multiplied with the specific weight of muscle tissue, which is 1.04 g/cm³ (30). Volumes and mass were indexed for body surface area (31).

For assessment of LV diastolic function, an electrocardiographically gated gradient-echo sequence with maximum velocity encoding was performed to measure blood flow across the mitral valve (32,33). Table 2 describes parameters for both 1.5- and 3-T MR. For both 1.5- and 3-T MR, 40 phases were reconstructed to ensure a high temporal resolution. Furthermore, a maximum velocity encoding of 150 cm/sec was used (34). In each cardiac phase, the area of the mitral valve was traced manually by using the software package FLOW (28). Flow at early diastole and at atrial contraction were assessed from the flow graph. The early peak filling rate, the atrial peak filling rate, and the early diastolic to atrial contraction peak filling rate (E/A_{peak}) ratio were assessed. Furthermore, the early diastolic peak deceleration gradients were calculated automatically (24). Moreover, LV filling pressures were estimated by the early

peak filling rate-to-early diastolic peak wall velocity ratio to correct for possible pseudo-normalization (35).

Contour segmentation was performed by one observer (A.B., with 1 year of experience in cardiac MR imaging) and was supervised by a radiologist (L.J.M.K., 12 years of experience in cardiac MR imaging).

Cerebral lesions

Brain MR imaging consisted of spin-echo T2-weighted and fluid-attenuated inversion recovery (FLAIR) sequences. Acquisition parameters for T2-weighted imaging were as follows: repetition time msec/echo time msec, 3951/80; flip angle, 90°; field of view, 224 mm; acquisition matrix, 448 × 448; reconstruction matrix, 1024 × 1024; section thickness, 3.6 mm; 40 sections without gap; and turbo-spin-echo factor, 16. The acquisition time was 2 minutes 46 seconds. Acquisition parameters for the FLAIR sequence were as follows: repetition time msec/echo time msec/inversion time msec, 10 000/100/2800; flip angle, 90°; field of view, 224 mm; acquisition matrix, 224 × 224; reconstruction matrix, 448 × 448; section thickness, 3.6 mm; and 40 sections without gap, with an acquisition time of 3 minutes 20 seconds.

Lacunar brain infarcts were defined as cavities within and not extending to the outer contours of the brain, with signal intensity similar to that of cerebrospinal fluid for all pulse sequences, surrounded by an area of parenchyma with a high signal intensity on T2-weighted and FLAIR images (14,25,36). WMHs were defined as areas of brain parenchyma with increased signal intensity on T2-weighted and FLAIR images and without mass effect. WMHs were subdivided into periventricular WMHs and deep WMHs and were classified according to Fazekas (26). Fazekas scores of 0 and 1 were considered normal, a score of 2 was considered abnormal below the age of 75 years, and a score of 3 was considered abnormal in any age group.

Lacunar brain infarcts and WMHs were visually scored by consensus reading by a researcher (A.B., with 1 year of experience in neuroradiology) and two experienced observers (M.A.v.B. and J.v.d.G., both with 15 years of experience in neuroradiology).

Statistical analysis

Statistical analysis was performed by using SPSS for Windows (version 14.0; SPSS, Chicago, Ill). Data are expressed as mean ± standard deviation unless stated otherwise. Univariable linear regression analyses were performed to analyze the association between aortic arch PWV and continuous data. Pearson correlation coefficients (r), p-values, and β regression coefficients are reported. Univariable logistic regression analyses were performed to analyze the association between aortic arch PWV and dichotomous data. Odds ratios (ORs), 95% confidence intervals (CIs), and p-values are reported. Multiple linear and logistic regression analyses were performed to identify variables that were independently associated with cardiac as well as cerebral indexes and to adjust for confounders. Age, sex, hypertension duration, and MR imager type were considered as confounders.

RESULTS

Aortic arch PWV

Mean aortic arch PWV was 7.3 ± 2.5 m/s, indicating increased aortic arch stiffness in comparison with normal MR imaging values from the literature (i.e., 5.7 ± 1.1 m/s for healthy volunteers (21)). Aortic arch PWV was statistically significantly associated with age ($r = 0.53$, $p < .01$, $\beta = 2.67$) and systolic blood pressure ($r = 0.30$, $p = .04$, $\beta = 2.55$). Sex, diastolic blood pressure, pulse pressure, heart rate, body mass index, smoking status, diabetes mellitus, and lipid status did not correlate with aortic arch PWV.

Association between aortic arch PWV and LV function and mass

Aortic arch PWV was statistically significantly associated with end-systolic LV volume indexed for body surface area ($r = 0.34$, $p = .02$, $\beta = 1.21$), ejection fraction ($r = -0.38$, $p = .01$, $\beta = -1.12$), LV mass index ($r = 0.30$, $p = .03$, $\beta = 1.73$), early peak filling rate ($r = -0.37$, $p = .02$, $\beta = -0.14$), atrial peak filling rate ($r = 0.42$, $p = .01$, $\beta = 20.10$), and E/A_{peak} ratio ($r = -0.44$, $p < .01$, $\beta = -0.11$) (Table 3). Mean ratio of early peak filling rate to early diastolic peak wall velocity was 4.2 ± 1.7 , indicating that the patients had a normal LV filling pressure (35).

Table 3. Association between aortic arch PWV and LV function and mass

	<i>n</i>	<i>mean ± sd</i>	<i>aortic arch PWV</i>		
			<i>r</i>	<i>p-value</i>	<i>β</i>
LVEDV-I (ml/m ²)	50	79.7 ± 12.2	0.12	0.43	0.56
LVESV-I (ml/m ²)	50	31.0 ± 9.2	0.34	0.02	1.21
LV ejection fraction (%)	50	61.3 ± 7.5	-0.38	0.01	-1.12
LVEDM-I (g/m ²)	50	60.4 ± 14.5	0.30	0.03	1.73
Early peak filling rate (ml/s)	41	507.7 ± 160.5	-0.37	0.02	-0.14
Early deceleration peak (ml/s ²)	41	-4.6 ± 2.0	0.29	0.06	0.23
Early deceleration mean (ml/s ²)	41	-2.6 ± 1.2	0.16	0.31	0.08
Early deceleration time (ms)	41	194.0 ± 77.9	-0.20	0.21	-6.11
Atrial peak filling rate (ml/s)	41	138.5 ± 121.9	0.42	0.01	20.10
E/A _{peak} ratio	41	1.5 ± 0.6	-0.44	<0.01	-0.11

Data are expressed as mean and standard deviations (sd) and Pearson correlation coefficients (*r*), *p*-values and β regression coefficients (β).

LVEDV-I: left ventricular end-diastolic volume corrected for body surface area, LVESV-I: left ventricular end-systolic volume corrected for body surface area, LVEDM-I: left ventricular end-diastolic LV mass corrected for body surface area, LV ejection fraction: left ventricular ejection fraction. E/A_{peak} ratio: Early diastolic to Atrial contraction peak filling rate ratio.

After adjustment for age, sex, and hypertension duration, aortic arch PWV was statistically significantly associated with LV mass index ($r = 0.37$, $p = .03$, $\beta = 2.11$). Aortic arch PWV was not statistically significantly associated with other indexes of LV diastolic, including E/A_{peak} ratio, and systolic function, including ejection fraction, after adjustment for age, sex, and

hypertension duration. Imager type was not statistically significantly associated with cardiac parameters (data not shown).

Association between aortic arch PWV and cerebral lesions

Lacunar brain infarcts were diagnosed in eight patients. Fazekas grade 2 or 3 periventricular WMHs were diagnosed in 12 patients. Fazekas grade 2 or 3 deep WMHs were diagnosed in 14 patients (Table 4).

Table 4. Association between aortic arch PWV and lacunar brain infarcts and periventricular and deep white matter hyperintensities

	<i>n</i>	<i>aortic arch PWV</i>		
		<i>OR</i>	<i>95% CI</i>	<i>p-value</i>
<i>Lacunar brain infarcts</i>		1.8	(1.2-2.5)	<0.01
No	42			
Yes	8			
<i>Periventricular WMHs</i>		1.5	(1.1-2.1)	0.01
No	38			
Yes	12			
<i>Deep WMHs</i>		1.6	(1.1-2.1)	0.01
No	36			
Yes	14			

Data are expressed as Odds ratios (OR) and 95% confidence intervals (CI) and p-values.

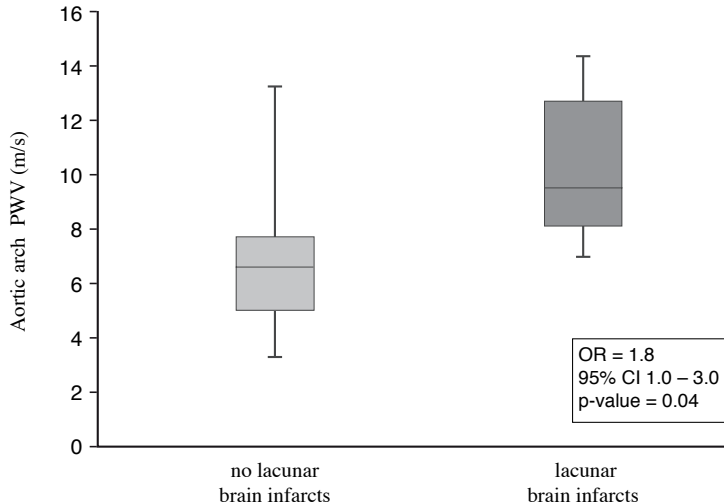
PWV: pulse wave velocity; WMHs: white matter hyperintensities

Univariable logistic regression analyses showed that aortic arch PWV was associated with lacunar brain infarcts (OR = 1.8; 95% CI: 1.2, 2.5; $p < .01$), Fazekas grade 2 or 3 periventricular WMHs (OR = 1.5; 95% CI: 1.1, 2.1; $p = .01$), and Fazekas grade 2 or 3 deep WMHs (OR = 1.6; 95% CI: 1.1, 2.1; $p = .01$) (Table 4).

After adjustment for age, sex, and hypertension duration, aortic arch PWV was statistically significantly associated with lacunar brain infarcts (OR = 1.8; 95% CI: 1.0, 3.0; $p = .04$). Aortic arch PWV was not statistically significantly associated with periventricular and deep WMHs after adjustment for age, sex, and hypertension duration. MR imager type was not statistically significantly associated with cerebral parameters (data not shown).

In Figure 2, aortic arch PWV in hypertensive patients with and those without lacunar brain infarcts is presented in a box plot that shows higher aortic arch PWV in patients with lacunar brain infarcts compared with patients without lacunar brain infarcts.

Figure 2. Box plot for aortic arch PWV in hypertensive patients with and those without lacunar brain infarcts. Median, 25th and 75th quartiles, and the range in aortic arch PWV measurements are shown. The OR, 95% CI, and p-value are given after adjustment for confounding factors of age, sex and hypertension duration.



DISCUSSION

We demonstrated that aortic arch PWV is statistically significantly associated with LV mass, as well as lacunar brain infarcts, in patients with hypertension, independently of age, sex, and hypertension duration.

We found that local stiffness of the aortic arch is related to early changes in LV mass, in the absence of overt cardiac failure. In our study most patients were adequately treated with mildly elevated systolic blood pressure, possibly explaining the mild degree of cardiac dysfunction. Our observations are in accordance with previous US studies that showed that aortic PWV is associated with LV hypertrophy (37–40). To our knowledge, only one previous study used MR imaging to demonstrate an association between decreased aortic distensibility and LV mass in 20 hypertensive patients (41).

In the current study, no associations between aortic arch stiffness and indexes of LV diastolic function (including E/A_{peak} ratio) and LV systolic function (including ejection fraction) were observed after correction for confounding factors of age, sex, and hypertension duration. Previous studies have shown that LV diastolic dysfunction occurs in hypertensive patients with increased aortic stiffness and preserved LV systolic function (42,43). In our study, LV systolic and diastolic function were still preserved, which is likely related to the less advanced stage of hypertensive heart disease. Furthermore, measurement of LV diastolic function was not obtained in nine patients, owing to technical problems. This could have affected the precision with which the association between aortic arch stiffness and LV diastolic function was determined.

Our study also reveals that aortic arch PWV in hypertensive patients is independently associated with lacunar brain infarcts, after correction for confounding factors of age, sex, and hypertension duration, whereas no significant association between aortic arch PWV and periventricular and deep WMHs is found after correction for confounding factors. These results are in line with a previous US study that assessed the relationship between brachial-ankle PWV and the risk of cerebral small vessel disease in 196 elderly patients with hypertension (44). These authors found a significant association between aortic PWV and lacunar brain infarcts but no relationship between the severity of periventricular WMHs and PWV after controlling for age (44).

The association between aortic stiffness and cerebral damage may be indirect through shared vascular risk factors or may be causative in nature (10,13,44,45). One possible mechanism is that increased aortic stiffness leads to a deficient absorption of the pulse wave and an increase in central pulse pressure, which may augment small vessel disease of the brain through high pulsatile flow (10,13,44). We hypothesize that large vessel disease of the aortic arch contributes to the occurrence of cerebral damage.

Although WMHs and lacunar brain infarcts share underlying risk factors, our results demonstrate that MR imaging-measured aortic arch PWV is not associated with WMHs after controlling for age, sex, and hypertension duration. It is plausible that aging has more effect on arteriosclerosis of the medullary arteries than on perforating arteries in hypertensive patients (44). Recent studies have suggested different pathogenic mechanisms between lacunar brain infarcts or WMHs (43,46).

Current recommendations for the care of hypertensive patients stress the importance of assessing early end-organ damage, allowing for better risk stratification with more therapeutic options and better follow-up. Increased PWV is an independent predictor of adverse cardiovascular events in various clinical settings (7,9,47,48). Of note, assessment of aortic PWV is not part of clinical routine in hypertensive patients. The results of our study suggest that aortic arch PWV could provide additional cardiovascular risk prediction beyond classical risk factors in hypertensive patients.

Our study had some limitations. First, this was a cross-sectional study, and therefore causative mechanisms cannot be determined. Outcome studies are required to assess the clinical significance of the relationship between aortic arch stiffness and LV mass and lacunar brain infarcts found in this study. Furthermore, no age-matched healthy subjects were included to serve as controls. However, the primary purpose of this study was to assess the possible relationship between aortic arch PWV and cardiac and cerebral end-organ damage in hypertensive patients.

In conclusion, aortic arch PWV is statistically significantly associated with LV mass index and lacunar brain infarcts in hypertensive patients, independent of age, sex, and hypertension duration. Further studies are required to assess the prognostic importance of these findings for risk stratification and optimization of therapy.

REFERENCES

1. Chobanian AV, Bakris GL, Black HR, et al. Seventh report of the joint national committee on prevention, detection, evaluation, and treatment of high blood pressure. *Hypertension* 2003;42(6):1206-1252.
2. Mancia G, de Backer G, Dominiczak A, et al. 2007 Guidelines for the management of arterial hypertension: The task force for the management of arterial hypertension of the European Society of Hypertension (ESH) and of the European Society of Cardiology (ESC). *J Hypertens* 2007;25(6):1105-1187.
3. Metafratzi ZM, Efremidis SC, Skopelitou AS, de Roos A. The clinical significance of aortic compliance and its assessment with magnetic resonance imaging. *J Cardiovasc Magn Reson* 2002;4(4):481-491.
4. Safar ME, Levy BI, Struijker-Boudier H. Current perspectives on arterial stiffness and pulse pressure in hypertension and cardiovascular diseases. *Circulation* 2003 10;107(22):2864-2869.
5. Isnard RN, Pannier BM, Laurent S, London GM, Diebold B, Safar ME. Pulsatile diameter and elastic modulus of the aortic arch in essential hypertension: a noninvasive study. *J Am Coll Cardiol* 1989;13(2):399-405.
6. O'Rourke MF. Mechanical principles. Arterial stiffness and wave reflection. *Pathol Biol (Paris)* 1999;47(6):623-633.
7. Laurent S, Cockcroft J, van Bortel L, et al. Expert consensus document on arterial stiffness: methodological issues and clinical applications. *Eur Heart J* 2006;27(21):2588-2605.
8. McEnery CM, Wilkinson IB, Avolio AP. Age, hypertension and arterial function. *Clin Exp Pharmacol Physiol* 2007;34(7):665-671.
9. Laurent S, Boutouyrie P, Asmar R, et al. Aortic stiffness is an independent predictor of all-cause and cardiovascular mortality in hypertensive patients. *Hypertension* 2001;37(5):1236-1241.
10. Laurent S, Katsahian S, Fassot C, et al. Aortic stiffness is an independent predictor of fatal stroke in essential hypertension. *Stroke* 2003;34(5):1203-1206.
11. Hamilton PK, Lockhart CJ, Quinn CE, McVeigh GE. Arterial stiffness: clinical relevance, measurement and treatment. *Clin Sci (Lond)* 2007;113(4):157-170.
12. Mandinov L, Eberli FR, Seiler C, Hess OM. Diastolic heart failure. *Cardiovasc Res* 2000;45(4):813-825.
13. O'Rourke MF, Safar ME. Relationship between aortic stiffening and microvascular disease in brain and kidney: cause and logic of therapy. *Hypertension* 2005;46(1):200-204.
14. Vermeer SE, Longstreth WT Jr., Koudstaal PJ. Silent brain infarcts: a systematic review. *Lancet Neurol* 2007;6(7):611-619.
15. Vermeer SE, Prins ND, den Heijer T, Hofman A, Koudstaal PJ, Breteler MM. Silent brain infarcts and the risk of dementia and cognitive decline. *N Engl J Med.* 2003;348(13):1215-1522.
16. Prins ND, van Dijk EJ, den Heijer T, et al. Cerebral white matter lesions and the risk of dementia. *Neurology* 2005;25;64(2):263-267.

17. Vermeer SE, Hollander M, van Dijk EJ, Hofman A, Koudstaal PJ, Breteler MM. Silent brain infarcts and white matter lesions increase stroke risk in the general population: the Rotterdam Scan Study. *Stroke* 2003;34(5):1126-1129.
18. Groenink M, de Roos A, Mulder BJ, Spaan JA, van der Wall EE. Changes in aortic distensibility and pulse wave velocity assessed with magnetic resonance imaging following beta-blocker therapy in the Marfan syndrome. *Am J Cardiol* 1998;82(2):203-208.
19. Stevanov M, Baruthio J, Gounot D, Grucker D. In vitro validation of MR measurements of arterial pulse-wave velocity in the presence of reflected waves. *J Magn Reson Imaging* 2001;14(2):120-127.
20. Grotenhuis HB, Ottenkamp J, Westenberg JJ, Bax JJ, Kroft LJ, de Roos A. Reduced aortic elasticity and dilatation are associated with aortic regurgitation and left ventricular hypertrophy in nonstenotic bicuspid aortic valve patients. *J Am Coll Cardiol* 2007;49(15):1660-1665.
21. Roes SD, Alizadeh DR, Westenberg JJ, et al. Assessment of aortic pulse wave velocity and cardiac diastolic function in subjects with and without the metabolic syndrome. *Diabetes Care* 2008;31(7):1442-1444.
22. Grotenhuis HB, Westenberg JJ, Steendijk P, et al. Validation and reproducibility of aortic pulse wave velocity as assessed with velocity-encoded MRI. *J Magn Reson Imaging* 2009;30(3):521-526.
23. Lamb HJ, Doornbos J, van der Velde EA, Kruit MC, Reiber JH, de Roos A. Echo planar MRI of the heart on a standard system: validation of measurements of left ventricular function and mass. *J Comput Assist Tomogr* 1996;20(6):942-949.
24. Lamb HJ, Beyerbach HP, van der Laarse, et al. Diastolic dysfunction in hypertensive heart disease is associated with altered myocardial metabolism. *Circulation* 1999 ;99(17):2261-2267.
25. Bokura H, Kobayashi S, Yamaguchi S. Distinguishing silent lacunar infarction from enlarged Virchow-Robin spaces: a magnetic resonance imaging and pathological study. *J Neurol* 1998;245(2):116-122.
26. Fazekas F. MR signal abnormalities at 1.5 T in Alzheimer's dementia and normal aging. *American Journal of Roentgenology* 1987;149(2):351-356.
27. Lee VS, Hecht EM, Taouli B, Chen Q, Prince K, Oesingmann N. Body and cardiovascular MR imaging at 3.0 T. *Radiology* 2007;244(3):692-705.
28. van der Geest RJ, de Roos A, van der Wall EE, Reiber JH. Quantitative analysis of cardiovascular MR images. *Int J Card Imaging* 1997;13(3):247-258.
29. Grothues F, Smith GC, Moon JC, et al. Comparison of interstudy reproducibility of cardiovascular magnetic resonance with two-dimensional echocardiography in normal subjects and in patients with heart failure or left ventricular hypertrophy. *Am J Cardiol* 2002;90(1):29-34.
30. Marcus JT, de Waal LK, Gotte MJ, van der Geest RJ, Heethaar RM, van Rossum AC. MRI-derived left ventricular function parameters and mass in healthy young adults: relation with gender and body size. *Int J Card Imaging* 1999;15(5):411-419.
31. Du Bois D, Du Bois EF. A formula to estimate the approximate surface area if height and weight be known. 1916. *Nutrition* 1989;5(5):303-311.
32. Paelinck BP, Lamb HJ, Bax JJ, van der Wall EE, de Roos A. Assessment of diastolic function by cardiovascular magnetic resonance. *Am Heart J* 2002;144(2):198-205.

33. Kayser HW, Stoel BC, van der Wall EE, van der Geest RJ, de Roos A. MR velocity mapping of tricuspid flow: correction for through-plane motion. *J Magn Reson Imaging* 1997;7(4):669-673.
34. Marsan NA, Westenberg JJ, Tops LF, et al. Comparison between tissue Doppler imaging and velocity-encoded magnetic resonance imaging for measurement of myocardial velocities, assessment of left ventricular dyssynchrony, and estimation of left ventricular filling pressures in patients with ischemic cardiomyopathy. *Am J Cardiol* 2008;102(10):1366-1372.
35. Paelinck BP, de Roos A, Bax JJ, et al. Feasibility of tissue magnetic resonance imaging: A pilot study in comparison with tissue Doppler imaging and invasive measurement. *J Am Coll Cardiol* 2005;45(7):1109-1116.
36. Braffman BH, Zimmerman RA, Trojanowski JQ, Gonatas NK, Hickey WF, Schlaepfer WW. Brain MR: pathologic correlation with gross and histopathology. 1. Lacunar infarction and Virchow-Robin spaces. *American Journal of Roentgenology* 1988;151(3):551-558.
37. Bouthier JD, de Luca N, Safar ME, Simon AC. Cardiac hypertrophy and arterial distensibility in essential hypertension. *Am Heart J* 1985;109(6):1345-1352.
38. Westerhof N, O'Rourke MF. Haemodynamic basis for the development of left ventricular failure in systolic hypertension and for its logical therapy. *J Hypertens* 1995;13(9):943-952.
39. Roman MJ, Ganau A, Saba PS, Pini R, Pickering TG, Devereux RB. Impact of arterial stiffening on left ventricular structure. *Hypertension* 2000;36(4):489-494.
40. Girerd X, Laurent S, Pannier B, Asmar R, Safar M. Arterial distensibility and left ventricular hypertrophy in patients with sustained essential hypertension. *Am Heart J* 1991;122(4 Pt 2):1210-1214.
41. Resnick LM, Militianu D, Cunnings AJ, Pipe JG, Evelhoch JL, Soulen RL. Direct magnetic resonance determination of aortic distensibility in essential hypertension: relation to age, abdominal visceral fat, and in situ intracellular free magnesium. *Hypertension* 1997;30(3 Pt 2):654-659.
42. Tsioufis C, Chatzis D, Dimitriadis K, et al. Left ventricular diastolic dysfunction is accompanied by increased aortic stiffness in the early stages of essential hypertension: a TDI approach. *J Hypertens* 2005;23(9):1745-1750.
43. Fernandes VR, Polak JF, Cheng S, et al. Arterial stiffness is associated with regional ventricular systolic and diastolic dysfunction: the Multi-Ethnic Study of Atherosclerosis. *Arterioscler Thromb Vasc Biol* 2008;28(1):194-201.
44. Kim DH, Kim J, Kim JM, Lee AY. Increased brachial-ankle pulse wave velocity is independently associated with risk of cerebral ischemic small vessel disease in elderly hypertensive patients. *Clin Neurol Neurosurg* 2008;110(6):599-604.
45. Altaf N, Morgan PS, Moody A, MacSweeney ST, Gladman JR, Auer DP. Brain white matter hyperintensities are associated with carotid intraplaque hemorrhage. *Radiology* 2008;248(1):202-209.
46. Hassan A, Hunt BJ, O'Sullivan M, et al. Markers of endothelial dysfunction in lacunar infarction and ischaemic leukoaraiosis. *Brain* 2003;126(Pt 2):424-432.
47. Cruickshank K, Riste L, Anderson SG, Wright JS, Dunn G, Gosling RG. Aortic pulse-wave velocity and its relationship to mortality in diabetes and glucose intolerance: an integrated index of vascular function? *Circulation* 2002;106(16):2085-2090.
48. Safar ME, London GM, Plante GE. Arterial stiffness and kidney function. *Hypertension* 2004;43(2):163-168.

Chapter 4

Aortic stiffness is associated with cardiac function and cerebral small vessel disease in patients with type 1 diabetes mellitus: assessment by MR imaging

SGC van Elderen, A Brandts, JJM Westenberg, J van der Grond, JT Tamsma, MA van Buchem, JA Romijn, LJM Kroft, JWA Smit, A de Roos

European Radiology 2010;20(5):1132-1138

ABSTRACT

Purpose

To evaluate, with the use of magnetic resonance imaging (MRI), whether aortic pulse wave velocity (PWV) is associated with cardiac left ventricular (LV) function and mass as well as with cerebral small vessel disease in patients with type 1 diabetes mellitus (DM).

Materials and Methods

We included 86 consecutive type 1 DM patients (49 male, mean age 46.9 ± 11.7 years) in a prospective, cross-sectional study. Exclusion criteria included aortic/heart disease and general MRI contra-indications. MRI of the aorta, heart and brain was performed for assessment of aortic PWV, as a marker of aortic stiffness, systolic LV function and mass, as well as for the presence of cerebral white matter hyperintensities (WMHs), microbleeds and lacunar infarcts. Multivariate linear or logistic regression was performed to analyse the association between aortic PWV and outcome parameters, with covariates defined as age, gender, mean arterial pressure, heart rate, BMI, smoking, DM duration and hypertension.

Results

Mean aortic PWV was 7.1 ± 2.5 m/s. Aortic PWV was independently associated with LV ejection fraction ($\beta = -0.406$, $p = 0.006$), LV stroke volume ($\beta = -0.407$, $p = 0.001$), LV cardiac output ($\beta = -0.458$, $p = 0.001$), and with cerebral WMHs ($p < 0.05$). There were no independent associations between aortic stiffness and LV mass, cerebral microbleeds or lacunar infarcts.

Conclusion

Aortic stiffness is independently associated with systolic LV function and cerebral WMHs in patients with type 1 DM.

INTRODUCTION

Type 1 diabetes mellitus (DM) patients show functional and structural alterations of the arterial vessel wall, resulting in arterial stiffness (1,2). Arterial stiffening has been described as an early phenomenon in subjects with type 1 DM, already apparent before clinical onset of cardiovascular (CV) complications, and also as an independent predictor of overt CV disease and mortality (3). Therefore, arterial stiffening may be related to the pathogenesis of CV complications in type 1 DM. This notion could be substantiated if an independent relationship could be established between arterial stiffness and cardiac function in type 1 DM. Furthermore, CV complications in type 1 DM also involve small vessel disease in the brain, and if a relationship between arterial stiffness and cerebral small vessel disease could be established as well, this would support the importance of arterial stiffness in CV complications in type 1 DM. An integrated study investigating the relationship between arterial stiffness, cardiac function and cerebral small vessel disease has not been performed in type 1 DM so far.

Stiffening of the aorta affects cardiac function by increasing the cardiac afterload and reducing diastolic coronary artery perfusion (4). Myocardial perfusion might fail to compensate for the increased metabolic energy demand, resulting in an impaired myocardial contractility function (5). Furthermore, stiffness of the central large arteries results in deficient absorption of the pulse wave. This high pulsatile flow is transmitted from the aorta to the brain causing damage to the endothelial and smooth muscle cells, disrupting the cerebral small vessels (6,7). Also, aortic stiffness may represent coronary and cerebral endothelial dysfunction or wall thickening caused by shared underlying mechanisms.

As aortic function plays a central role in maintaining adequate perfusion of both the heart and the brain, we hypothesized that aortic stiffness is associated with cardiac function as well as with cerebral small vessel disease in DM patients. To our knowledge, no previous magnetic resonance imaging (MRI) studies have evaluated the relationship between aortic function, cardiac function and cerebral small vessel disease in one comprehensive protocol. MRI is a non-invasive tool for the accurate assessment of aortic pulse wave velocity (PWV) (8) as a marker of aortic stiffness (9). Notably, MRI is not dependent on geometric assumptions about the aortic path length unlike ultrasound techniques (10). Furthermore, MRI is well suited to assess cardiac LV function (11). Moreover, MRI is a validated technique for the detection of cerebral small vessel disease manifesting as white matter hyperintensities (WMHs) (12), microbleeds (13) and lacunar infarcts (14).

Therefore, the purpose of the present study was to use a comprehensive MRI protocol to evaluate whether aortic PWV is associated with cardiac LV function and mass as well as with cerebral small vessel disease in patients with type 1 DM.

MATERIALS AND METHODS

Study participants

Between February 2008 and February 2009, consecutive patients with type 1 DM were recruited from our local outpatient clinic of the university medical centre. For inclusion, patients had to be older than 18 years and diagnosed with type 1 DM. A total of 86 patients (49 men, 37 women; mean age 46.9 ± 11.7 years) gave written informed consent to participate in the study and were prospectively included. Exclusion criteria included congenital aortic/heart disease, evidence of aortic or heart disease as evaluated by means of cardiac auscultation and ECG, and standard contra-indications to MRI such as claustrophobia, pacemaker and metal implantations.

Information about patient characteristics was obtained by means of a standardized interview and physical and laboratory examinations. Diabetes duration was estimated as the time passed between the reported age of diagnosis and the MRI examination. Body mass index (BMI) was calculated from body length and mass at the time of MRI. Blood pressure and heart rate were measured after MRI using a semi-automated sphygmomanometer (Dinamap, Critikon, Tampa, FL, USA, validated to ANSI/AAMI SP10 criteria). Pulse pressure was defined as the difference between systolic and diastolic blood pressure. Mean arterial pressure (MAP) was calculated by adding diastolic blood pressure to one-third of the pulse pressure. Smoking was defined as non-smoker or a current smoker. Hypertension was defined as the use of anti-hypertensive medication. Glycated hemoglobin (HbA1c), high-density lipoprotein (HDL), low-density lipoprotein (LDL), total cholesterol, triglycerides and C-reactive protein were determined. The albumin excretion ratio was calculated using the microalbumin and creatinine concentrations in the urine.

The study was approved by the local medical ethics committee, and the study was conducted according to the principles in the Declaration of Helsinki.

MR imaging protocol

Aortic and cardiac imaging was performed using 1.5 Tesla MRI (NT 15 Gyroscan Intera; Philips Medical Systems, Best, the Netherlands). All brain examinations were performed on 3.0 Tesla MRI (Achieva; Philips Medical Systems, Best, the Netherlands).

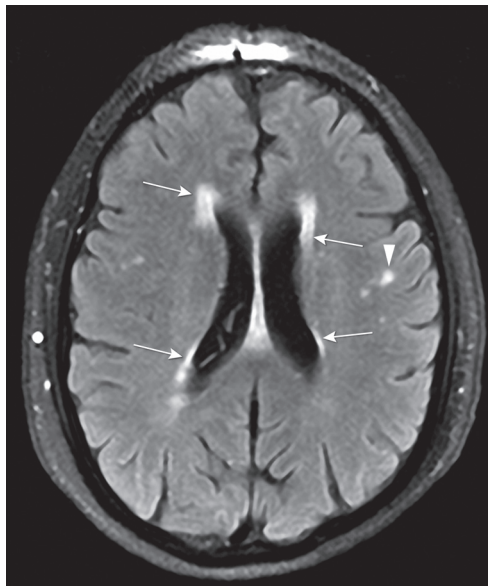
For the evaluation of aortic stiffness, aortic PWV was determined using a previously described protocol (15). In short, a scout view of the aorta was performed. Two velocity-encoded images were obtained: one perpendicular to the aorta at the level of the pulmonary trunk, and one at the level of the abdominal descending aorta 7.5 cm beneath the diaphragm. This resulted in through-plane flow measurements of the ascending and descending aorta at those levels. Aortic PWV was calculated for the aorta as $\Delta x/\Delta t$, where Δx is the aortic path length between the two measurement sites and Δt is the time delay between the arrivals of the foot of the pulse wave at the respective measurement sites. Data were analyzed with

MASS/FLOW (Medis, Leiden, the Netherlands) by a single observer (S.v.E., 2 years of experience in cardiac MRI) supervised by a senior researcher (J.W., 13 years of experience in cardiac MRI).

For the assessment of systolic LV function and LV mass, the entire heart was imaged in short-axis orientation as described previously (11). Endocardial and epicardial LV borders were manually traced on short-axis cine images using the software package MASS. Ejection fraction (EF), stroke volume (SV), cardiac output (CO), LV end-diastolic volume (LV ED volume), LV end-systolic volume (LV ES volume) and LV end-diastolic mass (LV ED mass) were assessed. Volumes and mass were indexed (i) for body surface area (BSA). All manual contour drawings were performed by a researcher (S.v.E., 2 years of experience in cardiac MRI), with supervision of a radiologist (L.K., 12 years of experience in cardiac MRI).

For evaluation of cerebral small vessel disease a spin-echo T2-weighted image, a fluid-attenuated inversion recovery (FLAIR) image and a T2*-weighted gradient echo sequence were assessed. WMHs were defined as areas of brain parenchyma with increased signal on T2-weighted and FLAIR images without mass effect. WMHs were distinguished as either periventricular (pv) WMHs or subcortical (sc) WMHs because of the different pathogenesis involved (16). WMHs were classified according to Fazekas et al. (16). For statistical analysis subjects were divided into those with normal [0] versus abnormal [1] amounts of pv and sc WMHs. Figure 1 demonstrates a case example with presence of pv and sc WMHs on a FLAIR

Figure 1. A 66-year-old male patient with type 1 diabetes mellitus with abnormal white matter hyperintensities (WMHs) on a FLAIR sequence and high aortic pulse wave velocity of 8.9 m/s. The four arrows point to periventricular WMHs, the arrowhead indicates an example of a subcortical WMH.



sequence. Microbleeds were defined as focal, nodular areas of signal loss in brain parenchyma on T2* images that are invisible or smaller on T2-weighted spin echo images (17). Microbleeds were scored as absent [0] or present [1]. Lacunar brain infarcts were defined as small (but >3 mm in size) cavities within the brain parenchyma, with similar signal intensity to that of cerebrospinal fluid on all pulse sequences, surrounded by an area of high signal intensity on T2 and FLAIR images (18,19). Their presence was defined on a binary scale: absent [0] or present [1]. WMHs, microbleeds and lacunar infarcts were visually scored by consensus reading by a researcher (S.v.E., 1 year of experience in neuroradiology) and a senior neuroscientist (J.v.d.G., 15 years of experience in neuroradiology) or a neuroradiologist (M.v.B., 15 years of experience in neuroradiology).

Statistical analysis

Statistical analysis was performed using SPSS for Windows (version 16.0; SPSS, Chicago, Illinois, USA). Data are expressed as mean \pm standard deviation, unless stated otherwise. Aortic PWV values were non-normally distributed (Kolmogorov-Smirnov test of normality, $p=0.002$). Spearman correlation analysis was performed to analyse the association between aortic PWV and continuous outcome parameters. Spearman correlation coefficients (r) and p values are reported. Univariate logistic regression was performed to analyse the association between aortic PWV and dichotomous outcome parameters. Odds ratios (OR), 95% confidence intervals (CI) and p values were reported. For adjustment of confounding factors, defined as age, gender, MAP, heart rate, BMI, smoking, DM duration and hypertension these covariates were entered into a multivariate linear or logistic regression model. Associations between cardiac parameters indexed for BSA were not corrected for BMI.

RESULTS

The characteristics of the study population are described in Table 1. All MRI examinations were successfully performed without any adverse events. Eighty-six patients with type 1 DM were included, with a mean age of 46.9 ± 11.7 years. The mean HbA1c values were 7.7 ± 1.0 %.

Mean aortic PWV was 7.11 ± 2.51 m/s. Aortic PWV was significantly associated with age ($r=0.674$, $p<0.001$), DM duration ($r=0.299$, $p=0.006$), BMI ($r=0.317$, $p=0.003$), systolic blood pressure ($r=0.484$, $p<0.001$), pulse pressure ($r=0.509$, $p<0.001$), MAP ($r=0.339$, $p=0.001$) and use of antihypertensive medication (OR=1.278, $p=0.017$). There were no statistically significant associations between aortic PWV and laboratory markers (Table 1).

Table 1. Patient characteristics

	Patients (n=86)	Association with aortic PWV
<i>Characteristics</i>		
Male gender, n (%)	49 (57)	p=0.586
Age (years)	46.9 ± 11.7	r=0.674, p<0.001*
Diabetes duration (years)	23.8 ± 11.0	r=0.299, p=0.006*
BMI (kg/m ²)	25.7 ± 3.4	r=0.317, p=0.003*
Systolic blood pressure (mmHg)	132 ± 18	r=0.484, p<0.001*
Diastolic blood pressure (mmHg)	74 ± 9	p=0.164
Pulse pressure (mmHg)	58 ± 16	r=0.509, p<0.001*
Mean arterial pressure (mmHg)	93 ± 11	r=0.339, p=0.001*
Heart rate (beats/min)	71 ± 10	p=0.286
Current smokers, n (%)	10 (12)	p=0.867
Use of antihypertensive medication, n (%)	31 (36)	OR=1.278, p=0.017*
<i>Laboratory markers</i>		
HbA1c (%)	7.7 ± 1.0	p=0.597
HDL cholesterol (mmol/l)	1.6 ± 0.5	p=0.905
LDL cholesterol (mmol/l)	2.8 ± 0.9	p=0.154
Total cholesterol (mmol/l)	4.7 ± 1.0	p=0.050
Triglycerides (mmol/l)	1.2 ± 0.8	p=0.193
C-reactive protein (mg/l)	2.1 ± 2.1	p=0.549
Microalbumin/creatinine ratio (µg/µmol)	1.2 ± 2.5	p=0.145

Data are presented as mean ± standard deviation or n (%). Spearman rho (r) and p-values are presented.

*p-value < 0.05, PWV: Pulse wave velocity; BMI: body mass index; HbA1c: glycated hemoglobin; HDL: high-density lipoprotein; LDL: low-density lipoprotein

Associations between aortic PWV and cardiac LV function and mass

The mean values of cardiac LV parameters and the associations with aortic PWV are summarised in Table 2. After statistical correction for confounder's age, gender, MAP, heart rate, BMI, smoking, DM duration and hypertension, aortic PWV was found to be significantly associated with systolic LV parameters: LV EF ($\beta=-0.402$, $p=0.006$), LV SVi ($\beta=-0.407$, $p=0.001$) and LV COi ($\beta=-0.458$, $p=0.001$). The inverse association between aortic PWV and LV SVi is illustrated in Figure 2. There was no statistically significant association between aortic PWV and LV mass.

Associations between aortic PWV and cerebral small vessel disease

According to their Fazekas score, 16 (18.6%) patients showed pv WMHs and 38 (44.2%) patients were diagnosed with sc WMHs. In 7 (8.1%) DM patients, microbleeds were detected. Two patients (2.3%) showed lacunar infarcts on brain MRI. The associations between aortic PWV and parameters of cerebral small vessel disease are summarized in Table 2. Univariate logistic regression analysis showed that aortic PWV was significantly associated with all MRI parameters of cerebral small vessel disease.

Table 2. Aortic PWV and the associations with MRI parameters

Cardiac MRI parameters	mean \pm sd	Univariate analysis		Multivariate analysis	
		r	p-value	β	p-value
Aortic PWV (m/s)	7.11 \pm 2.51				
LV EF (%)	59.7 \pm 6.1		0.201	-0.409	0.006*
LV SV (i) (ml/m ²)	46.7 \pm 8.1	-0.376	<0.001*	-0.407	0.001*
LV CO (i) (ml/m ²)	3100 \pm 542	-0.416	<0.001*	-0.457	0.001*
LV ED volume (i) (ml/m ²)	78.4 \pm 12.7	-0.310	0.004*		0.066
LV ES volume (i) (ml/m ²)	31.6 \pm 7.8		0.327		0.349
LV ED mass (i) (g/m ²)	47.4 \pm 9.7		0.848		0.666
<i>Brain MRI parameters</i>	<i>n (%)</i>	<i>OR</i>	<i>p-value</i>	<i>OR</i>	<i>p-value</i>
Periventricular WMHs	16 (18.6)	1.452	0.002*	1.426	0.048*
Subcortical WMHs	38 (44.2)	1.408	0.004*	1.479	0.020*
Microbleeds	7 (8.1)	1.301	0.042*		0.976
Lacunar infarct	2 (2.3)	1.492	0.036*		0.997

Data are presented as mean \pm standard deviations or n (%). Spearman's rho (r), standardised β values, odds ratios (OR) and p-values are reported for the association with aortic PWV, in univariate analysis or multivariate analysis with the covariates age, gender, MAP, heart rate, BMI, smoking, DM duration and hypertension. *p-value<0.05 PWV: Pulse wave velocity; MRI: magnetic resonance imaging; LV: left ventricular; EF: ejection fraction; SV: stroke volume; CO: cardiac output; ED: end-diastolic; ES: end-systolic; i: indexed for body surface area; WMHs: white matter hyperintensities

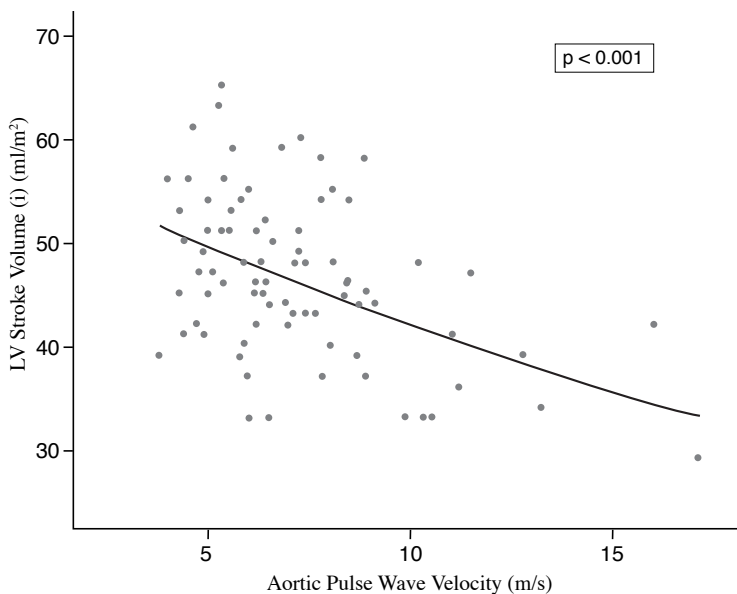
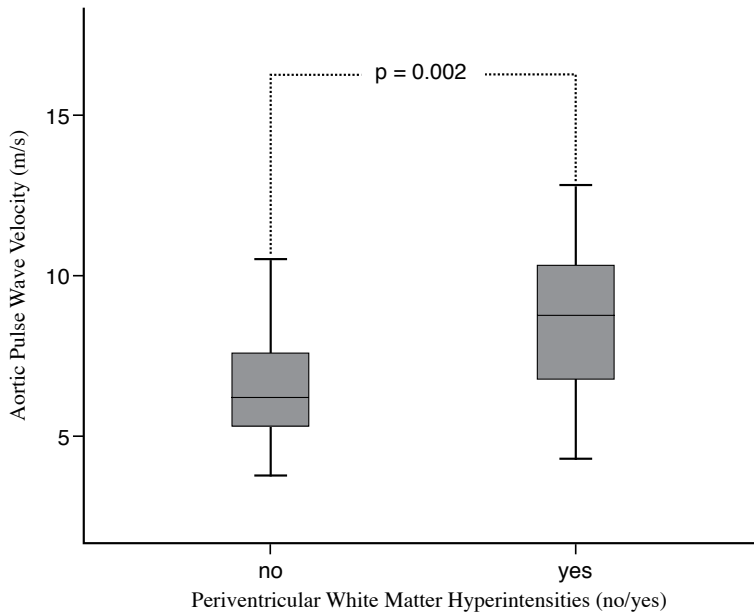
Figure 2. There is an inverse relation between aortic pulse wave velocity and systolic left ventricular (LV) function in patients with type 1 diabetes mellitus (n=86)

Figure 3. These boxplots show that type 1 diabetes mellitus patients with periventricular white matter hyperintensities in the brain have higher aortic pulse wave velocity values compared with those without periventricular white matter hyperintensities



After statistical adjustment for confounding factors, aortic PWV was significantly associated with pv WMHs (OR=1.425, 95% CI=1.003–2.026, $p<0.05$) and sc WMHs (OR=1.479, 95% CI=1.063–2.058, $p=0.02$). In Figure 3, aortic PWV in patients with type 1 DM with and without pv WMHs is presented in boxplots showing higher aortic PWV in patients with pv WMHs compared with patients without pv WMHs.

DISCUSSION

The purpose of the present study was to evaluate whether aortic PWV is associated with cardiac LV function and mass as well as with cerebral small vessel disease in patients with type 1 DM using a comprehensive MRI protocol.

The main findings of our study are that aortic stiffness in patients with type 1 DM is inversely associated with systolic LV function and is associated with cerebral WMHs, independently of age, gender, MAP, heart rate, BMI, smoking, DM duration and hypertension. No independent association between aortic stiffness and LV mass, cerebral microbleeds or lacunar infarcts was found.

This study is the first to report an integrated approach for detecting the relationship among arterial stiffness, cardiac function and cerebral small vessel disease. Indeed, in this cohort of

relatively young type 1 DM patients, aortic stiffness was found to be inversely associated with systolic LV function and with WMHs. Patients with type 1 DM are at increased risk of developing systolic LV dysfunction, with subsequent progressive heart failure and premature death (20). In addition, it is known that WMHs may progress and become manifest over time (21,22) but also that individuals with WMHs benefit from secondary stroke prevention therapies (23). We hypothesized that PWV as measured in the aorta by MRI may be a marker or risk factor for generalized vascular disease that might potentially be treated. Interestingly, this association between PWV and MRI manifestations of cardiac function and cerebral small vessel disease was independent of many major risk factors such as age and hypertension, suggesting that aortic stiffness might have an independent pathophysiological mechanism.

The present MRI data show that in type 1 DM patients aortic stiffness was inversely related to systolic LV function. To our knowledge, this is the first study to report a relationship between systolic LV function and aortic stiffness in a type 1 DM population. In our study population, the LV ejection fraction was in the normal range (24), which might emphasize an important role of aortic stiffness in cardiac function already manifesting before occurrence of cardiac dysfunction or failure and compensatory remodeling. High blood pressure is strongly associated with LV hypertrophy (25). However, in type 1 DM patients the presence of LV hypertrophy is not a well-known phenomenon (26,27). Therefore it is more likely that in patients with hypertension increased aortic stiffness is associated with LV hypertrophy (28,29). Our study on type 1 DM patients is in line with these findings; no relationship between aortic PWV and LV mass was found in a relatively young type 1 DM population with well-treated hypertension. Furthermore, a statistical correction for hypertension was performed.

In the present study, aortic PWV was independently associated with pv and sc WMHs. Although increased arterial stiffness in DM was related to microvascular complications of the kidneys and the retina in a previous study (3), the current study is the first to report on the potential relation between aortic stiffness and small vessel disease in the brain in patients with type 1 DM. Interestingly, this relationship between aortic stiffness and WMHs was independent of hypertension, a finding that has been reported recently (30), and independent of age as described before (31), suggesting an independent pathophysiological mechanism for aortic stiffness and WMHs in patients with type 1 DM.

No independent relationship was found between aortic stiffness and microbleeds. It is plausible that instead of a haemodynamic effect, other mechanisms including altered gluco-regulation and microvascular changes by advanced glycation end products are involved in the development of microbleeds in DM patients (32,33). The low prevalence of lacunar infarcts (n=2) in our study population may have hampered the statistical analyses.

In addition to arterial stiffness being a predictor of (fatal) myocardial infarction and stroke (3), our study results show that aortic stiffness is associated with reduced cardiac function and cerebral small vessel disease as shown by MRI. Of note, assessment of aortic PWV is currently not part of the clinical routine assessment in DM patients. Our study results suggest

that aortic PWV could be useful in the cardiovascular risk screening of patients with type 1 DM, if longitudinal studies confirm our initial observations and establish their prognostic implications in patients with type 1 DM.

As the study design is cross-sectional, a causal relationship between aortic PWV and systolic LV function or WMHs cannot be determined. However, the present study reveals that aortic stiffness reflects both cardiac function and cerebral small vessel disease. In our study design, we chose to measure aortic PWV with some distance of the aortic bifurcation to avoid wave reflections from the aortic bifurcation, which can corrupt the observer-independent automatic assessment of the PWV (34). However, more refined analysis of thoracic and abdominal aortic segments may allow local identification of aortic vessel wall condition, and its relationship with cardiac function and cerebral small vessel disease. A possible limitation of this study is the lack of a healthy control group. However, the main purpose of this study was to investigate the possible relationship between aortic PWV and cardiac function and mass as well as cerebral small vessel disease in type 1 DM patients.

In conclusion, this study shows that in patients with type 1 DM stiffness of the aorta is independently associated with systolic LV function as well as with cerebral WMHs. By documenting that aortic stiffness reflects stages of both cardiac function and cerebral small vessel disease, our study results suggest that aortic PWV assessment might be a useful marker of cardiac and cerebrovascular disease in patients with type 1 DM. Future studies are needed to assess the prognostic implications of our observations.

REFERENCES

1. Giannattasio C, Failla M, Piperno A, et al. Early impairment of large artery structure and function in type I diabetes mellitus. *Diabetologia* 1999;42(8):987-994.
2. Oxlund H, Rasmussen LM, Andreassen TT, Heickendorff L. Increased aortic stiffness in patients with type 1 (insulin-dependent) diabetes mellitus. *Diabetologia* 1989;32(10):748-752.
3. Schram MT, Chaturvedi N, Fuller JH, Stehouwer CD. Pulse pressure is associated with age and cardiovascular disease in type 1 diabetes: the Eurodiab Prospective Complications Study. *J Hypertens* 2003;21(11):2035-2044.
4. Leite-Moreira AF, Correia-Pinto J, Gillebert TC. Afterload induced changes in myocardial relaxation: a mechanism for diastolic dysfunction. *Cardiovasc Res* 1999;43(2):344-353.
5. Brooks B, Molyneaux L, Yue DK. Augmentation of central arterial pressure in type 1 diabetes. *Diabetes Care* 1999;22(10):1722-1727.
6. Byrom FB, Dodson LF. The causation of acute arterial necrosis in hypertensive disease. *Journal of Pathology and Bacteriology* 1948;60(3):357-368.
7. O'Rourke MF, Safar ME. Relationship between aortic stiffening and microvascular disease in brain and kidney: cause and logic of therapy. *Hypertension* 2005;46(1):200-204.
8. Grotenhuis HB, Westenberg JJ, Steendijk P, et al. Validation and reproducibility of aortic pulse wave velocity as assessed with velocity-encoded MRI. *J Magn Reson Imaging* 2009;30(3):521-526.
9. O'Rourke MF. Arterial aging: pathophysiological principles. *Vasc Med* 2007;12(4):329-341.
10. Laurent S, Cockcroft J, van Bortel L, et al. Expert consensus document on arterial stiffness: methodological issues and clinical applications. *Eur Heart J* 2006;27(21):2588-2605.
11. Lamb HJ, Doornbos J, van der Velde EA, Kruit MC, Reiber JH, de Roos A. Echo planar MRI of the heart on a standard system: validation of measurements of left ventricular function and mass. *J Comput Assist Tomogr* 1996;20(6):942-949.
12. Fazekas F, Kleinert R, Offenbacher H, et al. Pathologic correlates of incidental MRI white matter signal hyperintensities. *Neurology* 1993;43(9):1683-1689.
13. Cordonnier C, Al-Shahi SR, Wardlaw J. Spontaneous brain microbleeds: systematic review, subgroup analyses and standards for study design and reporting. *Brain* 2007;130(Pt 8):1988-2003.
14. Lastilla M. Lacunar infarct. *Clin Exp Hypertens* 2006;28(3-4):205-215.
15. van der Meer RW, Diamant M, Westenberg JJ, et al. Magnetic resonance assessment of aortic pulse wave velocity, aortic distensibility, and cardiac function in uncomplicated type 2 diabetes mellitus. *J Cardiovasc Magn Reson* 2007;9(4):645-651.
16. Fazekas F, Schmidt R, Scheltens P. Pathophysiologic mechanisms in the development of age-related white matter changes of the brain. *Dement Geriatr Cogn Disord* 1998;9 Suppl 1:2-5.
17. Greenberg SM, Vernooij MW, Cordonnier C, et al. Cerebral microbleeds: a guide to detection and interpretation. *Lancet Neurol* 2009;8(2):165-174.
18. Fazekas F, Chawluk JB, Alavi A, Hurtig HI, Zimmerman RA. MR signal abnormalities at 1.5 T in Alzheimer's dementia and normal aging. *AJR Am J Roentgenol* 1987;149(2):351-356.

19. Vermeer SE, Longstreth WT Jr., Koudstaal PJ. Silent brain infarcts: a systematic review. *Lancet Neurol* 2007;6(7):611-619.
20. Bell DS. Heart failure: the frequent, forgotten, and often fatal complication of diabetes. *Diabetes Care* 2003;26(8):2433-2441.
21. Prins ND, van Dijk EJ, den HT, et al. Cerebral white matter lesions and the risk of dementia. *Arch Neurol* 2004;61(10):1531-1534.
22. van Dijk EJ, Prins ND, Vrooman HA, Hofman A, Koudstaal PJ, Breteler MM. Progression of cerebral small vessel disease in relation to risk factors and cognitive consequences: Rotterdam Scan study. *Stroke* 2008;39(10):2712-2719.
23. Ovbiagele B, Saver JL. Cerebral white matter hyperintensities on MRI: Current concepts and therapeutic implications. *Cerebrovasc Dis* 2006;22(2-3):83-90.
24. Maceira AM, Prasad SK, Khan M, Pennell DJ. Normalized left ventricular systolic and diastolic function by steady state free precession cardiovascular magnetic resonance. *J Cardiovasc Magn Reson* 2006;8(3):417-426.
25. Chinali M, Devereux RB, Howard BV, et al. Comparison of cardiac structure and function in American Indians with and without the metabolic syndrome (the Strong Heart Study). *Am J Cardiol* 2004;93(1):40-44.
26. Di Cori A, Di Bello V, Miccoli R, et al. Left ventricular function in normotensive young adults with well-controlled type 1 diabetes mellitus. *Am J Cardiol* 2007;99(1):84-90.
27. Palmieri V, Capaldo B, Russo C, et al. Uncomplicated type 1 diabetes and preclinical left ventricular myocardial dysfunction: insights from echocardiography and exercise cardiac performance evaluation. *Diabetes Res Clin Pract* 2008;79(2):262-268.
28. Resnick LM, Militianu D, Cunnings AJ, Pipe JG, Evelhoch JL, Soulen RL. Direct magnetic resonance determination of aortic distensibility in essential hypertension: relation to age, abdominal visceral fat, and in situ intracellular free magnesium. *Hypertension* 1997;30(3 Pt 2):654-659.
29. Roman MJ, Ganau A, Saba PS, Pini R, Pickering TG, Devereux RB. Impact of arterial stiffening on left ventricular structure. *Hypertension* 2000;36(4):489-494.
30. Henskens LH, Kroon AA, van Oostenbrugge RJ, et al. Increased aortic pulse wave velocity is associated with silent cerebral small-vessel disease in hypertensive patients. *Hypertension* 2008;52(6):1120-1126.
31. Ohmine T, Miwa Y, Yao H, et al. Association between arterial stiffness and cerebral white matter lesions in community-dwelling elderly subjects. *Hypertens Res* 2008;31(1):75-81.
32. Craft S, Watson GS. Insulin and neurodegenerative disease: shared and specific mechanisms. *Lancet Neurol* 2004;3(3):169-178.
33. Qiu C, Cotch MF, Sigurdsson S, et al. Retinal and cerebral microvascular signs and diabetes: the age, gene/environment susceptibility-Reykjavik study. *Diabetes* 2008;57(6):1645-1650.
34. Stevanov M, Baruthio J, Gounot D, Grucker D. In vitro validation of MR measurements of arterial pulse-wave velocity in the presence of reflected waves. *J Magn Reson Imaging* 2001;14(2):120-127.

Chapter 5

Increased aortic stiffness measured by MR imaging in type 1 diabetes mellitus patients and the relationship with renal function

SGC van Elderen, JJM Westenberg, A Brandts, RW van der Meer,
JA Romijn, JWA Smit, A de Roos

American Journal of Roentgenology, accepted 2010

ABSTRACT

Purpose

Arterial stiffness is an important predictor of cardiovascular disease in type 1 diabetes mellitus (DM). The study purpose was 1. to investigate whether type 1 DM is associated with increased aortic stiffness measured by magnetic resonance imaging (MRI), independent of renal dysfunction; 2. to evaluate the relationship between aortic stiffness and renal function within the normal range in type 1 DM.

Materials and Methods

We included 77 type 1 DM patients (mean age 46 ± 12 years) and 36 healthy controls matched for age and renal function, in a cross-sectional study. Exclusion criteria consisted of microalbuminuria, renal impairment, aortic valve disease and standard MRI contra-indications. Aortic pulse wave velocity (PWV), a marker of aortic stiffness, was assessed by MRI. Renal function was expressed as estimated glomerular filtration rate (eGFR). Mann-Whitney U-test and Spearman correlation analysis were performed. Stepwise multivariable logarithmic regressions with forward entry analysis for eGFR were performed to study the relation with aortic PWV using interaction terms for type 1 DM.

Results

Type 1 DM patients without microalbuminuria or renal impairment show increased aortic PWV compared to controls ($p < 0.05$). There was a statistically significant correlation between eGFR and aortic PWV in type 1 DM patients ($p < 0.001$, $r = -.427$) and controls ($p = 0.002$, $r = -.502$) with aortic PWV being increased in type 1 DM patients for each given eGFR within normal range ($p < 0.001$). The decrease in eGFR per increase in aortic PWV was similar for type 1 DM patients and controls ($p = ns$).

Conclusion

Our data show that aortic stiffness, measured by MRI, is increased and inversely related to renal function in type 1 DM patients with normoalbuminuria and normal eGFR.

INTRODUCTION

Type 1 diabetes mellitus (DM) leads to functional and structural arterial vessel wall alterations, resulting in stiffening of the arterial system (1,2). In turn, increased arterial wall stiffness is an important predictor of cardiovascular disease in type 1 DM (3). A close relationship has been established between indices of arterial stiffening and progressive microvascular damage in the kidneys leading to renal failure (4). The mechanism of this relationship is complex, as a decrease in aortic wall elasticity may contribute to renal dysfunction by transmission of high pulsatile flow to the kidneys, but vice versa renal dysfunction may also contribute to increased aortic stiffness (5). Most of the studies reporting on arterial stiffness and the kidneys have been conducted in patients with chronic kidney disease (6), and similar findings have been noted in DM patients with microalbuminuria (7). However, whether type 1 DM per se is associated with increased aortic stiffness, independent of renal dysfunction has not been studied in detail before. Therefore, we selected type 1 DM patients with normal renal function to avoid the possible confounding effect of renal dysfunction that may aggravate reduction in vascular elasticity. On the other hand, diabetic nephropathy is one of the major complications of type 1 DM (8) and a gradual progressive process of aortic stiffening, renal damage and their interaction can be assumed in the chronic type 1 DM disease, appearing before onset of clinically detectable renal damage. This notion could be substantiated if an independent relationship can be established between aortic stiffness and renal function within the normal range in type 1 DM.

Velocity-encoded magnetic resonance imaging (MRI) is well-suited to assess aortic stiffness independent of geometric assumptions unlike other methods frequently used in clinical studies like tonometry and ultrasound (9). Furthermore, MRI-based pulse wave velocity measurements have been well-validated in comparison to invasive pressure recordings (10).

Accordingly, the purpose of the present study was twofold: 1. to investigate whether type 1 DM per se is associated with increased aortic stiffness measured by MRI, independent of renal dysfunction; 2. to evaluate the relationship between aortic stiffness and renal function within the normal range in type 1 DM patients.

MATERIALS AND METHODS

Study participants

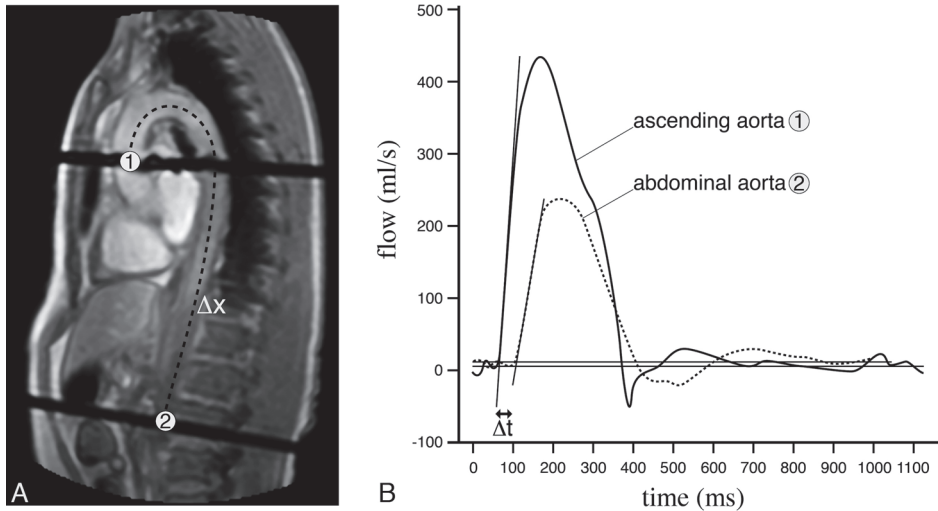
Between February 2008 and July 2009, 77 consecutive adult type 1 DM patients (mean duration of type 1 DM 24.3 ± 11.2 years) from our local outpatient clinic of the university medical centre participated in our study. Between March 2009 and September 2009 36 healthy controls (no history or clinical evidence of DM, hypertension and cardiovascular disease) similar in age and renal function were included. A retrospective subgroup analysis of a previous prospectively acquired population was performed. The type 1 DM patients included

for this study partly overlap with participants of a study described before (sixty-nine type 1 DM patients overlap with the formerly published study, and 8 type 1 DM patients were newly recruited because of the ongoing study design) (11). All type 1 DM patients were on insulin treatment. Study subjects were included if they had preserved renal function defined as estimated glomerular filtration rate (eGFR) ≥ 60 ml/min/1.73m² (12) and the presence of normoalbuminuria (i.e. <30 mg/24h microalbuminuria or microalbuminuria/creatinine ratio < 2.5 mg/mmol for men or <3.5 mg/mmol for women). Renal function was calculated with the Modification of Diet in Renal Diseases (MDRD) equation providing accurate GFR estimates using serum creatinine (13). Exclusion criteria included aortic valve stenosis or insufficiency and standard MRI contra-indications.

Blood pressure was measured after MRI using a semi-automated sphygmomanometer. Hypertension was diagnosed after repeated blood pressure measurements according to guidelines of the European Society of Hypertension (14). The study was approved by the local medical ethics committee, and conducted according to the principles in the Declaration of Helsinki. All study participants signed informed consent.

MR imaging evaluation of aortic stiffness

For the evaluation of aortic stiffness all participants underwent MRI scanning on a 1.5 Tesla whole-body MR scanner (Philips Medical Systems, Best, the Netherlands) using a five-element phased-array cardiac coil for data acquisition. Aortic pulse wave velocity (PWV, i.e. the propagation speed of systolic wave front through the aorta) was assessed with a validated technique (10) as previously described in detail (15). First, coronal and oblique sagittal scout views of the aorta were obtained. In these scout scans, two imaging planes; one perpendicular to the ascending aorta at the level of the pulmonary trunk and one perpendicular to the abdominal descending aorta 7.5 cm beneath the diaphragm were determined (Figure 1A). At those levels retrospectively electrocardiographically gated gradient-echo sequences with maximum velocity encoding were subsequently obtained during free breathing to assess the flow in the ascending and abdominal descending aorta. A maximal number of phases was reconstructed to ensure high (6–10 msec) temporal resolution. Maximum velocity encoding was set to 150 cm/sec in the ascending aorta and 100 cm/sec in the abdominal descending aorta. Aortic PWV was defined as the aortic path length (Δx) divided by the transit time (Δt) of the systolic wave front between the respective measurement sites. Δx is the distance between the ascending and abdominal descending aorta, measured along the centerline in the oblique sagittal aortic scout view. Δt is the time delay between arrival of the foot of the pulse wave at the ascending, respectively abdominal descending aorta (Figure 1B). Manual contour drawing in the aorta velocity maps was performed by a single observer (S.v.E., 3 years of experience in cardiac MRI) supervised by a senior researcher (J.W., 14 years of experience in cardiac MRI) using in-house developed software packages MASS and FLOW (Leiden University Medical Center, Leiden, The Netherlands).

Figure 1. Assessment of aortic pulse wave velocity

In Panel A, an oblique sagittal scout view of the aorta is shown. An oblique transverse pre-saturation slab in the ascending aorta and another pre-saturation slab perpendicular to the abdominal aorta result in black lines in the image. Velocity mapping was subsequently obtained at the same level of these lines in order to assess the flow graphs in the ascending and abdominal aorta. The aortic path length (Δx) between both levels was measured, indicated by the dashed line following the centerline of the aorta.

In Panel B, the flow curves in the ascending and abdominal aorta are illustrated. The horizontal lines represent the mean constant diastolic flow at the corresponding site in the aorta. The line following the upstroke is determined by linear regression between 20% and 80% of the range between diastolic flow and peak systolic flow. Time point of intersection between the upstroke and the baseline of the flow curve was considered being the arrival time of the pulse wave. The transit time (Δt) between arrival of the pulse wave at the ascending and respectively abdominal aorta was used to calculate aortic PWV, defined as the aortic path length (Δx) divided by (Δt).

Statistical analysis

Data are expressed as mean \pm standard deviation. Only aortic PWV values, because of non-normal distribution, were expressed as median (interquartile range). To compare clinical characteristics between type 1 DM and healthy controls independent samples t-test for continuous variables and Chi-Square test for dichotomous variables were used. Mann-Whitney U test was used to test aortic PWV values between type 1 DM and healthy subjects. The correlation between eGFR and aortic PWV was tested by the Spearman correlation analysis separate for type 1 DM and healthy controls. Stepwise multivariable logarithmic regressions with forward entry analysis for eGFR were performed to study the relation with aortic PWV using interaction terms for the presence of type 1 DM. To investigate the possible confounding effect of age, hypertension (14), heart rate, body mass index (BMI), smoking, DM duration and HbA1c multivariable logarithmic regression analysis was performed for the association between aortic PWV and eGFR in type 1 DM, using eGFR values uncorrected for age. P value < 0.05 was considered statistically significant. We used SPSS for Windows (version 16.0; SPSS, Chicago, Illinois, USA) for statistical analysis.

RESULTS

In all enrolled subjects, MRI scanning was completed and PWV was successfully obtained and interpreted. The clinical characteristics of the study population are shown in Table 1. There were no differences between type 1 DM patients and healthy controls with respect to renal function, age, gender, BMI, systolic blood pressure, smoking and HDL-cholesterol.

Type 1 DM patients showed significantly increased aortic PWV ($p < 0.05$), lower diastolic blood pressure ($p = 0.026$), a higher pulse pressure ($p < 0.001$), increased HbA1c ($p < 0.001$) and lower total cholesterol levels ($p = 0.010$) compared to healthy controls.

Table 1. Clinical characteristics and MRI results of the study population

Parameter	Diabetes mellitus (n=77)	Healthy controls (n=36)	p-value
<i>Clinical characteristics</i>			
Male gender, n (%)	39 (51)	23 (64)	0.2
Age (years)	46 ± 12	46 ± 16	0.9
DM duration (years)	24.3 ± 11.2	-	na
Body mass index (kg/m ²)	25.2 ± 3.2	25.7 ± 3.9	0.5
Systolic blood pressure (mmHg)	130 ± 17	124 ± 18	0.1
Diastolic blood pressure (mmHg)	73 ± 9	78 ± 11	0.026
Pulse pressure (mmHg)	57 ± 13	46 ± 15	<0.001
Current smoker, n (%)	10 (13)	4 (11)	0.7
HbA1c (%)	7.6 ± 1.0	5.0 ± 0.3 (n=10)	<0.001
Fasting plasma glucose (mmol/l)	-	4.9 ± 0.6	na
Total cholesterol (mmol/l)	4.7 ± 1.0	5.2 ± 1.0	0.010
HDL cholesterol (mmol/l)	1.6 ± 0.4	1.6 ± 0.4	0.7
Use of statin, n (%)	26 (34)	0 (0)	na
Use of antihypertensive drug, n (%)	23 (30)	0 (0)	na
<i>Renal function</i>			
Estimated GFR (ml/min/1.73m ²)	94 ± 16	89 ± 13	0.1
<i>Aortic stiffness</i>			
Aortic pulse wave velocity (m/s)	6.2 (5.4-7.8)	5.8 (4.4-7.1)	<0.05

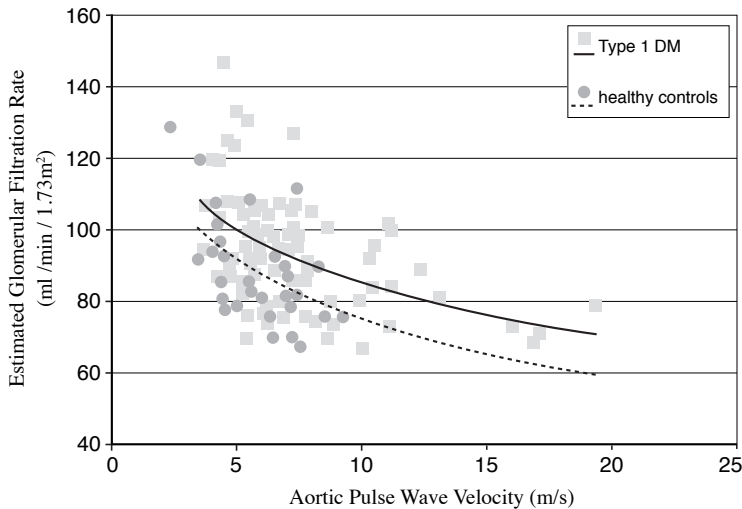
Data are means ± SD, number (%) or median (interquartile range). DM: diabetes mellitus; GFR: glomerular filtration rate; HbA1c: glycosylated haemoglobin; HDL: high density lipoprotein

Aortic pulse wave velocity and renal function

There was a statistically significant correlation between eGFR and aortic PWV in both type 1 DM patients ($p < 0.001$, $r = -.427$, corresponding regression line; $eGFR = -23 \times \ln(\text{aortic PWV}) + 137$) and healthy controls ($p = 0.002$, $r = -.502$, corresponding regression line; $eGFR = -24 \times \ln(\text{aortic PWV}) + 130$), which are shown in Figure 2. Interaction analyses showed that the association between eGFR and aortic PWV was significantly different between type 1 DM and healthy controls: 1. Type 1 DM patients show a higher aortic PWV than healthy controls for each given eGFR ($p < 0.001$); 2. The decrease in eGFR per increase in aortic PWV was not

significantly different between type 1 DM patients and healthy controls ($p=ns$). The inverse association between eGFR and aortic PWV in type 1 DM patients was independent of age, hypertension, heart rate, BMI, smoking, DM duration and HbA1c level ($p=0.026$, $\text{Beta}=-0.392$).

Figure 2. Figure showing the inverse relationship between eGFR and aortic PWV in type 1 DM patients and in healthy controls



		A ± SE	p	B ± SE	p	Spearman R
eGFR (ml/min/1.73m ²)	Type 1 DM	-23 ± 5 (p<0.001)	0.919	137 ± 9 (p<0.001)	<0.001	-0.427 (p<0.001)
	Controls	-24 ± 7 (p=0.002)		130 ± 12 (p<0.001)		-0.502 (p=0.002)

The table illustrates the linear regression analysis $eGFR=A \times \ln(\text{aortic PWV}) + B$ for type 1 DM and for healthy controls. P-values are reported from Interaction analysis, showing: 1. Increased aortic PWV in type 1 DM patients compared to healthy controls for each given eGFR ($p<0.001$); 2. The rate of decrease of eGFR per increase in aortic PWV did not statistically differ between type 1 DM patients and healthy controls ($p=0.919$).

DISCUSSION

The purpose of the present study was to investigate whether type 1 DM per se is associated with increased aortic stiffness measured by MRI, independent of renal dysfunction, and to evaluate the relationship between aortic stiffness and renal function within the normal range in type 1 DM patients. The main findings of our cross-sectional study are: 1. Type 1 DM patients

without microalbuminuria or renal impairment show increased aortic stiffness compared to matched healthy controls; 2. An inverse association between eGFR and aortic PWV was found in both type 1 DM patients and in healthy controls; aortic stiffness was increased for each given eGFR within normal range in type 1 DM, and the decrease in renal function per increase in aortic stiffness was similar for type 1 DM patients and healthy controls.

We found increased aortic stiffness in type 1 DM patients without microalbuminuria and renal impairment. The present finding of increased aortic PWV in type 1 DM patients compared to healthy controls extends the observations in previous studies showing augmentation of aortic stiffening in type 1 DM (2,16,17). Our findings confirm the hypothesis of an association between type 1 DM per se and increased aortic stiffness, irrespective of the potential detrimental effect on vascular elasticity of frequently present renal dysfunction.

Secondly, we showed a significant decrease in renal function within the normal range per increase in aortic stiffness which was similar for type 1 DM patients and healthy controls, but with an increased aortic stiffness for each given eGFR in type 1 DM (Figure 1). Our findings are consistent with earlier studies showing the significant relationship between eGFR values and arterial stiffness in a community population with normal renal function (18,19). However, in these studies the influence of type 1 DM was not reported. Interestingly, although aortic stiffness was increased in type 1 DM patients selected in our study, the increase in aortic stiffness itself did not show an additional deteriorative effect on renal function; the rate of decrease in eGFR per increase in aortic stiffness remained similar with healthy controls. A consequence of an increased aortic stiffness is that pulse waves propagate faster into peripheral arteries and therefore may induce early return of reflected waves, as manifested by the increased brachial pulse pressure shown by our data. Transmission of high pulsatile pressure is known to lead to renal microvascular damage (20). Apparently, the interaction between pulse wave velocity and renal function is also operational in presumed healthy subjects, indicating that this phenomenon may be physiological to some extent.

Of note, in our study aortic stiffness was associated with renal function in type 1 DM patients independent of other risk factors including age, hypertension and smoking or type 1 DM duration and glucose regulation. In contrast to our data, a previous study did not find this independent relationship between eGFR and aortic PWV in DM (21). These differences may be explained by their inclusion of both type 1 DM and type 2 DM patients. Risk profiles in patients with type 1 DM are usually different than in patients with type 2 DM. Type 2 DM is commonly associated with a high prevalence of other classical risk factors, such as obesity, abnormal lipid status and hypertension that also may affect aortic stiffness (22) and subsequently confound the relationship between aortic stiffness and renal function, as analyzed in our study independent of BMI and hypertension in type 1 DM patients. Another explanation for the difference in study outcome may be the methodology used for measuring aortic stiffness. In our study aortic PWV was assessed using velocity encoded MRI, a validated modality

which is not dependent on geometric estimations unlike applanation tonometry as used in the before mentioned study.

In perspective, MRI assessment of aortic PWV is currently not part of clinical routine in type 1 DM patients. However, our data show increased aortic stiffness in type 1 DM patients without microalbuminuria, whereas microalbuminuria is currently one of the most frequently used screening tools for the early detection of cardiovascular disease (23) in medical practice. Furthermore, arterial stiffness has been described as an independent predictor of cardiovascular disease and mortality in type 1 DM (3). Importantly, besides MRI assessed aortic stiffness being a marker of renal function in our current study, earlier studies have shown MRI assessed aortic stiffness to be an integrated marker of both cardiac function and cerebral small vessel disease (11) in type 1 DM patients. The results of our cross-sectional study and of earlier studies suggest that MRI assessment of aortic PWV could function as an integrated non-invasive screening tool for the detection of multi-organ cardiovascular complications in type 1 DM beyond classical risk factors. However, longitudinal studies are required to confirm a clinical role of aortic PWV in cardiovascular risk stratification and optimization of therapy.

In conclusion, this cross-sectional study demonstrates that aortic stiffness is increased in type 1 DM patients independent of renal dysfunction. Moreover, an inverse relation was found between aortic stiffness and renal function within the normal range in type 1 DM patients as well as in healthy controls. Longitudinal studies are needed to provide additional insight into the mechanisms of interaction between aortic stiffening and renal failure as a severe complication in type 1 DM and to further assess the clinical significance of our findings.

REFERENCES

1. Giannattasio C, Failla M, Piperno A, et al. Early impairment of large artery structure and function in type I diabetes mellitus. *Diabetologia* 1999;42(8):987-994.
2. Oxlund H, Rasmussen LM, Andreassen TT, Heickendorff L. Increased aortic stiffness in patients with type 1 (insulin-dependent) diabetes mellitus. *Diabetologia* 1989;32(10):748-752.
3. Schram MT, Chaturvedi N, Fuller JH, Stehouwer CD. Pulse pressure is associated with age and cardiovascular disease in type 1 diabetes: the Eurodiab Prospective Complications Study. *J Hypertens* 2003;21(11):2035-2044.
4. Safar ME, London GM, Plante GE. Arterial stiffness and kidney function. *Hypertension* 2004;43(2):163-168.
5. Karalliedde J, Smith A, DeAngelis L, et al. Valsartan improves arterial stiffness in type 2 diabetes independently of blood pressure lowering. *Hypertension* 2008;51(6):1617-1623.
6. Temmar M, Liabeuf S, Renard C, et al. Pulse wave velocity and vascular calcification at different stages of chronic kidney disease. *J Hypertens* 2010;28(1):163-169.
7. Lambert J, Smulders RA, Aarsen M, Donker AJ, Stehouwer CD. Carotid artery stiffness is increased in microalbuminuric IDDM patients. *Diabetes Care* 1998;21(1):99-103.
8. Finne P, Reunanen A, Stenman S, Groop PH, Gronhagen-Riska C. Incidence of end-stage renal disease in patients with type 1 diabetes. *JAMA* 2005;294(14):1782-1787.
9. Laurent S, Cockcroft J, van Bortel L, et al. Expert consensus document on arterial stiffness: methodological issues and clinical applications. *Eur Heart J* 2006;27(21):2588-2605.
10. Grotenhuis HB, Westenberg JJ, Steendijk P, et al. Validation and reproducibility of aortic pulse wave velocity as assessed with velocity-encoded MRI. *J Magn Reson Imaging* 2009;30(3):521-526.
11. van Elderen SG, Brandts A, Westenberg JJ, et al. Aortic stiffness is associated with cardiac function and cerebral small vessel disease in patients with type 1 diabetes mellitus: assessment by magnetic resonance imaging. *Eur Radiol* 2010;20(5):1132-1138.
12. Levey AS, Eckardt KU, Tsukamoto Y, et al. Definition and classification of chronic kidney disease: a position statement from Kidney Disease: Improving Global Outcomes (KDIGO). *Kidney Int* 2005;67(6):2089-2100.
13. Levey AS, Coresh J, Greene T, et al. Using standardized serum creatinine values in the modification of diet in renal disease study equation for estimating glomerular filtration rate. *Ann Intern Med* 2006;145(4):247-254.
14. Mancia G, de Backer G., Dominiczak A, et al. 2007 Guidelines for the management of arterial hypertension: The task force for the management of arterial hypertension of the European Society of Hypertension (ESH) and of the European Society of Cardiology (ESC). *J Hypertens* 2007;25(6):1105-1187.
15. van der Meer RW, Diamant M, Westenberg JJ, et al. Magnetic resonance assessment of aortic pulse wave velocity, aortic distensibility, and cardiac function in uncomplicated type 2 diabetes mellitus. *J Cardiovasc Magn Reson* 2007;9(4):645-651.
16. Brooks B, Molyneaux L, Yue DK. Augmentation of central arterial pressure in type 1 diabetes. *Diabetes Care* 1999;22(10):1722-1727.

17. Wilkinson IB, MacCallum H, Roijmans DF, et al. Increased augmentation index and systolic stress in type 1 diabetes mellitus. *QJM* 2000;93(7):441-448.
18. Kawamoto R, Kohara K, Tabara Y, et al. An association between decreased estimated glomerular filtration rate and arterial stiffness. *Intern Med* 2008;47(7):593-598.
19. Yoshida M, Tomiyama H, Yamada J, et al. Relationships among renal function loss within the normal to mildly impaired range, arterial stiffness, inflammation, and oxidative stress. *Clin J Am Soc Nephrol* 2007;2(6):1118-1124.
20. Giunti S, Barit D, Cooper ME. Mechanisms of diabetic nephropathy: role of hypertension. *Hypertension* 2006;48(4):519-526.
21. Aoun S, Blacher J, Safar ME, Mourad JJ. Diabetes mellitus and renal failure: effects on large artery stiffness. *J Hum Hypertens* 2001;15(10):693-700.
22. Sutton-Tyrrell K, Newman A, Simonsick EM, et al. Aortic stiffness is associated with visceral adiposity in older adults enrolled in the study of health, aging, and body composition. *Hypertension* 2001;38(3):429-433.
23. Go AS, Chertow GM, Fan D, McCulloch CE, Hsu CY. Chronic kidney disease and the risks of death, cardiovascular events, and hospitalization. *N Engl J Med* 2004;351(13):1296-1305.

Chapter 6

Cerebral perfusion and aortic stiffness are independent predictors of white matter brain atrophy in type 1 diabetes mellitus patients: assessment by MR imaging

SGC van Elderen, A Brandts, J van der Grond, JJM Westenberg,
LJM Kroft, MA van Buchem, JWA Smit, A de Roos

Submitted

ABSTRACT

Purpose

To identify vascular mechanisms of brain atrophy in type 1 diabetes mellitus (DM) patients by investigating the relationship between brain volumes and cerebral perfusion and aortic stiffness using magnetic resonance imaging (MRI).

Materials and Methods

Approval from the local institutional review board was obtained and patients gave informed consent. Fifty-one type 1 DM patients (30 men; mean age 44 ± 11 years; mean DM duration 23 ± 12 years) and 34 age and gender matched healthy controls, were prospectively enrolled. Exclusion criteria comprised hypertension, stroke, aortic disease and standard MRI contraindications. White matter (WM) and grey matter (GM) brain volumes, total cerebral blood flow (tCBF), total brain perfusion and aortic pulse wave velocity (PWV) were assessed using MRI. Multivariable linear regression analysis was used for statistics, with co-variables age, gender, mean arterial pressure, body mass index, smoking, heart rate, DM duration and HbA1c.

Results

Both WM and GM brain volumes were decreased in type 1 DM patients compared to controls (WM: $p=0.04$; resp. GM: $p=0.03$). Total brain perfusion was increased in type 1 DM compared to controls (Beta= -0.219 , $p<0.05$). Total CBF and aortic PWV predicted WM brain volume (Beta= 0.352 , $p=0.024$ for tCBF, resp. Beta= -0.458 , $p=0.016$ for aortic PWV) in type 1 DM. Age was the independent predictor of GM brain volume (Beta= -0.695 , $p<0.001$).

Conclusion

Type 1 DM patients without hypertension showed WM and GM volume loss compared to controls concomitant with a relative increased brain perfusion. Total CBF and stiffness of the aorta independently predicted WM brain atrophy in type 1 DM. Age only was predicting GM brain atrophy.

INTRODUCTION

In type 1 diabetes mellitus (DM) patients, early development of brain atrophy (1,2) which may affect cognitive functioning (3,4) has been demonstrated. Multiple pathophysiological mechanisms like repeated hypoglycemic episodes (5), chronic hyperglycemia (6) and alterations in insulin metabolism and associated insulin use (7) are suggested to be involved in the development of cerebral complications in type 1 DM. Although cerebral atrophy is common in neurodegenerative processes, decreased brain volumes have been associated with vascular risk factors (3,8), suggesting vascular mechanisms contributing to the development of brain atrophy. Indeed, the hyperglycemic state of DM induces structural changes and endothelial dysfunction of the macro- and microvasculature (9). Impaired cerebrovascular reactivity in type 1 DM has been demonstrated recently (10) and cerebral perfusion abnormalities have been found in type 1 DM patients in earlier studies (11,12). The cerebral circulation plays an important role in the maintenance of neuronal cell integrity, and therewith potentially in the development of brain atrophy.

Furthermore, arterial stiffening has shown to occur in type 1 DM, being an independent predictor of cardiovascular outcome (13). The elastic aorta is the predominant site of pathologic arterial stiffening. Aortic stiffening increases pulse wave velocity (PWV) and pulse pressure (PP), placing considerable pulsatile stress on the peripheral circulation. The brain is a high flow organ and therewith particularly susceptible to pulsatile stress. Therefore, it is conceivable that aortic stiffness is contributing to the pathogenesis of brain atrophy in type 1 DM.

Although the associations between type 1 DM and cerebral perfusion or arterial stiffening have been described, their relationship with brain volumes in this patient group, to investigate potential vascular mechanisms causing brain atrophy has not been assessed until so far.

Quantitative measurements of brain volumes can be accurately evaluated on scans obtained by magnetic resonance imaging (MRI) (14). MRI using phase-contrast is a reliable method for estimating total cerebral blood flow (tCBF) (15) as well as for evaluating aortic stiffness by means of PWV (16).

Accordingly, the purpose of the current study was to identify potential underlying vascular mechanisms of brain atrophy in type 1 DM patients by investigating the relationship between brain volumes and cerebral perfusion and aortic stiffness in this patient group using MRI.

METHODS

Study participants

Between February 2008 and January 2010, in total 51 consecutive type 1 DM patients from the local outpatient clinic of the Leiden university medical center and 34 age and gender matched healthy controls recruited by advertisement in local newspapers participated in

the study. Healthy controls did not have a history or clinical evidence of DM, hypertension or cardiovascular disease. Exclusion criteria for all participants included a clinical history or diagnosis of hypertension according to the guidelines of the European Society of Cardiology, stroke, aortic valve stenosis or insufficiency as evaluated by means of cardiac auscultation and velocity-encoded MR imaging, Marfan syndrome, and standard MRI contra-indications like claustrophobia, pacemaker and metal implantations.

Information about type 1 DM and healthy control characteristics was obtained by standardized interviews and physical and laboratory examinations. Type 1 DM duration was estimated as the time passed between the reported age of diagnosis and the MRI examination. Body mass index (BMI) was calculated from body length and mass at the time of MRI. Blood pressure (BP) and heart rate were measured after MRI using a semi-automated sphygmomanometer (Dinamap, Critikon, Tampa, FL, USA, validated to ANSI/AAMI SP10 criteria). Pulse pressure was defined as the difference between systolic and diastolic BP. Mean arterial pressure (MAP) was calculated by adding diastolic BP to one-third of the PP. Smoking was defined as non-smoker or a current smoker. Retinopathy was recognized on fundoscopy. Monofilament testing was used to diagnose peripheral neuropathies. Microalbuminuria was defined as 30-300 mg albumin/24h urine collection or microalbuminuria/creatinine ratio > 2.5 mg/mmol for men or >3.5 mg/mmol for women. Glycated hemoglobin (HbA1c) in type 1 DM, fasting glucose in healthy controls, high-density lipoprotein (HDL), total cholesterol, triglycerides and creatinine were furthermore determined.

The study was approved by the local medical ethics committee, and conducted according to the principles in the Declaration of Helsinki. All study participants signed informed consent.

MR imaging protocol

All brain examinations were performed on a 3.0 Tesla MRI (Achieva; Philips Medical Systems, Best, the Netherlands). Aortic imaging was performed using 1.5 Tesla MRI (NT 15 Gyroscan Intera; Philips Medical Systems, Best, the Netherlands).

Brain MR imaging consisted of a 3-dimensional T1 sequence for brain volume assessment and a 2-dimensional phase contrast scan at the level of the skull base for flow measurements in the internal carotid arteries and basilar artery.

For the evaluation of white matter (WM) and grey matter (GM) brain volumes the 3D T1 image (repetition time (TR) 9.8 msec, echo time (TE) 4.6 msec, flip angle (FA) 8° , field of view (FOV) 224 mm, 192x152 acquisition matrix, 256x256 reconstruction matrix, slice thickness 1.2 mm, 120 slices, no slice gap) was obtained. Software package SIENAX automatically segments brain from non-brain matter, calculates white, grey and total brain volume, and applies a normalization factor to correct for skull size (14). To avoid confounding brain volume measurements because not all scans included the full brain, the SIENAX analyses were restricted to a pre-specified interval along the z-axis, ranging from 75 to -52 mm in standard

MNI152 space. SIENAX is part of the FMRIB Software Library (FSL). All SIENAX analyses were performed using FSL version 2.6.

Total CBF was calculated from the electrocardiographic-triggered 2D phase contrast images (TR 13 msec, TE 8.3 msec, FA 10°, FOV 150 mm, 128x88 acquisition matrix, 256x256 reconstruction matrix, slice thickness 5 mm, no slice gap, velocity sensitivity 140 cm/s) using the software package FLOW (Leiden University Medical Center, Leiden, the Netherlands). An experienced researcher drew manual regions of interest closely around the vessel lumen of the internal carotid arteries and the basilar artery (S.v.E., 3 year of experience in neuroradiology). The flow through the three arteries was summed and multiplied by the individual's heart rate during MR scanning to calculate the tCBF (in ml/min). In three subjects (two type 1 DM patients, one healthy control) tCBF could not be obtained due to incorrect positioning of the phase-contrast imaging plane. Total brain perfusion (in ml/min per 100ml) was assessed by dividing tCBF (ml/min) by each individual's total brain volume (ml) and multiplying the obtained result by 100.

For the evaluation of aortic stiffness, aortic PWV was determined using a previously described protocol (16). In short, a scout view of the aorta was performed. Next, a velocity encoded image perpendicular to the ascending aorta at the level of the pulmonary trunk was assessed. This resulted in through-plane flow measurements of the ascending and proximal descending aorta at those levels. Linear regression between 20% and 80% of the range between diastolic flow and peak systolic flow determines the line following the upstroke. Time point of intersection between the upstroke and the baseline of the flow curve was considered being the arrival time of the foot of the pulse wave. Aortic PWV was subsequently calculated for the aorta as $\Delta x/\Delta t$, where Δx is the aortic path length between the two measurement sites measured in the aortic scout view and Δt is the time delay between the arrivals of the foot of the pulse wave at the respective measurement sites. Data were analyzed using MASS and FLOW (Leiden University Medical Center, Leiden, the Netherlands) by two observers (S.v.E. and A.B., both 4 years of experience in cardiac MRI) supervised by a senior researcher (J.W., 15 years of experience in cardiac MRI).

Statistical analysis

Data are expressed as mean \pm standard deviation. To compare clinical characteristics between type 1 DM and healthy controls independent samples t-test for continuous variables and Chi-Square test for dichotomous variables were used. Kolmogorov-Smirnov test showed that aortic PWV was non-normally distributed ($p < 0.001$). Therefore, a log transformation of aortic PWV values was used in the analyses. To compare MR findings between type 1 DM and healthy controls linear regression analysis with covariates age, gender and MAP was applied.

In type 1 DM multivariable linear regression analysis was performed to study the association between brain volumes and tCBF and aortic PWV, independent of potential confounders defined as age, gender, MAP, BMI, smoking, heart rate, DM duration and HbA1c. P value <

0.05 was considered statistically significant. We used SPSS for Windows (version 16.0; SPSS, Chicago, Illinois, USA) for statistical analysis.

RESULTS

The characteristics of the study population are described in Table 1. Fifty-one type 1 DM patients (30 male, 21 female, mean age 44 ± 11 years, mean type 1 DM duration 23 ± 12 years) and 34 healthy controls were included. All type 1 DM patients were on insulin treatment. Type

Table 1. Clinical characteristics and MRI parameters of type 1 DM patients and healthy controls

	Type 1 DM patients (n=51)	Healthy controls (n=34)	p-value
<i>Characteristics</i>			
Age, years	44 ± 11	46 ± 14	0.46
Male gender, n (%)	30 (59)	17 (50)	0.42
Body mass index, kg/m ²	25.0 ± 3.2	26.2 ± 3.9	0.18
Systolic blood pressure, mmHg	126 ± 18	128 ± 15	0.62
Diastolic blood pressure, mmHg	74 ± 10	80 ± 11	<0.01*
Pulse pressure, mmHg	52 ± 13	47 ± 13	0.11
Mean arterial pressure, mmHg	91 ± 11	96 ± 11	0.04*
Heart rate, beats/min	65 ± 10	61 ± 10	0.05
Current smoker, n (%)	8 (16)	2 (6)	0.17
Alcohol use yes, n (%)	33 (64)	26 (77)	0.30
<i>Laboratory markers</i>			
HbA1c, %	7.6 ± 1.0	na	na
Fasting glucose level, mmol/l	na	4.9 ± 0.6	na
HDL-cholesterol, mmol/l	1.7 ± 0.5	1.6 ± 0.4	0.34
Total cholesterol, mmol/l	4.7 ± 0.9	$5.3 \pm 1.2^*$	0.01*
Triglycerides, mmol/l	1.1 ± 0.6	$1.4 \pm 0.7^*$	0.04*
Creatinine, μ mol/l	74 ± 11	77 ± 17	0.32
<i>MRI findings</i>			
Aortic PWV, m/s	5.3 (4.7 - 6.1)	5.7 (4.6 - 7.6)	0.21
Total cerebral blood flow, mL/min	466 ± 131	424 ± 111	0.27
Total brain perfusion, mL/min per 100 mL brain tissue	41.3 ± 11.0	36.4 ± 9.0	<0.05 [#]
White matter brain volume, mL	567 ± 72	583 ± 70	0.04 [#]
Grey matter brain volume, mL	565 ± 59	584 ± 54	0.03 [#]
Total brain volume, mL	1132 ± 124	1167 ± 117	<0.01 [#]

* significantly different between groups using independent samples t-test, $p < 0.05$

[#] significantly different between groups, in multivariable linear regression analysis correcting for age, gender and MAP, $p < 0.05$

Abbreviations: DM: diabetes mellitus; HbA1c: glycated hemoglobin, HDL: high density lipoprotein; PWV: pulse wave velocity

1 DM and healthy controls were comparable in age, gender, BMI, systolic BP, PP, heart rate, current smokers, HDL-cholesterol and creatinine. Type 1 DM patients showed lower diastolic BP ($p<0.01$), lower total cholesterol ($p=0.01$) and lower triglyceride levels ($p=0.04$). Twelve type 1 DM patients used statins, whereas none of the healthy volunteers did. One out of the fifty-one type 1 DM patient used an ACE-inhibitor and an angiotensin II-antagonist for the presence of microalbuminuria. None of the type 1 DM patients were on beta-blocker use. None of the volunteers used antihypertensive medication.

WM brain volumes and GM brain volumes, normalized for skull size, were decreased in type 1 DM patients compared to healthy controls ($p=0.04$ for WM; resp. $p=0.03$ for GM brain volume). Total brain perfusion was significantly increased in type 1 DM compared to healthy controls presenting with similar systolic blood pressures and corrected for age, gender and MAP (Beta= -0.219, $p<0.05$). Aortic PWV values were in the normal range in type 1 DM patient and healthy controls ($p=0.21$).

Table 2 shows the results of multivariable linear regression analyses to assess independent predictors for WM and GM brain volume in type 1 DM. Both tCBF and aortic PWV were independent predictors of WM brain volume (Beta=0.352, $p=0.024$ for tCBF, resp. Beta=-0.458, $p=0.016$ for aortic PWV) in type 1 DM patients in a model including co-variables age, gender, MAP, BMI, smoking, heart rate, DM duration and HbA1c. In a similar multivariable linear regression model for GM brain volume age was a significant predictor (Beta=-0.695, $p<0.001$) and tCBF and aortic PWV were not. Both total CBF and aortic PWV did not independently predict WM or GM brain volumes in healthy controls.

Table 2. Results of multivariable linear regression analyses performed in type 1 DM patients to assess independent predictors of WM and respectively GM brain volumes

	WM brain volume		GM brain volume	
	Beta	p-value	Beta	p-value
Age, years	0.13	0.56	-0.70	<0.001
Male gender (n=30)	-0.27	0.06	0.14	0.21
Mean arterial pressure, mmHg	-0.04	0.80	-0.10	0.45
Body mass index, kg/m ²	0.20	0.15	-0.03	0.77
Current smoker (n=8)	0.06	0.68	0.12	0.28
DM duration, years	-0.18	0.35	0.02	0.91
HbA1c, %	-0.04	0.83	0.23	0.08
Aortic PWV, m/s	-0.46	0.02	0.07	0.62
Total cerebral blood flow, ml/min	0.35	0.02	0.11	0.36

Abbreviations: WM: white matter; GM: grey matter; DM: diabetes mellitus; HbA1c: glycated hemoglobin; PWV: pulse wave velocity

DISCUSSION

The purpose of the current study was to assess the possible association between brain volumes and cerebral perfusion and aortic stiffness in type 1 DM patients without hypertension by using MRI. The main findings of our study were: 1. Type 1 DM patients showed WM and GM volume loss compared to healthy controls concomitant with a relative increased brain perfusion. 2. Total CBF and stiffness of the aorta independently predicted WM brain atrophy; 3. Age was the only independent predictor of GM brain atrophy, whereas tCBF and aortic PWV were not.

Our findings of cortical and subcortical atrophy in type 1 DM are in line with previous studies reporting mild cerebral atrophy in type 1 DM compared to controls (1,2). Furthermore, we found concomitant hyperperfusion of the brain. Impaired echo Doppler measured cerebrovascular reactivity has been described before in type 1 DM in accordance with our findings (10,17). The Framingham heart study reported the exposure of cardiovascular disease risk factors, like DM, associated with high resting arterial flow and impaired vasoreactivity (18). The vasodilatory effect of persistent hyperinsulinemia was mentioned as a possible mechanism of the high resting arterial blood flow (19).

Furthermore, in our current study tCBF and aortic stiffness were both predictors of WM brain atrophy. Recently, two large cohort studies were the first to investigate and report associations between CBF and brain volumes (20,21). An elevation in CBF, particularly in the presence of factors that stiffen the aorta, may allow additional pulsatility to penetrate into and damage the microcirculation with subsequent cerebral tissue loss. A similar mechanism is a well known phenomenon in the kidneys; renal hyperperfusion is present in the earliest stages of type 1 DM and considered to contribute to renal injury and the progression to clinical nephropathy (22). It has been suggested that the brain and the kidneys, both high flow organs with low impedance vascular beds, present a common and unique vascular reactivity mechanism on blood pressure and flow fluctuations.

We found aortic stiffness as an independent predictor of WM brain atrophy. To the best of our knowledge, no studies investigated this relationship before. Measurements of aortic PWV represent propagation speed of the pulse pressure which is influenced by both functional and structural changes of the arterial vessel wall. An earlier study found a positive correlation between MR parameters of brain atrophy and wall thickness of the internal carotid artery as well as a diagnosis of DM and the current use of insulin in community-dwelling elderly (3), which is in congruence with our findings. Because vascular resistance in the brain is very low, pulsations can extend well into the microvascular cerebral bed. It is remarkable that the aortic PWV was still in the normal range without statistical significant difference as compared to that in healthy controls. We speculate that the brain of type 1 DM patients may be susceptible to small changes in aortic PWV, even when PWV appears to be relative normal. Moreover,

aortic stiffness may be a marker of arterial function and inflammatory processes manifesting in cerebral arteries and arterioles.

Of note, the association between aortic PWV and WM brain volume was found independent of tCBF suggesting two separate vascular mechanisms operating on WM brain atrophy.

The associations between WM brain volumes and tCBF as well as aortic PWV could not be shown for GM brain volumes. It is known that the blood flow in the GM is substantially higher to the amount of blood flow in the WM because of high metabolic activity in the GM (23). Subtle fluctuation in arterial blood flow or function may therefore spare GM brain volume in contrast to the vulnerable end-arterioles penetrating the WM. An earlier study suggested that persistent hyperglycemia and acute severe hypoglycemic events have an impact on early subtle alterations in GM structure in type 1 DM patients (24). In our study age was the only and strong predictor of GM brain atrophy, confirming the theory of accelerated brain ageing in DM.

Our results may have important implications. First, our study results reveal further insight into the pathophysiology of brain atrophy in type 1 DM. Our findings suggest two separate vascular mechanisms, namely tCBF and aortic stiffness, being involved in WM brain atrophy in type 1 DM patients, independent of glucose regulation. Second, our findings may have prognostic implications. Assessment of aortic PWV may have prognostic implications, even when values fall into the normal range, possibly due to increased brain susceptibility in DM patients. Furthermore, the arterial system is known to stiffen with older age and high blood pressure (25). When patients with type 1 DM become older or develop hypertension increased aortic stiffening may occur with subsequent adverse changes in WM brain volumes. On the other hand, methods likely to detect subtle changes in the brain are essential for evaluating the effects of type 1 DM on the brain since the gradual progress of cerebral changes may make them difficult to detect until years after onset of type 1 DM. Earlier detection of brain structural changes may increase the likelihood that treatment interventions can slow down the progression of these impairment. However, longitudinal studies are required to confirm our results and to investigate the clinical implications of our findings.

In conclusion, type 1 DM patients without hypertension showed WM and GM volume loss compared to healthy controls concomitant with a relative increased brain perfusion. Total CBF and stiffness of the aorta independently predicted WM brain atrophy in type 1 DM patients. Age only predicted GM brain atrophy. Future prospective studies are needed to assess the prognostic and clinical implications of these initial observations.

REFERENCES

1. Lunetta M, Damanti AR, Fabbri G, Lombardo M, Di Mauro M, Mughini L. Evidence by magnetic resonance imaging of cerebral alterations of atrophy type in young insulin-dependent diabetic patients. *J Endocrinol Invest* 1994;17(4):241-245.
2. Northam EA, Rankins D, Lin A, et al. Central nervous system function in youth with type 1 diabetes 12 years after disease onset. *Diabetes Care* 2009;32(3):445-450.
3. Longstreth WT, Jr., Arnold AM, Manolio TA, et al. Clinical correlates of ventricular and sulcal size on cranial magnetic resonance imaging of 3,301 elderly people. The Cardiovascular Health Study. Collaborative Research Group. *Neuroepidemiology* 2000;19(1):30-42.
4. Brands AM, Kessels RP, Hoogma RP, et al. Cognitive performance, psychological well-being, and brain magnetic resonance imaging in older patients with type 1 diabetes. *Diabetes* 2006;55(6):1800-1806.
5. Perros P, Deary IJ, Sellar RJ, Best JJ, Frier BM. Brain abnormalities demonstrated by magnetic resonance imaging in adult IDDM patients with and without a history of recurrent severe hypoglycemia. *Diabetes Care* 1997;20(6):1013-1018.
6. Wessels AM, Scheltens P, Barkhof F, Heine RJ. Hyperglycaemia as a determinant of cognitive decline in patients with type 1 diabetes. *Eur J Pharmacol* 2008;585(1):88-96.
7. Brands AM, Kessels RP, de Haan EH, Kappelle LJ, Biessels GJ. Cerebral dysfunction in type 1 diabetes: effects of insulin, vascular risk factors and blood-glucose levels. *Eur J Pharmacol* 2004;490(1-3):159-168.
8. Heijer T, Skoog I, Oudkerk M, et al. Association between blood pressure levels over time and brain atrophy in the elderly. *Neurobiol Aging* 2003;24(2):307-313.
9. Aronson D. Hyperglycemia and the pathobiology of diabetic complications. *Adv Cardiol* 2008;45:1-16.
10. Kozera GM, Wolnik B, Kunicka KB, et al. Cerebrovascular reactivity, intima-media thickness, and nephropathy presence in patients with type 1 diabetes. *Diabetes Care* 2009;32(5):878-882.
11. Quirce R, Carril JM, Jimenez-Bonilla JF, et al. Semi-quantitative assessment of cerebral blood flow with ^{99m}Tc-HMPAO SPET in type I diabetic patients with no clinical history of cerebrovascular disease. *Eur J Nucl Med* 1997;24(12):1507-1513.
12. Salem MA, Matta LF, Tantawy AA, Hussein M, Gad GI. Single photon emission tomography (SPECT) study of regional cerebral blood flow in normoalbuminuric children and adolescents with type 1 diabetes. *Pediatr Diabetes* 2002;3(3):155-162.
13. Schram MT, Chaturvedi N, Fuller JH, Stehouwer CD. Pulse pressure is associated with age and cardiovascular disease in type 1 diabetes: the Eurodiab Prospective Complications Study. *J Hypertens* 2003;21(11):2035-2044.
14. Smith SM, Zhang Y, Jenkinson M, et al. Accurate, robust, and automated longitudinal and cross-sectional brain change analysis. *Neuroimage* 2002;17(1):479-489.
15. Spilt A, Box FM, van der Geest RJ, et al. Reproducibility of total cerebral blood flow measurements using phase contrast magnetic resonance imaging. *J Magn Reson Imaging* 2002;16(1):1-5.

16. Grotenhuis HB, Westenberg JJ, Steendijk P, et al. Validation and reproducibility of aortic pulse wave velocity as assessed with velocity-encoded MRI. *J Magn Reson Imaging* 2009;30(3):521-526.
17. Fulesdi B, Limburg M, Bereczki D, et al. Impairment of cerebrovascular reactivity in long-term type 1 diabetes. *Diabetes* 1997;46(11):1840-1845.
18. Mitchell GF, Vita JA, Larson MG, et al. Cross-sectional relations of peripheral microvascular function, cardiovascular disease risk factors, and aortic stiffness: the Framingham Heart Study. *Circulation* 2005;112(24):3722-3728.
19. Baron AD, Brechtel-Hook G, Johnson A, Hardin D. Skeletal muscle blood flow. A possible link between insulin resistance and blood pressure. *Hypertension* 1993;21(2):129-135.
20. Muller M, van der Graaf Y, Visseren FL, Vlek AL, Mali WP, Geerlings MI. Blood pressure, cerebral blood flow, and brain volumes. The SMART-MR study. *J Hypertens* 2010;28(7):1498-1505.
21. van Es AC, van der Grond J, ten Dam VH, et al. Associations between total cerebral blood flow and age related changes of the brain. *PLoS One* 2010;5(3):e9825.
22. Mogensen CE. Early glomerular hyperfiltration in insulin-dependent diabetics and late nephropathy. *Scand J Clin Lab Invest* 1986;46(3):201-206.
23. Catafau AM, Lomena FJ, Pavia J, et al. Regional cerebral blood flow pattern in normal young and aged volunteers: a 99mTc-HMPAO SPET study. *Eur J Nucl Med* 1996;23(10):1329-1337.
24. Musen G, Lyoo IK, Sparks CR, et al. Effects of type 1 diabetes on gray matter density as measured by voxel-based morphometry. *Diabetes* 2006;55(2):326-333.
25. Benetos A, Waeber B, Izzo J, et al. Influence of age, risk factors, and cardiovascular and renal disease on arterial stiffness: clinical applications. *Am J Hypertens* 2002;15(12):1101-1108.

Chapter 7

Progression of brain atrophy and cognitive decline in diabetes mellitus, a 3 year follow-up

SGC van Elderen, A de Roos, AJM de Craen, RGJ Westendorp, GJ Blauw,
JW Jukema, ELEM Bollen, HAM Middelkoop, MA van Buchem, J van der Grond

Neurology 2010;75(11):997-1002

ABSTRACT

Purpose

To investigate progression of magnetic resonance imaging (MRI) assessed manifestations of cerebral degeneration related to cognitive changes in a population of elderly diabetes mellitus (DM) patients compared to age-matched control subjects.

Materials and Methods

From a randomized controlled trial (PROSPER-study) a study sample of 89 DM patients and 438 non-DM control subjects, aged 70-82 years, were included for brain MRI scanning and cognitive function testing at baseline and re-examination after 3-years. Changes in brain atrophy, white matter hyperintensities (WMHs), number of infarctions and cognitive function test results were determined in DM and non-DM subjects. Linear regression analysis was performed with correction for age, gender, hypertension, pravastatin treatment, educational level and baseline test results. In DM patients, baseline MRI parameters were correlated with change in cognitive function test result using linear regression analysis with covariates age and gender.

Results

DM patients showed increased progression of brain atrophy ($p < 0.01$) after follow-up compared to control subjects. No difference in progression of WMH volume or infarctions was found. DM patients showed increased decline in cognitive performance on Stroop ($p = 0.04$) and Picture Learning Test (PLT) ($p = 0.03$). Furthermore, in DM patients change in PLT was associated with baseline brain atrophy ($p < 0.02$).

Conclusion

Our data show that non-demented elderly DM patients have accelerated progression of brain atrophy with significant consequences in cognition compared to non-DM subjects. Our findings add further evidence to the hypothesis that diabetes exerts deleterious effects on neuronal integrity.

INTRODUCTION

Diabetes Mellitus (DM) is associated with cerebral atrophy, white matter hyperintensities (WMHs) and infarctions, observed on Magnetic Resonance Imaging (MRI) scans of the brain (1-4). In general the presence of these cerebral alterations is also associated with cognitive impairment (5-7) and dementia (8-10), and indeed previous studies have shown a higher prevalence of brain atrophy (11,12), WMHs (13,14) and infarctions (13), as well as a diminished cognitive function in DM patients compared to control subjects (14-18). For DM patients, little is known however about the progression in time of cerebral degeneration on MRI. Until now, only few longitudinal studies have investigated DM as possible risk factor for MRI assessed brain atrophy and WMHs, reporting conflicting results. Some studies reported DM as a risk factor for brain atrophy, WMH progression and new infarctions (1,19,20) while other studies did not find DM as a risk factor (3,21). Moreover, the potential predictive value of MRI parameters for cerebral degeneration for cognitive decline over time has not been studied before in DM.

The purpose of the present study was to investigate differences in progression rate of neurodegenerative changes (cerebral degeneration on MRI and cognitive function) between DM and non-DM subjects. Furthermore, we investigated whether MRI assessed brain atrophy, WMH volume and infarctions at baseline were associated with cognitive decline in DM after 3 year follow-up duration.

METHODS

Study participants

All study participants originated from the PROspective Study of Pravastatin in the Elderly at Risk (PROSPER) study (22), a large randomized controlled trial assessing the benefits of 40 mg pravastatin daily on vascular endpoints. Inclusion and exclusion criteria of the PROSPER study and extensive definition of PROSPER study endpoints have been described in detail elsewhere (22). In short, men and women between 70 and 82 years old with either pre-existing coronary (physician diagnosed stable angina, myocardial infarction), cerebral (stroke, transient ischemic attack) or peripheral vascular disease (physician diagnosed intermittent claudication, arterial surgery or amputation for vascular disease >6 months before study entry), or with increased risk of vascular disease because of smoking, hypertension (defined as currently receiving antihypertensive drug treatment) or DM (known diabetes mellitus) were enrolled. Individuals with pre-existing poor cognitive function, defined as a minimal mental state examination (MMSE) score of less than 24, or abnormal laboratory findings were excluded at baseline. Additional exclusion criteria for this MRI sub-study were general MRI contra-indications (pacemaker, metal implantations, claustrophobia). From the 1100 Dutch

participants in the PROSPER study, 646 participants consented for the MRI sub-study. Forty of the 646 original study participants died during the 3 year follow-up period. From the remaining 606 study subjects, MRI data and cognitive function test results at baseline and at end of follow-up were available from in total 527 participants. Reasons for exclusion of follow-up examination were claustrophobia or illness during MRI (n=41), technical problems of the MRI (n=2), MRI contra-indications (n=3), artifacts on MRI (n=27), and 6 withdrew their informed consent. Compared with the follow up participants, those who dropped out had higher baseline total WMH volumes and performed worse on the Stroop and Letter-Digit Coding Test (LDCT). All participating study subjects experienced MRI scanning and cognitive function testing at the same day. In total 89 of the 527 participants were DM patients. All participants gave their written informed consent according to the Declaration of Helsinki. Our local ethics committee approved the study protocol.

MRI scanning

Similar MRI protocols were performed on a 1.5 T MR system (Philips Medical Systems, Best, the Netherlands) at baseline and at follow-up. The MRI protocol included dual fast spin echo (TR/TE₁/TE₂= 3000/27/120ms; flip angle 90°, echo train length 10; 48 continuous 3mm slices; matrix 256x256; FOV 220mm) and fluid-attenuated inversion recovery (FLAIR) (TR/TE= 8000/100ms; 48 continuous 3mm slices; matrix 256x256; FOV=220mm) sequences.

Automatic quantification of intracranial volume, brain parenchyma volume and WMH volume was performed on T2-weighted and FLAIR images using Software for Neuro-Image Processing in Experimental Research (SNIPER) (23). A measure reflecting acquired brain volume loss was calculated using the equation: brain atrophy (%) = [(intracranial volume – parenchymal volume)/intracranial volume] x 100% (24). Hyperintensities connected to the lateral ventricles were labeled as periventricular WMHs. Hyperintensities not connected to the lateral ventricles were labeled as deep WMH (25). The volume of periventricular WMH and deep WMH was calculated automatically. Brain infarctions included symptomatic and silent (lacunar) infarctions. Infarction was defined as a parenchyma defect (>3 mm in size) seen on a FLAIR scan with the same signal intensity as cerebrospinal fluid and corresponding focal hyperintensity on T2-weighted images. The total number of infarctions for each patient was visually scored by a neuroradiologist with more than 15 years of experience in neuroradiology.

Cognitive function testing

For the assessment of cognition, three different cognitive function tests reflecting the main cognitive domains affected in DM (26,27) were performed at baseline and subsequently repeated at end of follow-up, including Stroop test, LDCT and Picture Learning Test (PLT). Since the MMSE is not suitable for longitudinal research because of learning and ceiling effects, MMSE scores are not reported here. The third part of the Stroop test was used for the evaluation of selective attention (28). In this study an abbreviated version of the Stroop

Color-Word test was used in which the stimuli were reduced from 100 to 40 items, which is a very reliable estimate of the performance on the complete test (29). The LDCT was performed to measure speed of processing of general information, which tests visual scanning, perception, visual memory, visuoconstruction and motor functions. The PLT consists of 12 pictures which subjects should recall in any order after the pictures has been shown to them, to test recent memory. The PLT performed comprised an immediate and a 20 minute delayed recall.

Statistical analysis

Statistical analysis was performed using the SPSS-16.0.2 statistical software package (SPSS Inc., Chicago, IL). Baseline differences between DM and control subjects in demographic variables, MRI parameters and cognitive function test results were analyzed using regression analysis, adjusting for age and gender. We calculated change in scores for each subject final visit (change in score (Δ) = follow-up value minus baseline value) for each MRI parameter and cognitive function test result, respectively defined as Δ Atrophy, Δ WMH, Δ infarction, Δ Stroop, Δ LDCT and Δ PLT. Differences between DM and control subjects in Δ MRI parameters and Δ cognitive function test results were tested using linear regression models. Age, gender, hypertension, pravastatin treatment and corresponding baseline test result were defined as possible confounders and entered as co-variates in the multivariate regression model. Educational level (age left school) was added as a co-variate in the linear regression analysis for Δ cognitive function tests. A potential predictive role of MRI assessed brain atrophy, WMH volume and infarction for cognitive decline over time in DM was investigated by correlating baseline MRI parameters with Δ cognitive function test scores, which were significantly increased for DM versus non-DM subjects. For this analysis linear regression analysis was used with correction for age and gender. A p-value ≤ 0.05 was considered significant.

RESULTS

The demographic characteristics of the study population are shown in Table 1. At baseline, there were no differences in age, gender, pravastatin use, MMSE score and educational level between the DM and control subjects. The DM patients showed higher body mass index (BMI) ($p=0.01$), higher glucose level after overnight fasting ($p<0.01$), less hypertension ($p<0.01$) but with similar systolic blood pressure levels, and a slightly better cholesterol profile ($p<0.05$) compared to control subjects. There was no difference in use of drugs with an effect on cognition between groups including the use of anticholinergics, antipsychotics, antiepileptics and benzodiazepines. Out of the 89 DM patients, 11 (12.4%) DM patients were on insulin treatment, 56 (62.8%) DM patients used oral glucose lowering drugs, two (2.2%) DM patients used both insulin treatment and an oral glucose lowering drug and 24 (27.0%) DM patients did not receive medical treatment for their DM (lifestyle interventions).

Table 1. Baseline characteristics of the study population

	<i>DM patients (n = 89)</i>	<i>Control subjects (n = 438)</i>	<i>p-value</i>
Age, years	74.7 ± 3.1	75.0 ± 3.2	0.39
Male gender, n (%)	53 (60)	244 (56)	0.51
MMSE, total test score	28.1 ± 1.4	28.2 ± 1.5	0.55
Education level, age in years left school	15.3 ± 2.80	15.5 ± 2.89	0.41
BMI, kg/m ²	27.6 ± 3.8	26.5 ± 3.6	0.01*
Systolic blood pressure, mmHg	161 ± 21	157 ± 22	0.09
Diastolic blood pressure, mmHg	84 ± 12	86 ± 11	0.19
Pravastatin treatment, n (%)	41 (46)	218 (50)	0.52
Current smoker, n (%)	14 (16)	97 (22)	0.18
Hypertension, n (%)	43 (48)	290 (66)	<0.01*
TIA or stroke, n (%)	9 (10)	72 (16)	0.13
Myocardial infarction, n (%)	14 (16)	51 (12)	0.29
Peripheral vascular disease, n (%)	29 (33)	194 (44)	0.03*
Fasting glucose, mmol/l	8.32 ± 2.39	5.26 ± 0.69	<0.01*
Total cholesterol, mmol/l	5.56 ± 0.78	5.80 ± 0.87	0.02*
LDL cholesterol, mmol/l	3.76 ± 0.70	3.95 ± 0.76	0.03*
HDL cholesterol, mmol/l	1.19 ± 0.30	1.25 ± 0.32	0.13
Triglycerides, mmol/l	1.57 ± 0.67	1.49 ± 0.68	0.30
Use of anticholinergicum, n (%)	6 (6.7)	16 (3.7)	0.30
Use of antiepilepticum, n (%)	0 (0)	0 (0)	na
Use of antipsychoticum, n (%)	1 (1.1)	1 (0.1)	0.31
Use of benzodiazepine, n (%)	5 (5.6)	16 (3.7)	0.38

Data are expressed as mean ± standard deviation or number of subjects with numbers in parentheses being percentages. List of abbreviations: DM: diabetes mellitus; MMSE: mini mental state examination; BMI: body mass index; TIA: transient ischemic attack; LDL: low-density lipid; HDL: high density lipid; *significant difference between DM and control subjects corrected for age and gender, $p < 0.05$

The average time period (\pm SD) between baseline and follow up visit was 33 ± 1.4 months. Follow-up duration was slightly shorter in DM patients compared to control subjects ($p < 0.05$).

MRI parameters of DM and control subjects at baseline, and change between follow-up and baseline (Δ) MRI parameters are shown in Table 2. At baseline DM patients had more brain atrophy compared to control subjects ($p = 0.02$). No difference in baseline WMH volume and number of infarctions per patient was found between DM patients and control subjects. DM patients showed increased progression of total brain atrophy ($p < 0.01$, $\text{Beta} = 0.136$) compared to control subjects, after correction for age, gender, hypertension, pravastatin treatment and baseline level of atrophy. DM subjects did not show increased progression of total, periventricular or subcortical WMHs or infarctions compared to control subjects.

In addition, a linear regression analysis was performed to investigate the possible role of hyperglycemia or insulin use on the progression of atrophy (Δ atrophy as a dependent variable and age, gender, hypertension, pravastatin treatment, baseline level of atrophy and fasting glucose respectively insulin treatment entered as co-variates). There was a significant

association between Δ atrophy and fasting glucose levels ($p=0.003$, $\text{Beta}=0.127$), and between Δ atrophy and insulin treatment ($p=0.002$, $\text{Beta}=0.131$).

Table 2. MRI and cognitive function test results at baseline and after follow-up

	DM patients (n = 89)	Control subjects (n = 438)	p-value
Time between follow-up and baseline visit, wks (SD)	170 \pm 14	173 \pm 13	0.03*
<i>MRI findings</i>			
Baseline total brain atrophy, %	26.9 \pm 0.37	26.1 \pm 0.14	0.02*
Baseline total WMH volume, cc	4.19 \pm 0.82	5.34 \pm 0.48	0.31
Baseline periventricular WMH volume, cc	3.29 \pm 0.69	4.19 \pm 0.42	0.36
Baseline subcortical WMH volume, cc	0.90 \pm 0.16	1.15 \pm 0.08	0.20
Baseline infarction, number per patient	1.39 \pm 3.02	0.98 \pm 1.84	0.53
Δ total brain atrophy, %	1.57 \pm 0.26	0.96 \pm 0.10	<0.01 [†]
Δ total WMH volume, cc	1.78 \pm 0.29	2.21 \pm 0.17	0.41
Δ periventricular WMH volume, cc	1.38 \pm 0.24	1.78 \pm 0.16	0.32
Δ subcortical WMH volume, cc	0.39 \pm 0.12	0.44 \pm 0.05	0.87
Δ infarction, number per patient	0.40 \pm 1.23	0.19 \pm 0.68	0.07
<i>Cognitive function test</i>			
Baseline Stroop time, sec	59.0 \pm 1.94	54.1 \pm 0.84	0.02*
Baseline LDCT score, digits/min	26.6 \pm 0.76	28.0 \pm 0.34	0.09
Baseline PLT immediate, recalled pictures	9.70 \pm 0.18	10.23 \pm 0.08	0.01*
Baseline PLT delayed, recalled pictures	10.67 \pm 0.30	11.31 \pm 0.12	0.04*
Δ Stroop time, sec	3.8 \pm 2.48	0.6 \pm 0.65	0.04 [†]
Δ LDCT score, digits/min	-1.9 \pm 0.37	-1.3 \pm 0.21	0.06
Δ PLT immediate, recalled pictures	-0.16 \pm 0.16	0.07 \pm 0.09	0.03 [†]
Δ PLT delayed, recalled pictures	-0.15 \pm 0.27	-0.04 \pm 0.12	0.12

Data are expressed as mean \pm standard error unless stated otherwise. List of abbreviations: DM: diabetes mellitus; MRI: magnetic resonance imaging; WMH: white matter hyperintensity; LDCT: letter digit coding test; PLT: picture learning test

Δ : change in test score between baseline and follow-up

*Significant difference ($p < 0.05$) between DM and control subjects adjusted for age and gender

[†]Significant difference ($p < 0.05$) between DM and control subjects adjusted for age, gender, hypertension, pravastatin treatment, educational level and corresponding baseline test results

Cognitive function test results of DM and control subjects at baseline, and change between follow-up and baseline (Δ) cognitive function test results are shown in Table 2. At baseline, DM patients showed worse performance on Stroop testing ($p=0.02$) and immediate and delayed PLT scores ($p < 0.05$) compared to control subjects. No difference in LDCT test results between the DM and the control subjects were found at baseline. After follow-up, DM subjects showed worse decline in cognitive function test results on Stroop ($p=0.04$, $\text{Beta}=-0.090$) and PLT immediate ($p=0.03$, $\text{Beta}=-0.090$) compared to control subjects, corrected for age, gender, hypertension, pravastatin treatment, educational level and respective baseline test

result. No independent significant association was found between DM and change in LDCT and PLT delayed test score.

In the DM group, change in immediate PLT scores was correlated with baseline brain atrophy ($p=0.01$, $r=-0.292$). Changes in Stroop did not show a significant association with baseline MRI parameters of cerebral degeneration in patients with DM.

DISCUSSION

The main findings of our study are an accelerated progression of total brain atrophy in non-demented elderly DM patients compared to control subjects. In addition, DM patients showed accelerated decline in cognitive performance on Stroop and immediate PLT compared to control subjects. Moreover, change in immediate recall was associated with baseline brain atrophy in DM patients.

We investigated the progression of MRI assessed manifestations of cerebral degeneration in DM and we found accelerated progression of brain atrophy, but not of WMHs or infarctions in DM compared to control subjects. Although many cross-sectional studies have reported an association between DM and brain atrophy (2,12,30-32), to our knowledge only two longitudinal studies have reported on this (3,19). Our finding on accelerated progression of brain atrophy in DM compared to control subjects is in line with one of these studies (19), which showed that DM subjects had a high rate of brain atrophy after a 6-year follow-up period. Our results are in contrast with an earlier published study (3) which did not find DM as a risk factor of progression in brain atrophy. In our study, DM patients did not have accelerated progression of WMHs, which is supported by previous studies in which hypertension (33), high blood pressure and smoking (21) were determinants of WMH progression, whereas DM was not. On the contrary, others have found that DM is a risk factor for WMH progression within a comparable follow-up period of 3 years (1). The conflicting results in the latter study compared to our results may be explained by the difference in methodological approach. In our study semiautomated quantification of WMHs was performed, whereas WMHs were visually rated in the latter study. This rating method may be less sensitive compared to absolute measurements in studying longitudinal white matter changes (34). The finding that the number of new infarctions during follow-up in DM patients was not different from control subjects is in line with earlier longitudinal studies investigating risk factors of incidental brain infarcts which reported no association with DM (1,21).

A possible explanation for accelerated progression of brain atrophy and not of WMHs and infarctions in DM patients could be due to differences in underlying pathophysiological mechanisms. Our results indicate that the increased progression of brain atrophy in DM is mediated mostly by mechanisms other than hemodynamic causes, since there was a low prevalence of hypertension in the DM group compared to the control group. In this respect,

a direct neurotoxic effect of hyperglycemia or hyperinsulinaemia as proposed in previous studies (31,35,36) could be important determinants of brain atrophy in DM. Importantly, additional analyses showed a significant role for glucose levels and for the use of insulin on brain atrophy progression.

Another important finding in our study is that DM subjects demonstrated an accelerated decline in selective attention and immediate recall. This finding is in line with previous studies reporting an association between DM and increased decline in cognitive function test scores (15-18), including the cognitive domains of attention and memory. In contrast to our findings, one study did not find an accelerated cognitive decline in DM (37). However, in this study the oldest old beyond the age of 85 were investigated, compared to a mean age of 75 years in our study. Although we found a progressive decline in cognitive functioning in DM, the changes in cognitive function test scores were relatively small (Δ Stroop: 3.8 sec, Δ PLT immediate: -0.16 recalled pictures). Still, in daily practice patients can already experience subtle inconvenience from this cognitive decline, for instance being in stressful situations. Importantly, DM can be well treated and elderly DM patients on oral hypoglycemic therapy have been shown to perform comparable on cognitive function tests over time to subjects without DM (38).

In the current longitudinal study we reported the predictive value of cerebral degeneration on cognitive decline over time in DM. Our study results show that brain atrophy at baseline is a predictor of verbal memory loss in DM implying a causative mechanism of loss of brain volume on impaired memory. Previous cross-sectional studies reported brain atrophy and WMHs observed on MRI scans of elderly DM patients to be associated with several domains of cognitive impairment including memory (13,39). However, to our knowledge, there are no previous studies specifically addressing the longitudinal relation between brain MRI abnormalities and cognitive functioning in DM patients.

A strength of our study is the large number of DM patients investigated. Although a limitation of the present study is the relatively short follow-up duration, it should be noted that even in a relatively small follow-up period of three years accelerated progression of brain atrophy with clinical consequences can already be detected.

REFERENCES

1. Gouw AA, van der Flier WM, Fazekas F, et al. Progression of white matter hyperintensities and incidence of new lacunes over a 3-year period: the Leukoaraiosis and Disability study. *Stroke* 2008;39(5):1414-1420.
2. Knopman DS, Mosley TH, Catellier DJ, Sharrett AR. Cardiovascular risk factors and cerebral atrophy in a middle-aged cohort. *Neurology* 2005;65(6):876-881.
3. Meyer JS, Rauch GM, Crawford K, et al. Risk factors accelerating cerebral degenerative changes, cognitive decline and dementia. *Int J Geriatr Psychiatry* 1999;14(12):1050-1061.
4. Pantoni L, Garcia JH. Pathogenesis of leukoaraiosis: a review. *Stroke* 1997;28(3):652-659.
5. de Groot JC, de Leeuw FE, Oudkerk M, et al. Periventricular cerebral white matter lesions predict rate of cognitive decline. *Ann Neurol* 2002;52(3):335-341.
6. Kramer JH, Mungas D, Reed BR, et al. Longitudinal MRI and cognitive change in healthy elderly. *Neuropsychology* 2007;21(4):412-418.
7. van den Heuvel DM, ten Dam VH, de Craen AJ, et al. Increase in periventricular white matter hyperintensities parallels decline in mental processing speed in a non-demented elderly population. *J Neurol Neurosurg Psychiatry* 2006;77(2):149-153.
8. Ikram MA, Vrooman HA, Vernooij MW, et al. Brain tissue volumes in relation to cognitive function and risk of dementia. *Neurobiol Aging* 2008.
9. Kuller LH, Lopez OL, Newman A, et al. Risk factors for dementia in the cardiovascular health cognition study. *Neuroepidemiology* 2003;22(1):13-22.
10. Whitwell JL, Przybelski SA, Weigand SD, et al. 3D maps from multiple MRI illustrate changing atrophy patterns as subjects progress from mild cognitive impairment to Alzheimer's disease. *Brain* 2007;130(Pt 7):1777-1786.
11. Jongen C, van der Grond J, Kappelle LJ, Biessels GJ, Viergever MA, Pluim JP. Automated measurement of brain and white matter lesion volume in type 2 diabetes mellitus. *Diabetologia* 2007;50(7):1509-1516.
12. Kumar R, Anstey KJ, Cherbuin N, Wen W, Sachdev PS. Association of type 2 diabetes with depression, brain atrophy, and reduced fine motor speed in a 60- to 64-year-old community sample. *Am J Geriatr Psychiatry* 2008;16(12):989-998.
13. Manschot SM, Brands AM, van der Grond J, et al. Brain magnetic resonance imaging correlates of impaired cognition in patients with type 2 diabetes. *Diabetes* 2006;55(4):1106-1113.
14. van Harten B, Oosterman J, Muslimovic D, van Loon BJ, Scheltens P, Weinstein HC. Cognitive impairment and MRI correlates in the elderly patients with type 2 diabetes mellitus. *Age Ageing* 2007;36(2):164-170.
15. Fontbonne A, Berr C, Ducimetiere P, Alperovitch A. Changes in cognitive abilities over a 4-year period are unfavorably affected in elderly diabetic subjects: results of the Epidemiology of Vascular Aging Study. *Diabetes Care* 2001;24(2):366-370.
16. Gregg EW, Yaffe K, Cauley JA, et al. Is diabetes associated with cognitive impairment and cognitive decline among older women? Study of Osteoporotic Fractures Research Group. *Arch Intern Med* 2000;160(2):174-180.

17. Hassing LB, Grant MD, Hofer SM, et al. Type 2 diabetes mellitus contributes to cognitive decline in old age: a longitudinal population-based study. *J Int Neuropsychol Soc* 2004;10(4):599-607.
18. Yaffe K, Blackwell T, Kanaya AM, Davidowitz N, Barrett-Connor E, Krueger K. Diabetes, impaired fasting glucose, and development of cognitive impairment in older women. *Neurology* 2004;63(4):658-663.
19. Enzinger C, Fazekas F, Matthews PM, et al. Risk factors for progression of brain atrophy in aging: six-year follow-up of normal subjects. *Neurology* 2005;64(10):1704-1711.
20. Vermeer SE, den Heijer T, Koudstaal PJ, Oudkerk M, Hofman A, Breteler MM. Incidence and risk factors of silent brain infarcts in the population-based Rotterdam Scan Study. *Stroke* 2003;34(2):392-396.
21. van Dijk EJ, Prins ND, Vrooman HA, Hofman A, Koudstaal PJ, Breteler MM. Progression of cerebral small vessel disease in relation to risk factors and cognitive consequences: Rotterdam Scan study. *Stroke* 2008;39(10):2712-2719.
22. Shepherd J, Blauw GJ, Murphy MB, et al. The design of a prospective study of Pravastatin in the Elderly at Risk (PROSPER). PROSPER Study Group. PROspective Study of Pravastatin in the Elderly at Risk. *Am J Cardiol* 1999;84(10):1192-1197.
23. Admiraal-Behloul F, van den Heuvel DM, Olofsen H, et al. Fully automatic segmentation of white matter hyperintensities in MR images of the elderly. *Neuroimage* 2005;28(3):607-617.
24. van der Flier WM, van den Heuvel DM, Weverling-Rijnsburger AW, et al. Magnetization transfer imaging in normal aging, mild cognitive impairment, and Alzheimer's disease. *Ann Neurol* 2002;52(1):62-67.
25. van den Heuvel DM, Admiraal-Behloul F, ten Dam VH, et al. Different progression rates for deep white matter hyperintensities in elderly men and women. *Neurology* 2004;63(9):1699-1701.
26. Awad N, Gagnon M, Messier C. The relationship between impaired glucose tolerance, type 2 diabetes, and cognitive function. *J Clin Exp Neuropsychol* 2004;26(8):1044-1080.
27. Stewart R, Liolitsa D. Type 2 diabetes mellitus, cognitive impairment and dementia. *Diabet Med* 1999;16(2):93-112.
28. Houx PJ, Jolles J, Vreeling FW. Stroop interference: aging effects assessed with the Stroop Color-Word Test. *Exp Aging Res* 1993;19(3):209-224.
29. Klein M, Ponds RW, Houx PJ, Jolles J. Effect of test duration on age-related differences in Stroop interference. *J Clin Exp Neuropsychol* 1997;19(1):77-82.
30. Manolio TA, Kronmal RA, Burke GL, et al. Magnetic resonance abnormalities and cardiovascular disease in older adults. The Cardiovascular Health Study. *Stroke* 1994;25(2):318-327.
31. Manschot SM, Biessels GJ, de Valk H, et al. Metabolic and vascular determinants of impaired cognitive performance and abnormalities on brain magnetic resonance imaging in patients with type 2 diabetes. *Diabetologia* 2007;50(11):2388-2397.
32. Schmidt R, Launer LJ, Nilsson LG, et al. Magnetic resonance imaging of the brain in diabetes: the Cardiovascular Determinants of Dementia (CASCADE) Study. *Diabetes* 2004;53(3):687-692.
33. Silbert LC, Nelson C, Howieson DB, Moore MM, Kaye JA. Impact of white matter hyperintensity volume progression on rate of cognitive and motor decline. *Neurology* 2008;71(2):108-113.

34. van den Heuvel DM, ten Dam VH, de Craen AJ, et al. Measuring longitudinal white matter changes: comparison of a visual rating scale with a volumetric measurement. *AJNR Am J Neuroradiol* 2006;27(4):875-878.
35. Gispen WH, Biessels GJ. Cognition and synaptic plasticity in diabetes mellitus. *Trends Neurosci* 2000;23(11):542-549.
36. Greene DA, Lattimer SA, Sima AA. Sorbitol, phosphoinositides, and sodium-potassium-ATPase in the pathogenesis of diabetic complications. *N Engl J Med* 1987;316(10):599-606.
37. van den Berg E, de Craen AJ, Biessels GJ, Gussekloo J, Westendorp RG. The impact of diabetes mellitus on cognitive decline in the oldest of the old: a prospective population-based study. *Diabetologia* 2006;49(9):2015-2023.
38. Logroscino G, Kang JH, Grodstein F. Prospective study of type 2 diabetes and cognitive decline in women aged 70-81 years. *BMJ* 2004;328(7439):548.
39. Akisaki T, Sakurai T, Takata T, et al. Cognitive dysfunction associates with white matter hyperintensities and subcortical atrophy on magnetic resonance imaging of the elderly diabetes mellitus Japanese elderly diabetes intervention trial (J-EDIT). *Diabetes Metab Res Rev* 2006;22(5):376-384.

Part II:

Innovative MR techniques

Chapter 8

Phosphorus-31 MR spectroscopy of skeletal muscle in maternally inherited diabetes and deafness A3243G mitochondrial mutation carriers

SGC van Elderen, J Doornbos, EHR van Essen, HHPJ Lemkes,
JA Maassen, JWA Smit, A de Roos

Journal of Magnetic Resonance Imaging 2009;29(1):127-131

ABSTRACT

Purpose

To investigate high-energy phosphate metabolism in striated skeletal muscle of patients with Maternally Inherited Diabetes and Deafness (MIDD) syndrome.

Materials and Methods

In 11 patients with the MIDD mutation (six with diabetes mellitus (DM) and five non-DM) and eight healthy subjects, phosphocreatine (PCr) and inorganic phosphate (Pi) in the vastus medialis muscle was measured immediately after exercise using ^{31}P -magnetic resonance spectroscopy (MRS). The half-time of recovery ($t_{1/2}$) of monoexponentially fitted (PCr+Pi)/PCr was calculated from spectra obtained every 4 seconds after cessation of exercise. A multiple linear regression model was used for statistical analysis.

Results

Patients with the MIDD mutation showed a significantly prolonged $t_{1/2}$ (PCr+Pi)/PCr after exercise as compared to controls (13.6 ± 3.0 vs. 8.7 ± 1.3 sec, $p = 0.01$). No association between the presence of DM and $t_{1/2}$ (PCr + Pi)/PCr was found ($p = 0.382$).

Conclusion

MIDD patients showed impaired mitochondrial oxidative phosphorylation in skeletal muscle shortly after exercise, irrespective of the presence of DM.

INTRODUCTION

The maternally inherited diabetes and deafness (MIDD) syndrome is known as a phenotype of the adenosine to guanine mutation at position 3243 (A3243G) in the tRNA gene (1,2). The key identifying features of MIDD patients are characterized by a triad of diabetes mellitus (DM), developing in 80% of patients with the MIDD mutation carriers, sensorineural deafness, and a history of these conditions in maternal relatives (3-6). Diagnosis of the MIDD syndrome is based on the pattern of inheritance, the presence of clinical features, and DNA analysis. Although MIDD is often unrecognized, it is estimated that MIDD affects between 0.6-1.5% of DM patients (7).

Besides the characteristic triad, MIDD patients may present with other symptoms such as renal disease, cardiomyopathy, gastrointestinal complaints, and muscle cramps or muscle weakness (3). A transition of adenosine to guanine at nucleotide position 3243 affects the encoding of mitochondrial proteins. This mutation causes the formation of dysfunctional mitochondria and subsequently reduced mitochondrial oxidative adenosinetriphosphate (ATP) energy production (4). The striated skeletal muscle depends largely on mitochondrial oxidative phosphorylation for generation of high-energy phosphates. Associations have been suggested between (sub)clinical myopathies and mitochondrial dysfunction in the MIDD syndrome (5,6).

Phosphorus-31 magnetic resonance spectroscopy (^{31}P -MRS) is a sensitive and specific noninvasive method for the assessment of skeletal muscle mitochondrial ATP production. Observations at rest are not specific for mitochondrial disorders. During exercise patients with mitochondrial myopathies will display rapid phosphocreatine (PCr) depletion. During recovery, ^{31}P -MRS measurements are the most sensitive and the most specific indices used to assess skeletal muscle mitochondrial ATP production (8-11). To our knowledge, only a limited number of MIDD patients have been studied by skeletal muscle ^{31}P -MRS and the potential confounding effect of the presence of DM has not been systematically evaluated before (12-14). As the A3243G mutation potentially results in decreased oxidative phosphorylation and some MIDD patients show signs of muscle involvement, we hypothesized that alterations in phosphate energy metabolism of the striated muscles can be detected in these patients after exercise.

Accordingly, the objective of the current study was to investigate with ^{31}P -MRS whether the presence of the A3243G mitochondrial mutation in the MIDD phenotype affects high-energy phosphate metabolism in the striated skeletal muscle of patients with the A3243G MIDD mutation. As alterations in phosphate metabolism in MIDD patients may be attributed to DM (15-19), we included both DM and non-DM MIDD patients.

MATERIALS AND METHODS

Study participants

The local medical ethics committee approved the study and informed consent was obtained from all participants prior to enrolment in the study.

A ^{31}P -MRS examination was performed in 11 MIDD patients (five male; age 36 ± 10 years; six with DM and five non-DM) and eight healthy control subjects (five male; age 35 ± 8 years), matched for age, height, and body weight. Patients were recruited from the local MIDD database of the DM outpatient clinic of our institution. A standard oral glucose tolerance test (OGTT) was performed in the MIDD patient group - except for the DM patients - to differentiate between DM and patients with normal glucose tolerance (non-DM). The patient group showed no signs of increased muscle weakness or fatigue during normal daily activities. Control subjects and patients were not actively engaged in sports or training activities. Other exclusion criteria comprised general contraindications to MRI.

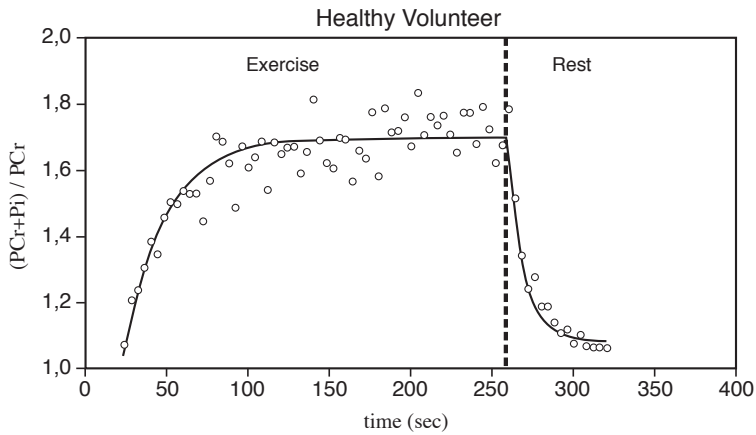
MR spectroscopy protocol

In order to apply an individually adjusted exercise load, the maximal isokinetic potential of the leg muscles was measured prior to MRS in a standardized setting with a dynamometer (EnKnee, Enraf Nonius, Delft, The Netherlands). Subjects were positioned in the test chair with the lower leg secured above the ankle, and hip and thigh strapped down to avoid involuntary movements. After extending the knee 15 times in rapid succession the isokinetic muscle strength was expressed as the maximum peak torque produced in these knee extensions.

The subjects were subsequently instructed to exercise by leg extension in the scanner with a weight attached to the ankle of the dominant leg. The weight consisted of lead-containing rubber strips and corresponded to 25% of the individually assessed maximal isokinetic potential. The knee of the subject was supported to enable extension. Exercise was performed by repeated extension once per second during 3 minutes to reach a steady state, which was validated in a pilot study before onset of this study, depicted in Figure 1. During exercise the subjects were in a supine position in a 1.5 T MRI-system (Gyrosan ACS/NT15; Philips, Best, The Netherlands, Philips Medical Systems). A 6 cm diameter circular surface coil was positioned at the anatomical localization of the vastus medialis muscle. After exercise the subject kept the leg immobilized for 3 minutes, in which the spectra were obtained. The whole procedure was repeated after 15 minutes of rest.

Immediately after cessation of the exercise, ^{31}P -MRS from the vastus medialis muscle were obtained every 4 seconds (sweep width 2000 Hz, 1024 samples, flip angle 20° , 6 cm diameter circular surface coil, four signal averages obtained at $\text{TR} = 1$ sec). Shimming of the magnetic field was performed with the proton imaging body coil, yielding a water resonance of 0.2-0.3 parts/million full-width at half-maximum. Relative concentrations of high-energy phosphates (PCr and inorganic phosphate (Pi)) were measured.

Figure 1. ^{31}P -MRS derived phosphor-curve during exercise in a healthy volunteer, showing a steady state of phosphor metabolism at 3 minutes.



Data analysis

Ratios of $(\text{PCr}+\text{Pi})/\text{PCr}$ were calculated from spectra obtained during the recovery period using time-domain spectral fitting (MRUI-software, AMARES) (20). Recovery rate, reflecting efficiency and rate of oxidative phosphorylation (21), was characterized by the half-time of recovery ($t_{1/2}$) of monoexponential fitted $(\text{PCr}+\text{Pi})/\text{PCr}$ (22).

As each subject performed exercise twice in the scanner, we obtained two phosphorus spectra from each individual. From each obtained phosphorus spectrum the half-time of PCr recovery was calculated. Subsequently the average of the two measurements in each subject was used for statistical analysis.

Laboratory assessment

Venous blood samples were obtained prior to and after exercise to determine blood glucose, insulin, connecting-peptide (C-peptide), glycated hemoglobin (HbA1c), creatine-phosphokinase (CPK), and lactate levels.

Statistical analysis

Multiple linear regression analysis and one-way analysis of variance (ANOVA) were used for statistical evaluation. Results are expressed as mean \pm standard deviation. A multiple linear regression analysis was performed for analysis of the ^{31}P -MRS results. To identify independent predictors of skeletal phosphorus-metabolism, $t_{1/2} (\text{PCr}+\text{Pi})/\text{PCr}$ was entered as a dependent variable and MIDD mutation (yes/no) and DM (yes/no) were subsequently entered as independent variables into the model. For comparison of isokinetic potentials and laboratory measurements between groups one-way ANOVA analysis was used, with post-hoc Bonfer-

roni correction when comparing healthy subjects with patients both with DM and without DM. Statistical significance was indicated by a p-value less than 0.05.

RESULTS

The results of patients and healthy subjects are summarized in Table 1.

Table 1. Clinical characteristics and ^{31}P -MRS results of the study population

	A3243G MIDD carriers			
	Healthy subjects (n=8)	DM (n=6)	Non-DM (n=5)	Total MIDD (n=11)
<i>Clinical characteristics</i>				
Gender (male/female)	5 / 3	3 / 3	3 / 2	6 / 5
Age (years)	35 ± 6	39 ± 6	36 ± 5	38 ± 5
Body mass Index (kg/m ²)	23.7 ± 2.4	22.6 ± 3.6	24.4 ± 3.1	23.4 ± 3.3
HbA1c (%)	4.5 ± 0.4	7.2 ± 2.5*	5.0 ± 0.2*	6.2 ± 2.1*
Max isokinetic potential (Newton)	103 ± 27	88 ± 47	137 ± 70	110 ± 61
Ankle load (kg)	6.6 ± 1.3	5.6 ± 2.7	7.3 ± 2.0	6.4 ± 2.5
<i>^{31}P-MRS result</i>				
t _{1/2} (PCr+Pi)/PCr	8.7 ± 1.3	14.2 ± 3.8*	12.9 ± 1.9*	13.6 ± 3.0*
<i>Laboratory measurements</i>				
Glucose prior exercise (mmol/l)	5.0 ± 0.8	6.7 ± 2.1	4.7 ± 0.4	5.8 ± 1.9
Glucose after exercise (mmol/l)	5.2 ± 1.0	6.4 ± 1.8	5.8 ± 1.3	6.1 ± 1.5
Insulin prior exercise (mU/l)	17 ± 19	12 ± 8	15 ± 6	13 ± 7
Insulin after exercise (mU/l)	13 ± 18	37 ± 60	19 ± 18	29 ± 45
C-Peptide prior exercise (nmol/l)	1.05 ± 0.71	0.61 ± 0.43	1.06 ± 0.24	0.81 ± 0.41
C-Peptide after exercise (nmol/l)	0.79 ± 0.67	0.67 ± 0.53	1.36 ± 1.07	0.97 ± 0.84
Lactate prior exercise (mmol/l)	1.1 ± 0.3	1.5 ± 0.4	1.9 ± 1.4	1.7 ± 1.0
Lactate after exercise (mmol/l)	1.6 ± 0.7	2.1 ± 0.9	2.5 ± 2.2	2.3 ± 1.5
CPK prior exercise (U/l)	99 ± 29	239 ± 191	210 ± 134	226 ± 159
CPK after exercise (U/l)	95 ± 31	221 ± 183	191 ± 131	208 ± 153

Data are expressed as mean ± standard deviation.* Results were significantly different from healthy subjects (p < 0.05). A3243G: adenosine to guanine mutation at position 3243; MIDD: maternally inherited diabetes and deafness; DM: diabetes mellitus; HbA1c: glycated hemoglobin; Max: maximal; ^{31}P -MRS: 31-phosphorus magnetic resonance spectroscopy; t_{1/2}: recovery half time; Pi: inorganic phosphate; PCr: phosphocreatine; C-peptide: connecting-peptide; CPK: creatine-phosphokinase

Patient characteristics

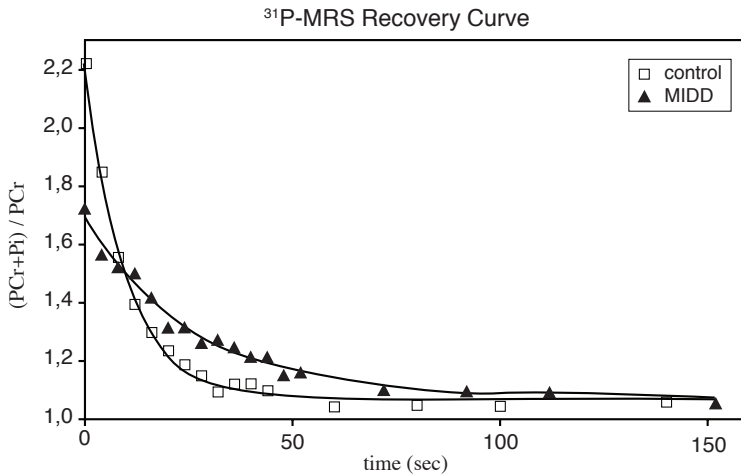
Comparison of the study groups shows similar age and body mass index (BMI) due to matching (Table 1). Four of the DM patients used insulin, one of them in combination with an oral glucose-lowering sulfonylurea derivate; the other two DM patients showed abnormal glucose levels on OGTT. HbA1C levels were significantly higher in the MIDD group, reflecting the

inclusion of MIDD patients diagnosed with DM in this group. Differences in values of maximal isokinetic potential in exercise and the subsequently used ankle loads were nonsignificant. All subjects tolerated the exercise well.

Skeletal muscle mitochondrial function

^{31}P -MRS was performed successfully and a steady state was reached in all participants. Figure 2 shows typical examples of skeletal muscle ^{31}P -MRS recovery curves of an MIDD patient and a healthy subject from which PCr recovery $t_{1/2}$ was calculated. The MIDD mitochondrial mutation showed a statistically significant association with half-time of PCr recovery after exercise (beta: 0.611, $p = 0.01$). In the multiple linear regression model no association of the presence of DM was found with $t_{1/2}$ (PCr + Pi)/PCr ($p = 0.382$).

Figure 2. Phosphorus metabolite ratio recovery curves. Example of an MIDD patient ($t_{1/2} = 18.0$ sec) and a healthy control subject ($t_{1/2} = 6.9$ sec). Solid lines indicate fitted curves.



Laboratory measurements

Glucose, insulin, and C-peptide measurements before and after exercise did not significantly differ between all groups. Lactate levels were normal in all subjects, before and after exercise. High baseline CPK levels were seen in A3243G MIDD mutation carriers (borderline significance with controls, $p = 0.058$), but in both groups CPK levels did not increase after the exercise.

DISCUSSION

This study revealed that mitochondrial function is impaired in the skeletal muscle in carriers of the MIDD mutation compared to healthy subjects. Furthermore, in the mutation carriers

no additional effect of DM on mitochondrial function was demonstrated. The latter observation, however, could be due to insufficient statistical power in the small study sample size of this rare mutation.

In the present study PCr recovery half-time was significantly prolonged in the MIDD mutation carriers as compared to healthy controls. During recovery from exercise, PCr is resynthesized as a consequence of oxidative ATP synthesis (23). Therefore, $t_{1/2}(\text{PCr}+\text{Pi})/\text{PCr}$ provides information about mitochondrial function. Our results support the studies of Chinnery et al, who observed mitochondrial dysfunction in the calf muscle in a case report (13) and in A3243G mutation families (14). However, in their study not all A3243G mutation carriers were of the MIDD phenotype, in contrast to our carefully selected MIDD patient population. Furthermore, those authors speculated that physical training or the use of coenzyme Q (12) or dichloroacetate contributed to the ^{31}P -MRS detected impaired oxidative phosphorylation rather than the mutation itself. In our study none of the participants used this medication and none were actively engaged in sports or training activities, excluding for the potential confounding effect of these factors. In the current study all participants performed individually adjusted exercise to equal the exercise level. Similar maximal isokinetic potentials at a succession of knee extensions were seen, which confirms comparable baseline physical exercise capacity between the groups. So we suggest that MIDD patients show subclinical muscular impaired mitochondrial phosphorylation. This is supported by the high CPK baseline levels in the patient group, without clinical signs of muscle weakness.

We did not find an association of DM and PCr recovery values, as no effect of DM in our MIDD patient population on skeletal oxidative phosphorylation was observed. Recently, Schrauwen-Hinderling et al (18) applied ^{31}P -MR spectroscopy in the vastus lateralis muscle to study mitochondrial function in overweight type 2 DM patients and BMI-matched control subjects. They reported a longer PCr recovery half-time in the type 2 diabetes group when compared to the control group. On the basis of their results we expected an additional effect of DM in the MIDD patient group with DM as compared to the non-DM MIDD subgroup, which was not confirmed by our results. The recently published results of de Feyter et al (15) did not show an effect of insulin resistance or type 2 DM on mitochondrial function when compared to healthy normoglycemic controls, which is in accordance with our study results. In the current study we did not perform proton MRS to further evaluate mitochondrial dysfunction and the association with insulin resistance, as shown in previous studies (15,18). Thus, the exact relationship between DM per se and skeletal muscle phosphate metabolism remains to be clarified, but our results clearly indicate an effect of the MIDD mutation itself on phosphate metabolism.

Our study has limitations. We studied a limited number of patients and controls, although the MIDD phenotype of the A3243G mutation is a very rare entity and previous reports in the literature described mainly case reports. As the mutation is not a common entity, international collaboration is required to collect larger numbers of MIDD subjects, including DM and non-DM patients.

In conclusion, the present study demonstrates subclinical mitochondrial dysfunction of the skeletal muscle in MIDD patients. The presence of DM does not seem to affect the mitochondrial function of the skeletal muscle in the MIDD population independently.

REFERENCES

1. Hansrote S, Croul S, Selak M, Kalman B, Schwartzman RJ. External ophthalmoplegia with severe progressive multiorgan involvement associated with the mtDNA A3243G mutation. *J Neurol Sci* 2002;197(1-2):63-67.
2. van den Ouweland JM, Lemkes HH, Ruitenbeek W, et al. Mutation in mitochondrial tRNA(Leu) (UUR) gene in a large pedigree with maternally transmitted type II diabetes mellitus and deafness. *Nat Genet* 1992;1(5):368-371.
3. Guillausseau PJ, Massin P, Dubois-Laforgue D, et al. Maternally inherited diabetes and deafness: a multicenter study. *Ann Intern Med* 2001;134(9 Pt 1):721-728.
4. Maassen JA. Mitochondrial diabetes: pathophysiology, clinical presentation, and genetic analysis. *Am J Med Genet* 2002;115(1):66-70.
5. Suzuki Y, Taniyama M, Muramatsu T, et al. Diabetes mellitus associated with 3243 mitochondrial tRNA(Leu(UUR)) mutation: clinical features and coenzyme Q10 treatment. *Mol Aspects Med* 1997;18 Suppl:S181-S188.
6. Takano M, Fujita N, Kamoi K, Makino K, Nagai H. [Exercises on a bicycle ergometer in a family of diabetes mellitus associated with a mutation of mitochondrial DNA]. *Rinsho Shinkeigaku* 1998;38(7):683-685.
7. Murphy R, Turnbull DM, Walker M, Hattersley AT. Clinical features, diagnosis and management of maternally inherited diabetes and deafness (MIDD) associated with the 3243A>G mitochondrial point mutation. *Diabet Med* 2008;25(4):383-399.
8. Arnold DL, Taylor DJ, Radda GK. Investigation of human mitochondrial myopathies by phosphorus magnetic resonance spectroscopy. *Ann Neurol* 1985;18(2):189-196.
9. Kuhl CK, Layer G, Traber F, Zierz S, Block W, Reiser M. Mitochondrial encephalomyopathy: correlation of P-31 exercise MR spectroscopy with clinical findings. *Radiology* 1994;192(1):223-230.
10. Mattei JP, Bendahan D, Cozzone P. P-31 magnetic resonance spectroscopy. A tool for diagnostic purposes and pathophysiological insights in muscle diseases. *Reumatismo* 2004;56(1):9-14.
11. Taylor DJ, Kemp GJ, Radda GK. Bioenergetics of skeletal muscle in mitochondrial myopathy. *J Neurol Sci* 1994;127(2):198-206.
12. Barbiroli B, Iotti S, Lodi R. Improved brain and muscle mitochondrial respiration with CoQ. An in vivo study by 31P-MR spectroscopy in patients with mitochondrial cytopathies. *Biofactors* 1999;9(2-4):253-260.
13. Chinnery PF, Taylor DJ, Brown DT, Manners D, Styles P, Lodi R. Very low levels of the mtDNA A3243G mutation associated with mitochondrial dysfunction in vivo. *Ann Neurol* 2000;47(3):381-384.
14. Chinnery PF, Taylor DJ, Manners D, Styles P, Lodi R. No correlation between muscle A3243G mutation load and mitochondrial function in vivo. *Neurology* 2001;56(8):1101-1104.
15. De Feyter HM, van den Broek NM, Praet SF, Nicolay K, van Loon LJ, Prompers JJ. Early or advanced stage type 2 diabetes is not accompanied by in vivo skeletal muscle mitochondrial dysfunction. *Eur J Endocrinol* 2008;158(5):643-653.
16. Petersen KF, Befroy D, Dufour S, et al. Mitochondrial dysfunction in the elderly: possible role in insulin resistance. *Science* 2003;300(5622):1140-1142.

17. Schrauwen-Hinderling VB, Roden M, Kooi ME, Hesselink MK, Schrauwen P. Muscular mitochondrial dysfunction and type 2 diabetes mellitus. *Curr Opin Clin Nutr Metab Care* 2007;10(6):698-703.
18. Schrauwen-Hinderling VB, Kooi ME, Hesselink MK, et al. Impaired in vivo mitochondrial function but similar intramyocellular lipid content in patients with type 2 diabetes mellitus and BMI-matched control subjects. *Diabetologia* 2007;50(1):113-120.
19. Szendroedi J, Schmid AI, Chmelik M, et al. Muscle mitochondrial ATP synthesis and glucose transport/phosphorylation in type 2 diabetes. *PLoS Med* 2007;4(5):e154.
20. Vanhamme L, van den Boogaart A, van Huffel S. Improved method for accurate and efficient quantification of MRS data with use of prior knowledge. *J Magn Reson* 1997;129(1):35-43.
21. Kemp GJ, Meyerspeer M, Moser E. Absolute quantification of phosphorus metabolite concentrations in human muscle in vivo by 31P MRS: a quantitative review. *NMR Biomed* 2007;20(6):555-565.
22. Kushmerick MJ, Meyer RA, Brown TR. Regulation of oxygen consumption in fast- and slow-twitch muscle. *Am J Physiol* 1992;263(3 Pt 1):C598-C606.
23. Quistorff B, Johansen L, Sahlin K. Absence of phosphocreatine resynthesis in human calf muscle during ischaemic recovery. *Biochem J* 1993;291 (Pt 3):681-686.

Chapter 9

Initial results on in vivo human coronary MR angiography at 7 Tesla

SGC van Elderen, MJ Versluis, AG Webb, JJM Westenberg,
J Doornbos, NB Smith, A de Roos, M Stuber

Magnetic Resonance in Medicine 2009;62(6):1379-1384

ABSTRACT

Seven Tesla (T) MR imaging is potentially promising for the morphologic evaluation of coronary arteries because of the increased signal-to-noise ratio compared to lower field strengths, in turn allowing improved spatial resolution, improved temporal resolution, or reduced scanning times. However, there are a large number of technical challenges, including the commercial 7 T systems not being equipped with homogeneous body radiofrequency coils, conservative specific absorption rate constraints, and magnified sample-induced amplitude of radiofrequency field inhomogeneity. In the present study, an initial attempt was made to address these challenges and to implement coronary MR angiography at 7 T. A single-element radiofrequency transmit and receive coil was designed and a 7 T specific imaging protocol was implemented, including significant changes in scout scanning, contrast generation, and navigator geometry compared to current protocols at 3 T. With this methodology, the first human coronary MR images were successfully obtained at 7 T, with both qualitative and quantitative findings being presented.

INTRODUCTION

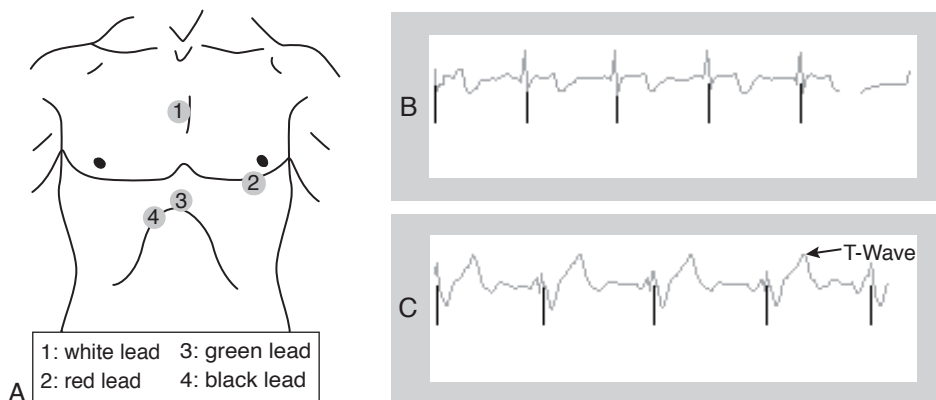
Coronary magnetic resonance angiography (MRA) has been shown to be a promising tool for the noninvasive identification of significant proximal coronary artery disease (1,2). The most commonly used magnetic field strength for coronary MRA is 1.5 Tesla (T), involving many years of sequence, parameter, and radiofrequency (RF) coil optimization. In common with many MRI applications, the use of higher magnetic field strengths for coronary MRA is attractive, with advantages arising from increases in signal-to-noise ratio (SNR), smaller voxel sizes, a higher temporal resolution, and/or shortened scanning times. Individually or in combination, these improvements are likely to result in improved image quality and ultimately better access to small diameter and branching vessels. As a first step in this direction, implementation of coronary MRA at 3 T has been found to result in increased SNR, increased contrast-to-noise ratio, and increased measured coronary vessel lengths compared to 1.5 T (3-5). Voxel sizes as low as $0.35 \times 0.35 \times 1.5 \text{ mm}^3$ have been obtained at 3 T (6) in selected cases. Although initial studies comparing 1.5 T coronary MRA with 3 T coronary MRA and the gold standard x-ray coronary angiography showed little advantage of 3 T for the identification of significant luminal coronary artery disease, a more recent report (4) appears much more promising, and other studies that take advantage of new high-field specific improvements are ongoing. Notably, the increase in magnetic field strength between 1.5 and 3 T produces a series of challenges, including adequate electrocardiograph (ECG) triggering (7), sophisticated higher-order shimming (8) to account for increased magnetic field susceptibility, and spatially homogeneous magnetization preparation for contrast generation (9).

Given the promising indicators at 3 T, the recent availability of commercial human whole-body high-field 7 T MR systems might offer great potential for cardiovascular imaging in general (10). However, because of the large resonance frequency increase between 3 T and 7 T, roughly three times that between 1.5 T and 3 T, considerable challenges are expected for cardiovascular studies at 7 T. Initial feasibility for cardiac MRI at 7 T has been demonstrated by Snyder et al. (10), who showed a series of very promising anatomic and functional cardiac scans in normal volunteers, using a highly sophisticated multiple-transmit array. In the present paper, we investigated the feasibility of coronary MRA in humans at 7 T. The methodology adopted was to use a custom-built RF transmit and receive surface coil, a 7 T specific scout scanning approach, specific navigator adaptations, and segmented gradient echo free-breathing three-dimensional (3D) coronary MRA with adiabatic inversion recovery for fat saturation.

MATERIALS AND METHODS

All imaging protocols were approved by the Leiden University Medical Center medical ethics committee. Ten healthy adult volunteers (seven men, age 32.7 ± 8.1 years) without known history of cardiovascular disease, were studied on a commercial human whole-body 7 T MR system (Philips Achieva; Philips Healthcare, Best, The Netherlands). The MR system is equipped with a commercial vector ECG module (7). The electrodes of the vector ECG were placed at the anterior chest wall, with two electrodes on the sternum, one electrode on the left thorax, and one below the sternum, as shown in Figure 1a. All subjects were positioned head first and in the supine position in the magnet.

Figure 1. Electrocardiogram at 7 T. The position of the four ECG electrodes (dots) on the thorax is shown in (a). A normal ECG signal from outside (b) and inside (c) the 7 T magnet is shown with enhanced T-wave (arrow) due to the magneto-hydrodynamic effect. Despite the amplified artifactual signal on the T-wave, R-wave triggering was reliable, as demonstrated by the vertical black lines that indicate the computer-identified position of the R-wave.



RF coil

For coronary imaging, a 13-cm-diameter RF transmit and receive surface coil was developed for operation at 298.1 MHz. The coil was constructed using copper tape with a width of 1.6 cm (3M, Minneapolis, MN). Eight segments, with a length of 4.3 cm each, were segmented by 5.1-pF nonmagnetic capacitors (ATC, Series B, Huntington Station, NY). Three variable capacitors (1-40 pF; Johansson, Camarillo, CA) were used for fine tuning and impedance matching in a balanced configuration. A lattice balun was used to improve the balancing of the coil. The coil was constructed in an end-on configuration to reduce electric field coupling to the patient (11). In addition, short lengths of copper foil were placed on the plastic former between the capacitors and the patient to reduce the conservative electric fields within the patient. Finally, a 1-cm-diameter gap between the coil and patient was introduced using foam rubber

to reduce patient-induced losses (12). The RF coil was connected via an RG-58 cable to the interface box of the scanner. The patient loading of the coil was dominant, with a loaded-to-unloaded Q-ratio of 1:10, and the coil was well matched to 50 ohm for all of the subjects irrespective of body size. Therefore, there was no need for manual adjustment for individual subjects, although the use of variable capacitors does leave the option open. Amplitude of RF field (B_1) homogeneity was tested using a phantom that was filled with mineral oil: the sensitivity pattern usual for this coil size was obtained (data not shown). Specific absorption rate (SAR) calculations were based upon previous work by Collins and Smith (13), using the appropriate scaling factors outlined in the publication. The RF pulses were calibrated by measuring the flip angle averaged over an aligned slice through the center of the imaging volume, which results in a more accurate flip angle calibration than the standard scheme where the flip angle is measured in a transverse plane through the isocenter of the magnet.

Coronary MR angiography

Coronary MR angiography was performed as follows: one low-resolution scout scan preceded a two-dimensional (2D) axial multislice cine scout scan and volume-targeted 3D coronary MRA.

Scout scans

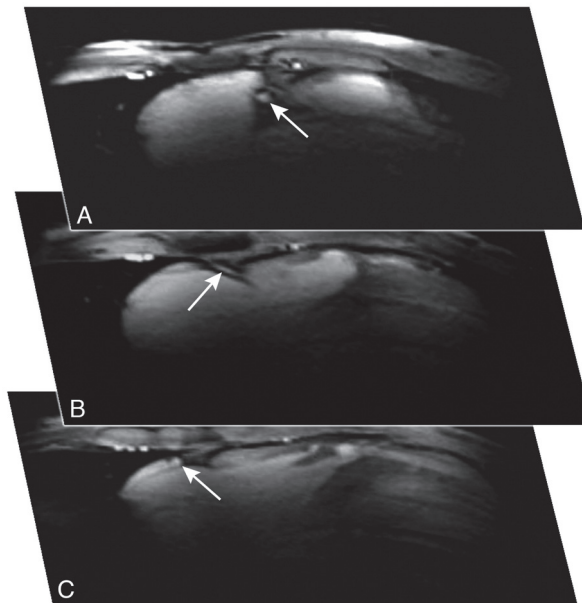
Two scout scans were acquired to localize the navigator volume for identification of the period of minimal coronary motion and for anatomic localization of the right coronary artery (RCA).

The first scout scan was a multistack, 2D, segmented, k-space, gradient-echo acquisition obtained in coronal, axial, and sagittal orientations. The images were collected without ECG triggering during free breathing of the volunteers (pulse repetition time = 4.0 ms, echo time = 1.82 ms, RF excitation angle = 20°, acquisition matrix = 192 × 96, reconstruction matrix = 256 × 256, field of view = 450 × 450 mm², slice thickness = 10 mm, no slice gap, 20 slices per stack, scan duration ~25 sec). This scout scan was utilized for scan plane localization of the subsequent cine scout scan and for the localization of the 2D selective navigator.

After the first scout scan, an ECG-triggered, multislice, 2D, axial cine scout scan (Figure 2) was localized using the coronal images of the first scout. This scan replaces the low-resolution whole-heart 3D scout scan that is commonly used for the identification and volume targeting of the coronaries at 3 T. However, since the use of standard T_2 preparation (9,14) was impractical at 7 T due to conservative SAR constraints, an alternative mechanism for improved visualization of the coronaries was required. This was accomplished by taking advantage of the in-flow contrast on 2D cine images. Therefore, the second scout was performed using a retrospectively ECG-gated, segmented, k-space, gradient-echo, cine imaging sequence. Thirty-three cine acquisitions per RR interval were obtained, resulting in a temporal resolution of ~25-35 ms, dependent on individual heart rate. Ten 8-mm-thick slices with a slice gap

of 4 mm covered the whole heart from base to apex in an axial plane (pulse repetition time = 4.0 ms, echo time = 2.4 ms, RF excitation angle = 15°, breath-hold duration ~15 sec per slice). This scan was utilized for the identification of the period of minimal coronary motion needed for identifying the acquisition time delay (= trigger delay) and for volume targeting of the subsequent 3D stack in parallel to the RCA.

Figure 2. Multislice 2D axial cine scout scans. Multislice cine scout scans were acquired in an axial plane covering the whole heart. The figure shows selected images at multiple anatomic levels: basal (a), midventricular (b), and closer to the apex (c). The RCA (arrows) was visually identified at the period of minimal coronary motion in these slices. Subsequently, a three-point-plan-scan tool was used for volume targeting in parallel to the RCA.



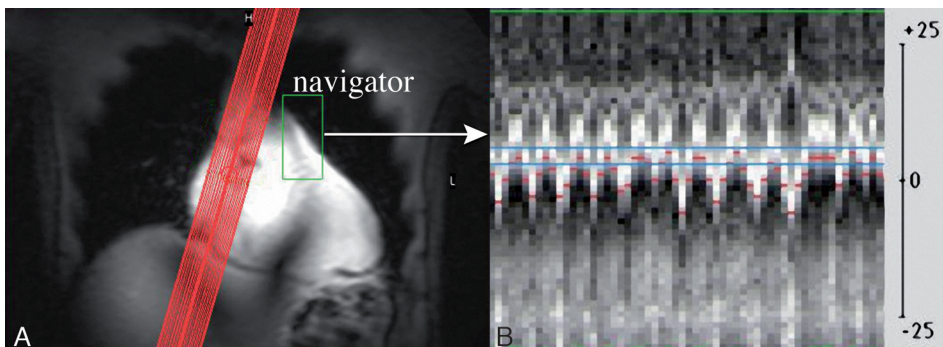
3D coronary MRA

Scan plane localization for volume-targeted 3D MRA of the RCA was performed on the multislice cine scout scans. In cine slices at multiple anatomic levels (basal (Figure 2a), midventricular (Figure 2b) and closer to the apex (Figure 2c)), the RCA was identified at time point trigger delay. Subsequently, a previously described three-point-plan-scan tool (15) was used for volume targeting of the stack in parallel to the RCA. A 3D segmented k-space gradient-echo sequence was used with prospective ECG triggering. In total, 15 slices with a slice thickness of 4 mm were acquired and reconstructed to thirty 2-mm-thick slices. A field of view of $420 \times 269 \text{ mm}^2$ and a scan matrix of 512×312 led to an in-plane voxel size of $0.82 \times 0.86 \text{ mm}^2$. The RF excitation angle was 15°, pulse repetition time = 4.3 ms, echo time = 1.4 ms, signal readout bandwidth = 335 Hz/pixel, and the duration of the acquisition window was

116 ms. The 3D volume-targeted coronary MRA data were acquired during free breathing, using prospective navigator gating and tracking. The 2D selective navigator was localized at the anterior wall of the left ventricle (16), as identified in the coronal (Figure 3a) and sagittal images of the first scout scan. To minimize T_2^* -related susceptibility artifacts on the navigator signal, the duration of the 2D selective navigator RF pulse was shortened from 7 ms in the 3 T protocol to 4.4 ms by reducing the number of cycles in k-space from 16 to eight. The navigator gating window was 3-5 mm, and both RF excitation and signal reception for the navigator were obtained with the local RF transmit and receive surface coil. Since the navigator was localized at the heart and not at the lung-liver interface, a correction factor of 1.0, rather than the conventional 0.6 (17), was used.

Contrast enhancement between the coronary lumen blood pool and the epicardial fat was obtained by using a spectrally selective adiabatic RF inversion pulse for fat suppression. The duration of this pulse was 18 ms, the B_1 was 7.3 μ T, and the center frequency was -850 Hz relative to the water resonance frequency (f_0). The pulse was adiabatic over a range of B_1 values, with a lower limit of 60% of the expected B_1 . The bandwidth was 800 Hz, which represents a tradeoff between the measured line width of the water and fat peaks after shimming and the adiabaticity of the pulse. In a few initial volunteers, the time delay between this fat saturation prepulse and data acquisition at the center of k-space that leads to the best visual fat suppression was experimentally determined. A spectrally selective adiabatic RF inversion pulse with an inversion time of 200 ms was found to null the signal from fat effectively. The fat saturation prepulse preceded the navigator not only to reduce the fat signal for the navigator signal readout but also to minimize the time delay between the navigator and the imaging part of the sequence (18). First-order local volume shimming in a volume of $50 \times 140 \times 50$ mm localized at the level of the RCA was performed in all cases. The off-center and angulations of the shim volume were identical to that of the imaged volume.

Figure 3. Navigator gating at 7 T. a: A coronal scout scan with the navigator (rectangle) positioned at the left heart-lung interface is shown. The scan plane (contiguous slices) localized in parallel to the RCA is visible. The navigator signal received from the 2D selective excitation is shown in (b). The navigator window width was 3 mm, which resulted in a navigator efficiency of 36% in this example.



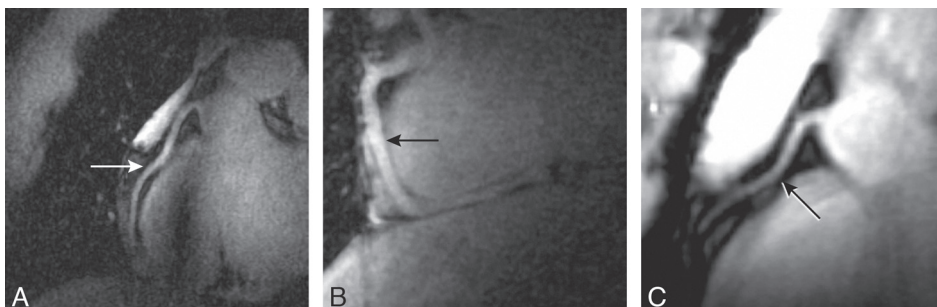
Postprocessing

3D coronary MRAs were reformatted using the “Soapbubble” tool (19). Measurements of vessel length, diameter, and sharpness (19) of the first 4 cm of the RCA were subsequently performed. SNR of the blood was measured for the RCA and the left main coronary artery (LM) as described before (20) if it could be identified on the image. The difference in SNR between RCA and LM was compared using a paired Student’s t test. A p value of <0.05 was considered statistically significant.

RESULTS

Images of the RCA were successfully obtained in nine of the 10 subjects, with a total 3D coronary MRA scan duration of 232 ± 36 sec. In one volunteer, data collection could not be completed due to navigator failure related to insufficient SNR of the navigator signal. Quantitative coronary length, diameter, and vessel sharpness measurements could be performed in all 3D coronary MRA. However, the LM could only successfully be identified and used for subsequent SNR analysis in six out of the nine available datasets because of rapid signal drop-off more distant from the surface coil. The average contiguous length of the RCA was 66 ± 38 mm, and the average diameter of the first 4 cm of the RCA was 2.8 ± 0.4 mm, with an average vessel sharpness of $49 \pm 10\%$. The SNR of the RCA was 18.1 ± 3.4 , and that of the LM 8.3 ± 1.5 ($p < 0.001$). Representative examples of MR images of the RCA obtained at 7 T are displayed in Figure 4, which shows sharply delineated contiguous segments with good contrast between the coronary lumen blood pool and the epicardial fat.

Figure 4. Representative examples of MR images of the RCA obtained at 7 T. Proximal (a,c) and more distal (b) segments of the RCA are visualized. The 13-cm RF transmit and receive coil provides sufficient penetration depth to visualize a considerable RCA segment length. Sharply delineated contiguous coronary segments with good contrast between the coronary lumen blood pool and the epicardial fat are shown.



The 13-cm-diameter RF transmit and receive surface coil was sufficient to cover the heart in the superior-inferior and left-right direction, but the coverage was limited in the anterior-

posterior direction. The coil coverage supported adequate scan planning, navigator gating and tracking, and 3D data acquisition of the RCA. The RF penetration depth of the surface coil was also sufficient to follow the RCA for a considerable distance, as shown in Figure 4. The coil coverage was not large enough for the simultaneous visualization of the RCA, LM, left anterior descending, and the left circumflex coronary arteries. Although the effects of B_1 inhomogeneity were visible in the scout images and in certain areas of the coronary MRA, this did not adversely affect the regions in which the RCA was visible.

Despite a significantly amplified magneto-hydrodynamic effect at 7 T that led to considerable artificial augmentation of the T-wave of the ECG, the vector ECG algorithm allowed reliable R-wave triggering in all subjects. Representative ECG traces are shown in Figure 1, where the recordings from outside (Figure 1b) and inside (Figure 1c) the magnet are displayed. In Figure 1c, the artifactual T-wave augmentation is clearly visible, as indicated by the arrow.

With the navigator volume localized at the anterior wall of the left ventricle, the navigator could adequately track breathing motion, resulting in a navigator efficiency between 36 and 82% (mean $70 \pm 16\%$). In Figure 2b the navigator signal received by the surface coil is shown.

DISCUSSION

This initial report demonstrates that in vivo human right coronary MRA is feasible on a commercial high-field 7 T scanner equipped with a custom-built RF transmit and receive cardiac surface coil. The present study, to our knowledge, is the first to report on coronary MRA at this field strength. These findings complement those from a recently published study by Snyder et al. (10), in which successful in vivo human anatomic and cardiac cine imaging was demonstrated at 7 T.

The 7 T coronary MR images allowed quantitative measurements of RCA length and diameter, as well as vessel sharpness. While we did not perform a direct comparison with lower-field-strength coronary MRA, the 7 T scanning time was similar to that of earlier reports performed at lower field strength (21,22) and without parallel imaging. However, and using the present 7 T approach, an increased visible vessel length and a higher image quality may be expected at both 1.5 T (20) and 3 T (5). Nevertheless, measurements of RCA diameter and vessel sharpness were similar to those reported in an early study on in vivo human coronary MRA at 3 T (23).

When compared to contemporary 1.5 T or 3 T protocols, the current 7 T methodology was different in that a local RF transmit and receive surface coil with limited volumetric coverage was utilized, and in that both the scout scanning approach and the coronary MRA data collection had to be adapted, primarily due to SAR constraints. These conservative SAR constraints at 7 T limit the use of more common cardiac pulse sequences and certainly remove flexibility for pulse sequence design. The use of steady state free precession sequences with

T_2 -preparation considerably augments image quality in comparison to 3D gradient echo sequences (24) at 1.5 T and is currently the most commonly used technique at 1.5 T. However, implementation of steady state free precession sequences at higher field strength is challenging due to increased magnetic susceptibility, banding artifacts, and SAR constraints that limit the use of minimal pulse repetition time. While sophisticated higher-order shimming approaches have helped to improve image quality for steady state free precession at 3 T (8), most of the research with (25) and without contrast agents at 3 T is currently done with more conventional segmented k-space gradient echo imaging sequences. Since amplitude of static field inhomogeneity and SAR constraints are already limiting factors for steady state free precession at 3 T, its adoption for 7 T use is currently not straightforward. For these reasons, a segmented k-space gradient echo technique similar to that described in this article will most likely be the method of choice for future coronary MRA implementations at 7 T. Successful contrast enhancement mechanisms at 1.5 T include T_2 -preparation (14,26) and inversion recovery (27), in combination with contrast agents. While inversion recovery in combination with slow contrast infusion was very successful at 3 T (25), the use of conventional T_2 -preparation is more challenging and an adiabatic version of the T_2 -preparation had to be developed to account for amplitude of static field and B_1 inhomogeneities at 3 T. However, at 7 T, the SAR constraints on our system did not permit the use of an adiabatic T_2 -preparation for contrast generation. Therefore, the slow infusion approach described by Liu et al. (4) holds great promise at 7 T but remains to be explored. Similarly, spin labeling techniques that do not depend on two acquisitions and subtraction, as that described by Katoh et al. (28), may be valuable alternatives that deserve further investigation.

The RF penetration depth of the surface coil was sufficient for coverage of the proximal segments of the RCA, but more distal segments may not easily be visualized. The coil coverage was also not large enough for the simultaneous visualization of the left coronary arterial system. The lower SNR of the LM when compared to the RCA confirms a signal loss in the region of the left coronary arterial system that is more distant from the surface coil. This is attributable to both limited RF penetration and coil sensitivity of the small-diameter transmit and receive coil. Therefore, the development of larger surface coils or coil arrays will be critical to improve volumetric coverage (10). The RF coil setup used in these initial experiments is extremely simple. This has both advantages and disadvantages. Recent studies have shown that homogeneous transmit fields can be produced using transmit arrays and sophisticated B_1 shimming routines (29). Although this represents the optimum strategy, it does require hardware that is not yet standard on most commercial MRI scanners, and it currently necessitates the development of sophisticated hardware and software interfaces. No doubt, such hardware will become more widely available on commercial systems. However, the aim of this article was to demonstrate feasibility of motion-compensated 3D coronary MRA data acquisition at 7 T with an RF transmit and receive surface coil architecture that is relatively straightforward to construct and which can be easily interfaced with a commercial 7-T system.

Both intrinsic cardiac and extrinsic respiratory motion suppression was effective at 7 T. Augmented T-waves of the ECG were observed in all subjects while positioned in the magnet. However, with careful positioning of the ECG leads, the vector ECG module enabled reliable R-wave detection, despite the high magnetic field strength. A reduction in the duration of the navigator RF pulse compared to that used at 3 T helped to minimize T_2^* -related susceptibility artifacts on the navigator signal and improved navigator performance. While the diameter of the 2D selective RF pulse remained unchanged, increased aliasing of the navigator signal may be expected. However, due to the limited sensitivity of the surface coil outside the heart, this is a minor concern. Nevertheless, this will have to be revisited if larger coils or coil arrays will be used, and dedicated navigator signal receive coils (23) may have to be exploited to account for that problem. Because of the relatively small field of view of the 13-cm surface coil, the right hemidiaphragm was outside the field of view, and therefore navigator localization at the lung-liver interface was not practical. With the navigator localized at the anterior wall of the left ventricle, a workaround was found and adequate respiratory motion suppression was ensured. However, this strategy works only for 2D selective excitations with small RF excitation angles. Navigators that consist of echoes obtained from intersecting planes may not be useful since the presence of local signal voids has to be considered. Finally, the navigator efficiency was quite high when compared to that commonly reported at lower magnetic field strength. However, in the present report, the navigator was localized directly at the heart-lung interface where the respiration-induced motion in the foot-head direction is reduced when compared to that at the lung-liver interface. This may have contributed to improved navigator efficiency.

The use of 3D-segmented gradient echo sequences with relatively short echo times and spectrally selective adiabatic RF inversion pulses for fat suppression enabled this initial feasibility study of coronary MRA at 7 T. No direct comparison with data obtained at lower magnetic field strength was performed and no patient data were collected.

Neither a higher spatial resolution, temporal resolution, nor an abbreviated scanning time was obtained when compared to lower field strengths. However, the purpose of this initial study was to test feasibility of coronary MR angiography at 7 T. To fully benefit from the potential for improved image quality at 7 T, the limits of spatial resolution and temporal resolution remain to be explored as methodology advances. Nevertheless, significant challenges have been addressed, and it has been demonstrated that coronary MRA at 7 T can be successfully obtained. Future steps include the design of improved RF transmit/receive coils in conjunction with novel approaches to pulse sequence design.

CONCLUSION

This initial report demonstrates feasibility of 3D motion compensated in vivo human right coronary MRA at 7 T while quantitative measurements of RCA length, diameter, vessel sharpness, and SNR could successfully be obtained. The combination of a home-built RF transmit and receive surface coil, vector ECG hardware, navigator adaptations, specifically designed scout scanning procedures, segmented k-space gradient echo imaging, and adiabatic inversion of the magnetization for fat suppression was critical to address some of the 7 T specific challenges. Further improvements in coil design and a strong focus on contrast enhancement mechanisms will critically support continued progress.

REFERENCES

1. Kim WY, Danias PG, Stuber M, et al. Coronary magnetic resonance angiography for the detection of coronary stenoses. *N Engl J Med* 2001;345(26):1863-1869.
2. Sakuma H, Ichikawa Y, Chino S, Hirano T, Makino K, Takeda K. Detection of coronary artery stenosis with whole-heart coronary magnetic resonance angiography. *J Am Coll Cardiol* 2006;48(10):1946-1950.
3. Bi X, Deshpande V, Simonetti O, Laub G, Li D. Three-dimensional breathhold SSFP coronary MRA: a comparison between 1.5T and 3.0T. *J Magn Reson Imaging* 2005;22(2):206-212.
4. Liu X, Bi X, Huang J, Jerecic R, Carr J, Li D. Contrast-enhanced whole-heart coronary magnetic resonance angiography at 3.0 T: comparison with steady-state free precession technique at 1.5 T. *Invest Radiol* 2008;43(9):663-668.
5. Sommer T, Hackenbroch M, Hofer U, et al. Coronary MR angiography at 3.0 T versus that at 1.5 T: initial results in patients suspected of having coronary artery disease. *Radiology* 2005;234(3):718-725.
6. Ustun A, Desai M, Abd-Elmoniem KZ, Schar M, Stuber M. Automated identification of minimal myocardial motion for improved image quality on MR angiography at 3 T. *AJR Am J Roentgenol* 2007;188(3):W283-W290.
7. Fischer SE, Wickline SA, Lorenz CH. Novel real-time R-wave detection algorithm based on the vectorcardiogram for accurate gated magnetic resonance acquisitions. *Magn Reson Med* 1999;42(2):361-370.
8. Schar M, Kozerke S, Fischer SE, Boesiger P. Cardiac SSFP imaging at 3 Tesla. *Magn Reson Med* 2004;51(4):799-806.
9. Nezafat R, Stuber M, Ouwerkerk R, Gharib AM, Desai MY, Pettigrew RI. B1-insensitive T2 preparation for improved coronary magnetic resonance angiography at 3 T. *Magn Reson Med* 2006;55(4):858-864.
10. Snyder CJ, Delabarre L, Metzger GJ, et al. Initial results of cardiac imaging at 7 Tesla. *Magn Reson Med* 2009;61(3):517-524.
11. Ong KC, Wen H, Chesnick AS, DUEWELL S, Jaffer FA, Balaban RS. Radiofrequency shielding of surface coils at 4.0 T. *J Magn Reson Imaging* 1995;5(6):773-777.
12. Suits BH, Garroway AN, Miller JB. Surface and gradiometer coils near a conducting body: the lift-off effect. *J Magn Reson* 1998;135(2):373-379.
13. Collins CM, Smith MB. Calculations of B(1) distribution, SNR, and SAR for a surface coil adjacent to an anatomically-accurate human body model. *Magn Reson Med* 2001;45(4):692-699.
14. Brittain JH, Hu BS, Wright GA, Meyer CH, Macovski A, Nishimura DG. Coronary angiography with magnetization-prepared T2 contrast. *Magn Reson Med* 1995;33(5):689-696.
15. Stuber M, Botnar RM, Danias PG, et al. Double-oblique free-breathing high resolution three-dimensional coronary magnetic resonance angiography. *J Am Coll Cardiol* 1999;34(2):524-531.
16. Stuber M, Botnar RM, Danias PG, Kissinger KV, Manning WJ. Submillimeter three-dimensional coronary MR angiography with real-time navigator correction: Comparison of navigator locations. *Radiology* 1999;212(2):579-587.

17. Wang Y, Riederer SJ, Ehman RL. Respiratory motion of the heart: kinematics and the implications for the spatial resolution in coronary imaging. *Magn Reson Med* 1995;33(5):713-719.
18. Spuentrup E, Manning WJ, Botnar RM, Kissinger KV, Stuber M. Impact of navigator timing on free-breathing submillimeter 3D coronary magnetic resonance angiography. *Magn Reson Med* 2002;47(1):196-201.
19. Etienne A, Botnar RM, van Muiswinkel AM, Boesiger P, Manning WJ, Stuber M. "Soap-Bubble" visualization and quantitative analysis of 3D coronary magnetic resonance angiograms. *Magn Reson Med* 2002;48(4):658-666.
20. Roes SD, Korosoglou G, Schar M, et al. Correction for heart rate variability during 3D whole heart MR coronary angiography. *Journal of Magnetic Resonance Imaging* 2008;27(5):1046-1053.
21. Gharib AM, Herzka DA, Ustun AO, et al. Coronary MR angiography at 3T during diastole and systole. *J Magn Reson Imaging* 2007;26(4):921-926.
22. Huber ME, Kozerke S, Pruessmann KP, Smink J, Boesiger P. Sensitivity-encoded coronary MRA at 3T. *Magnetic Resonance in Medicine* 2004;52(2):221-227.
23. Stuber M, Botnar RM, Fischer SE, et al. Preliminary report on in vivo coronary MRA at 3 Tesla in humans. *Magnetic Resonance in Medicine* 2002;48(3):425-429.
24. Spuentrup E, Katoh M, Buecker A, et al. Free-breathing 3D steady-state free precession coronary MR angiography with radial k-space sampling: Comparison with cartesian k-space sampling and cartesian gradient-echo coronary MR angiography - Pilot study. *Radiology* 2004;231(2):581-586.
25. Bi X, Carr JC, Li D. Whole-heart coronary magnetic resonance angiography at 3 Tesla in 5 minutes with slow infusion of Gd-BOPTA, a high-relaxivity clinical contrast agent. *Magn Reson Med* 2007;58(1):1-7.
26. Botnar RM, Stuber M, Danias PG, Kissinger KV, Manning WJ. Improved coronary artery definition with T2-weighted, free-breathing, three-dimensional coronary MRA. *Circulation* 1999;99(24):3139-3148.
27. Deshpande VS, Cavagna F, Maggioni F, Schirf BE, Omary RA, Li D. Comparison of gradient-echo and steady-state free precession for coronary artery magnetic resonance angiography using a gadolinium-based intravascular contrast agent. *Invest Radiol* 2006;41(3):292-298.
28. Katoh M, Spuentrup E, Barmet C, Stuber M. Local re-inversion coronary MR angiography: arterial spin-labeling without the need for subtraction. *J Magn Reson Imaging* 2008;27(4):913-917.
29. Vaughan TT, Snyder CJ, DelaBarre LJ, et al. Whole-body imaging at 7T: preliminary results. *Magnetic Resonance in Medicine* 2009;61(1):244-248.

Chapter 10

Right coronary MR angiography at 7 Tesla: a direct quantitative comparison with 3 Tesla in young healthy volunteers

SGC van Elderen, MJ Versluis, JJM Westenberg, H Agarwal,
NB Smith, M Stuber, A de Roos, AG Webb

Radiology 2010;257(1):254-259

ABSTRACT

Purpose

To objectively compare parameters related to image quality of coronary magnetic resonance angiography (MRA) of the right coronary artery (RCA) obtained with 7 Tesla (T) and 3 T MRI.

Materials and Methods

Approval from our institutional review board was obtained, and participants gave informed consent. Ten healthy adult subjects (mean age 25 ± 4 years, 7 men) underwent navigator-gated 3D MRA of the RCA at 7 T and 3 T. For 7 T, a custom-built quadrature radiofrequency (RF) transmit/receive surface coil was utilized. At 3 T, a commercial body RF transmit coil and a cardiac coil array for signal reception were used. Segmented k-space gradient echo imaging with spectrally selective adiabatic fat suppression was performed and scan parameters were similar at both field strengths. Contrast-to-noise ratio (CNR) between blood and epicardial fat, signal-to-noise ratio (SNR) of the blood-pool, RCA vessel sharpness, diameter and length as well as navigator efficiency were quantified at both field strengths and compared using Mann-Whitney-U test.

Results

The CNR between blood and epicardial fat was significantly improved at 7 T when compared to 3 T (87 ± 34 versus 52 ± 13 , $p=0.01$). SNR of the blood-pool was increased at 7 T (109 ± 47 versus 67 ± 19 , $p=0.02$). Vessel sharpness obtained at 7 T was also higher ($58 \pm 9\%$ versus $50 \pm 5\%$, $p=0.04$). Simultaneously RCA vessel diameter, length and navigator efficiency showed no significant field strength dependent difference.

Conclusion

In our quantitative and qualitative study comparing in vivo human imaging of the RCA at 7 T and 3 T in young healthy volunteers, parameters related to image quality obtained at 7 T equal or surpass those from 3 T.

INTRODUCTION

Currently, relatively few (~40) seven Tesla (T) magnetic resonance imaging (MRI) systems are available for human use to our knowledge, most of them situated in research centers. High field cardiac MRI was initially thought to be very problematic due to magnetic field inhomogeneity and specific absorption rate (SAR) constraints. Further, contemporary commercial 7 T units are not routinely equipped with body radiofrequency (RF) transmit coils or surface RF receive coils. Despite these major challenges, a number of research groups have already demonstrated the feasibility of cardiac imaging at 7 T and beyond (1-5). Initial attempts focusing on coronary artery imaging at 7 T have shown that these barriers can successfully be removed and initial in vivo human images were very promising (6). While these early 7 T studies were conducted using single channel RF transmit/receive coil architecture, recent advances in surface coil technology seem particularly promising. However, and while an improvement in image quality may be expected at higher magnetic field strength (7), there have been no reports to our knowledge on cardiac MR imaging studies that directly and objectively compare parameters related to image quality at 7 T with those obtained at lower field strength.

Therefore, the purpose of our study was to objectively compare quantitative parameters related to image quality of coronary MRA of the right coronary artery (RCA) obtained at 7 T and 3 T.

MATERIALS AND METHODS

Our study was approved by our institutional review board and all volunteers signed informed consent. Three-dimensional MRA of the right coronary system was performed in 10 healthy adult young subjects (mean age 25 ± 4 years, 3 women) scanned at 7 T and 3 T (Philips Achieva; Philips Healthcare, Best, NL) in a prospective study design. For practical reasons, 7 T scanning always occurred prior to 3 T MRI. Coronary MRA were acquired with prospective navigator technology and vector ECG-triggering (8). All volunteers were studied in head-first and supine position. None of the volunteers received nitroglycerin before MRI. The interval between the two examinations was 8 ± 5 weeks on average.

7 T imaging

A quadrature transmit/receive surface coil consisting of two overlapping loops (13 cm diameter each) was constructed in-house (Figure 1). The coil size is larger than described previously (4,6) to improve volumetric coverage. First, a non-ECG triggered scout scan in coronal, axial and sagittal orientations was acquired to plan subsequent scans and to localize the 2D selective navigator. At 7 T, the navigator was placed at the lung-heart interface because of the

Figure 1. The custom-built quadrature RF transmit/receive surface coil consisting of two 13 cm elements used for our study at 7 T is shown.



limited sensitive volume of the surface coil. Secondly, an ECG-triggered, breath-hold multi-slice axial cine scout scan was performed for both the determination of the period of minimal coronary motion (=trigger delay) and volume targeting of the 3D stack in parallel to the mid-diastolic RCA. Finally, volume-targeted coronary MRA was obtained using a 3D segmented k-space gradient echo imaging technique (parameters Table 1) combined with a spectrally selective adiabatic inversion recovery (SPAIR) pulse (TI=200 ms) for fat saturation. First-order local volume shimming at the anatomical level of the RCA was performed in all cases.

3 T imaging

On the 3 T system, the body coil was used for RF transmission, with a commercial six-element cardiac coil array for signal reception. Scout scanning included a free-breathing, retrospectively ECG-gated, 2D cine balanced turbo-gradient echo scan in a horizontal long-axis view (4-chamber) to determine the trigger delay. Further, an ECG-triggered free-breathing navigator gated and corrected 3D gradient echo whole heart scan was obtained for the anatomical localization of the RCA. After scout scanning, two coronary imaging sequences were performed at 3 T with different navigator localization in random order; 1.) with navigator localization at the lung-heart interface (navigator at heart), 2.) with navigator localization at the lung-liver interface (navigator at liver). Both 3 T coronary imaging sequences consisted of a 3D segmented k-space gradient echo technique with SPAIR (TI=150 ms) for fat saturation. The coronary MRA scan parameters were very similar (Table 1) at both field strengths to support a fair quantitative comparison.

Table 1. Scan parameters of the coronary MRA sequences at 7 T and 3 T

Field strength	7 Tesla	3 Tesla	3 Tesla
Sequence	3D gradient echo	3D gradient echo	3D gradient echo
Navigator position / correction factor	Lung-heart interface / 1.0	Lung-heart interface / 1.0	Lung-liver interface / 0.6
Coil	Quadrature two-element surface coil transmit/receive	Body coil transmit / six-element phased array receive	Body coil transmit / six-element phased array receive
Fat suppression	Adiabatic SPIR	Adiabatic SPIR	Adiabatic SPIR
TR (ms)	4.3	4.3	4.3
TE (ms)	1.38	1.38	1.38
TI (ms)	200	150	150
Acquired voxel size (mm ³)	0.82x0.86x2.00	0.82x0.86x2.00	0.82x0.86x2.00
Reconstructed voxel size (mm ³)	0.82x0.82x1.00	0.82x0.82x1.00	0.82x0.82x1.00
Number of slices	30	30	30
Field of view (mm ²)	420x268	420x269	420x269
Matrix	512x312	512x312	512x312
Flip angle (°)	15	15	15
Acquisition window (ms)	107	108	108

Abbreviations; SPIR: spectrally selective inversion recovery; TR: repetition time; TE: echo time; TI: inversion time

Data analysis

Images were processed and analyzed using the Soap bubble tool (9). Both a visual qualitative description and a direct quantitative comparison between 7 T and 3 T images were performed. All data analyses were performed by one physician (S.G.C.v.E., 4 years of experience in cardiac MRI) with supervision of a senior researcher (M.S., 18 years of experience in cardiac MRI).

The following parameters were measured: contrast-to-noise ratio (CNR) between the blood-pool and the epicardial fat, signal-to-noise ratio (SNR) of the blood-pool, RCA vessel sharpness and diameter of the first 4cm and visible vessel length. The CNR was defined as the difference in signal intensity between a manually placed region of interest (ROI) in the aortic root (mean ROI area $1.80 \pm 0.60 \text{ cm}^2$) near the offspring of the RCA, and that of a ROI placed in the epicardial fat adjacent to the proximal RCA (mean ROI area $0.90 \pm 0.61 \text{ cm}^2$), divided by the standard deviation (SD) of the background signal from a ROI positioned anterior to the chest wall (=noise) (mean ROI area: $9.95 \pm 3.98 \text{ cm}^2$). The SNR was calculated for the blood signal in the above-described ROI localized in the aortic root. The average signal intensity from this ROI was divided by the noise. Vessel sharpness was measured using signal intensity gradients perpendicular to the 3D course of the RCA, and was calculated for the proximal 4cm of the RCA (9). The RCA vessel length was measured manually and both vessel sharpness and diameter for the proximal 4 cm of the RCA were automatically calculated by the software.

Statistical analysis

Data are presented as mean \pm SD. Comparisons were made between the results obtained at 7 T and 3 T, and between those obtained with the different navigator positions at 3 T.

For comparisons, a nonparametric Mann-Whitney-U test was used. $P < 0.05$ was considered statistically significant.

RESULTS

Coronary MRA was successfully performed in all volunteers at both field strengths. At 7 T, one study participant complained about vertigo while the table was moving. All quantitative findings are listed in Table 2. Total time in the magnet was on average 30 minutes at 7 T and 20 minutes at 3 T.

Table 2. Quantitative results obtained from ten healthy volunteers

	7 Tesla, navigator on lung-heart interface	3 Tesla, navigator on lung-heart interface	3 Tesla, navigator on lung-liver interface
CNR blood-pool – epicardial fat	87.5 ± 33.9*	51.7 ± 12.7	47.8 ± 15.2
SNR blood-pool	109.2 ± 46.9*	66.9 ± 19.4	67.2 ± 24.9
RCA vessel sharpness (%)	58.3 ± 8.9*	49.7 ± 5.1	48.9 ± 7.5
RCA vessel length (cm)	7.24 ± 2.34	8.21 ± 2.19	7.99 ± 2.73
RCA diameter, first 4 cm (mm)	2.97 ± 0.27	3.07 ± 0.38	3.07 ± 0.37
Navigator efficiency (%)	54 ± 20	53 ± 20	46 ± 14
Acquisition time (sec)	469 ± 225	410 ± 180	470 ± 191
Heart rate (beats/min)	70 ± 15	67 ± 10	69 ± 10

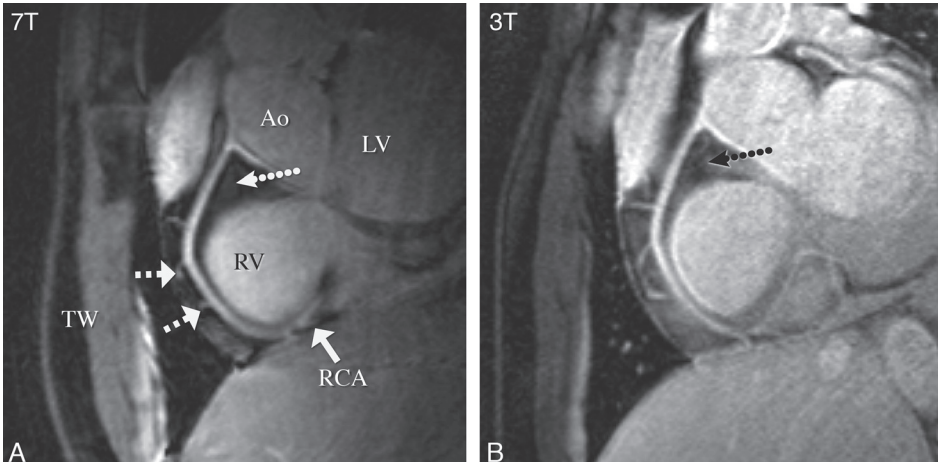
All data are expressed as mean ± SD; * significantly different from 3 T ($p < 0.05$);

Abbreviations; CNR: contrast-to-noise ratio between blood-pool and epicardial fat surrounding the proximal right coronary artery; RCA: right coronary artery; SNR: signal-to-noise ratio

Figure 2, 3 and 4 illustrate example coronary MRA reformations obtained at 7 T and at 3 T. All images show high signal intensity of the coronary artery lumen while that of the surrounding epicardial fat is suppressed. At 7 T, suppression of the epicardial fat appears visually improved when compared to 3 T (Figure 2).

Consistent with these findings, quantitative CNR between the blood-pool and epicardial fat was significantly improved at 7 T (7 T vs. 3 T navigator at heart: $p = 0.013$, 7 T vs. 3 T navigator at liver: $p = 0.009$). Visually, the contrast between the myocardium and the blood-pool in the left ventricle is rather shallow at 7 T as shown in Figures 3 and 4. When compared to 3 T, the SNR of the blood-pool measured on the 7 T images was 60% higher (7 T vs. 3 T navigator at heart: $p = 0.023$, 7 T vs. 3 T navigator at liver: $p = 0.027$). Improved delineation of the RCA at 7 T is visible in Figure 3, with good depiction of RCA branches and distal segments. Consistent with these findings, objective vessel sharpness analysis demonstrated improved quantitative vessel conspicuity at 7 T (vs. 3 T navigator at heart $p = 0.038$, vs. 3 T navigator at liver $p = 0.031$).

Figure 2. An example of a coronary magnetic resonance angiogram of the RCA obtained at 7 T (a) and at 3 T (b) in the same healthy 18 year old male volunteer is illustrated (double oblique volume targeted plane parallel to the right coronary artery). Improved suppression of the epicardial fat (dotted arrows) with high contrast between the blood and epicardial fat is visible at 7 T. At both field strengths a number of small branching vessels can be depicted (larger hatched arrows). Also, at 7 T a long portion of the RCA can be visualized. The solid arrow indicates the distal part of the RCA.



Abbreviations; Ao: aortic root; LV: Left ventricle; RCA: right coronary artery; RV: Right ventricle; TW: thoracic wall

Figure 3. These right coronary artery (RCA) images (double oblique volume targeted plane parallel to the right coronary artery) from a healthy 26 year old male subject display a high visual vessel definition (dotted arrows with small arrow heads) in the 7 T image (a) compared to 3 T (b). At 7 T there is limited contrast between the myocardium (2 dots) and the blood pool (1 dot). Multiple RCA side-branches (squared arrows) and distal parts of the RCA (plain arrow) are clearly depicted at both field strengths.

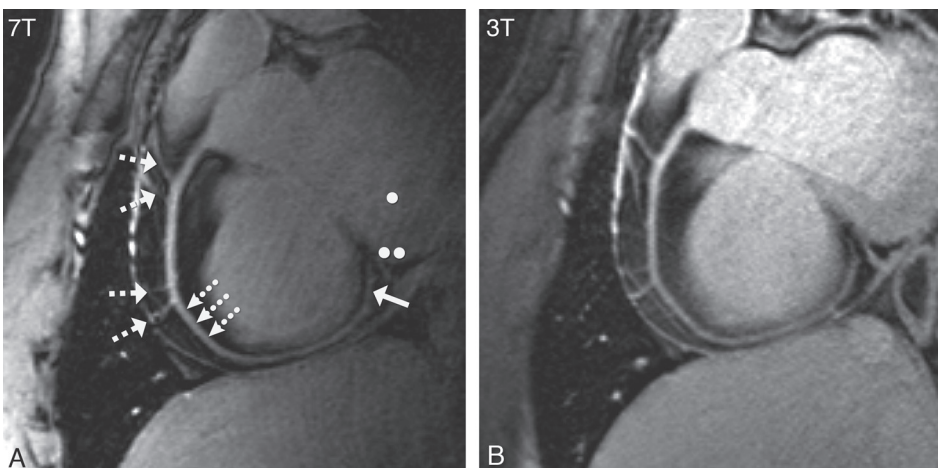
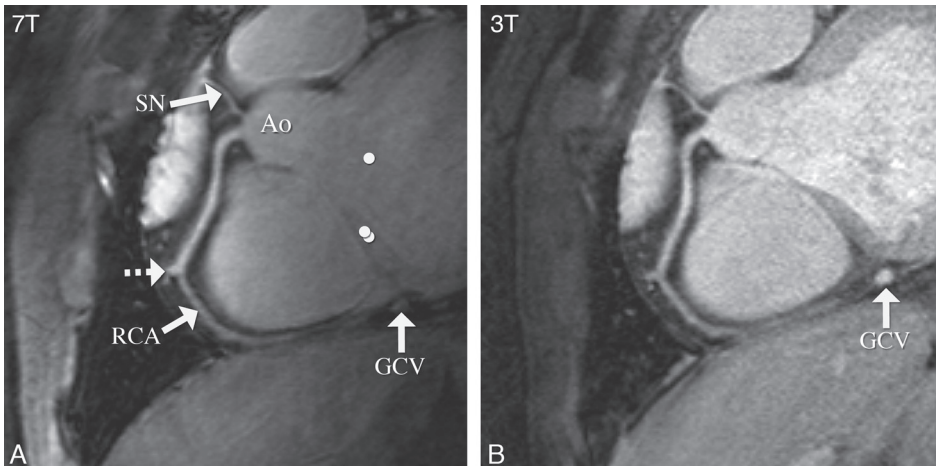


Figure 4. The SN and a proximal branch of the RCA (image obtained in a double oblique volume targeted plane parallel to the right coronary artery) from a healthy 28 year old male subject is depicted. At 7 T (a), there is not much difference in signal between the blood pool (dot) and the myocardium (2 dots). At 3 T (b), this contrast is slightly improved. On the 3 T image, the GCV can easily be identified but this structure is less visible on the 7 T counterpart likely due to shortened T2* at 7 T as well as limited surface coil RF penetration. The squared arrow points out a RCA side-branch.



Abbreviations; Ao: aortic root; GCV: great cardiac vein; RCA: right coronary artery; SN: sinoatrial nodal artery; RF: radiofrequency

Even though constraints related to the B1 field and coil sensitivity adversely affect the signal more distant to the surface transmit/receive coil at 7 T (Figures 2-4), there was no significant difference in vessel length (7 T vs. 3 T navigator at heart; $p=0.233$, 7 T vs. 3 T navigator at liver: $p=0.414$) or vessel diameter (7 T vs. 3 T navigator at heart; $p=0.653$, 7 T vs. 3 T navigator at liver: $p=0.567$) measurements among the images from the different field strengths. Navigator efficiency (7 T vs. 3 T navigator at heart: $p=0.970$, 7 T vs. 3 T navigator at liver: $p=0.272$) and the total data acquisition time (7 T vs. 3 T navigator at heart: $p=0.520$, 7 T vs. 3 T navigator at liver: $p=0.821$) were also not field strength dependent.

No significant difference in CNR between the blood-pool and epicardial fat, SNR of the blood-pool, RCA vessel sharpness, vessel length, vessel diameter, navigator efficiency or acquisition time was found between the 3 T scans acquired with different navigator localization.

DISCUSSION

In our study comparing 7 T and 3 T RCA coronary MRA in young healthy volunteers, we found an improved CNR between the blood-pool and the epicardial fat, enhanced SNR of

the blood-pool and increased vessel sharpness at 7 T. These findings may have implications since vessel conspicuity and well-defined borders of the coronary arteries support improved identification of significant coronary artery stenoses.

Considering the results of a most recent multicenter study, multi detector computed tomography (CT) is highly promising and superior to MRA for the non-invasive evaluation of significant proximal coronary stenoses (10). However, most recent data from a coronary MRA multicenter trial (11) demonstrate significant progress, and with a further improvement in SNR diagnostic quality approaching that of CTA may soon be expected. Therefore, the development of new MRI methodology at higher magnetic field strength is of particular interest.

Approximately a two-fold increase in SNR is predicted at 7 T when compared to 3 T (7,12) while a 60% SNR improvement was found in our study. This may be explained with the prolonged T1 at 7 T and the depth penetration of the RF transmit/receive coil, which was clearly inferior to that at 3 T. However, a significant 60% increase in SNR with a simple coil design is encouraging and emphasizes the need for further developments in coil technology. Recent advances in RF transmit arrays (2,3) are a step in this direction. Previous studies comparing 1.5 T and 3 T coronary MRA (13-15) clearly demonstrated that the expected 100% improvement in SNR could not be obtained. At 7 T the lack of commercially available RF coils and the only recent availability of 7 T for whole body human use comprise additional 7 T specific limitations. Despite these limitations, the reported 60% improvement in SNR, when going from 3 T to 7 T, is consistent with that reported for direct 1.5 T vs. 3 T comparisons.

Our findings of increased vessel sharpness at 7 T suggest that motion suppression works effectively at 7 T since vessel sharpness depends on the performance of ECG-triggering and the respiratory navigator. Two similar scans with different navigator localizations were performed at 3 T to exclude the influence of navigator localization on the quantitative parameters related to image quality. Consistent with earlier findings (16), no navigator-dependent quantitative differences were observed.

The results from the RCA vessel length and diameter measurements were similar for both field strengths. This suggests that coverage and RF penetration of the surface coil at 7 T may not be limiting factors for visualization of the RCA.

The situation for the left coronary system (LCS) is different. On the one hand, the penetration depth of the current transmit/receive coil is limited and therefore, parts of the LCS may not easily be visualized. On the other hand, an enhancement of the contrast between myocardium and the blood-pool is mandatory for the visualization of the LCS. At 3 T, such contrast enhancement has been obtained with adiabatic T2 preparation (T2Prep) (17) or by the combination of extracellular contrast agents and inversion-recovery (18). However, at 7 T, SAR constraints preclude the use of T2Prep and alternative 7 T-specific solutions with or without contrast agents remain to be explored. Finally, and even though a 60% increase in SNR was obtained at 7 T, we have not used this gain for an increased spatial resolution. However, the objective of our work was a direct, quantitative and objective comparison with 3 T.

In conclusion, while there are substantial challenges associated with 7 T cardiac MRI, a number of these have been successfully addressed. In our study directly comparing in vivo human imaging of the right coronary artery at 7 T and 3 T in young healthy volunteers, quantitative parameters related to image quality obtained at 7 T equal or surpass those from 3 T. Our results clearly warrant further evaluation in patients with coronary artery disease to assess the potential of our 7 T approach for the visualization of luminal RCA disease. Future work will concentrate on refinements in coil technology and contrast generation to support concomitant imaging of the left coronary system.

REFERENCES

1. Maderwald S, Orzada S, Schafer LC, et al. 7T Human in vivo cardiac imaging with an 8-channel transmit/receive array. *Proc Intl Soc Mag Reson Med* 2009;17:821.
2. Snyder CJ, Delabarre L, Metzger GJ, et al. Initial results of cardiac imaging at 7 Tesla. *Magn Reson Med* 2009;61(3):517-524.
3. Vaughan TT, Snyder CJ, DelaBarre LJ, et al. Whole-body imaging at 7T: preliminary results. *Magnetic Resonance in Medicine* 2009;61(1):244-248.
4. Versluis MJ, Tsekos N, Smith NB, Webb AG. Simple RF design for human functional and morphological cardiac imaging at 7tesla. *J Magn Reson* 2009;200(1):161-166.
5. Frauenrath T, Hezel F, Heinrichs U, et al. Feasibility of cardiac gating free of interference with electro-magnetic fields at 1.5 Tesla, 3.0 Tesla and 7.0 Tesla using an MR-stethoscope. *Invest Radiol* 2009;44(9):539-547.
6. van Elderen SG, Versluis MJ, Webb AG, et al. Initial results on in vivo human coronary MR angiography at 7 T. *Magn Reson Med* 2009;62(6):1379-1384.
7. Wen H, Denison TJ, Singerman RW, Balaban RS. The intrinsic signal-to-noise ratio in human cardiac imaging at 1.5, 3, and 4 T. *J Magn Reson* 1997;125(1):65-71.
8. Fischer SE, Wickline SA, Lorenz CH. Novel real-time R-wave detection algorithm based on the vectorcardiogram for accurate gated magnetic resonance acquisitions. *Magn Reson Med* 1999;42(2):361-370.
9. Etienne A, Botnar RM, van Muiswinkel AM, Boesiger P, Manning WJ, Stuber M. "Soap-Bubble" visualization and quantitative analysis of 3D coronary magnetic resonance angiograms. *Magn Reson Med* 2002;48(4):658-666.
10. Miller JM, Rochitte CE, Dewey M, et al. Diagnostic performance of coronary angiography by 64-row CT. *N Engl J Med* 2008;359(22):2324-2336.
11. Kato S, Kitagawa K, Ishida N, et al. Assessment of coronary artery disease using magnetic resonance coronary angiography: a national multicenter trial. *J Am Coll Cardiol* 2010;in press.
12. Vaughan JT, Garwood M, Collins CM, et al. 7T vs. 4T: RF power, homogeneity, and signal-to-noise comparison in head images. *Magn Reson Med* 2001;46(1):24-30.
13. Bi X, Deshpande V, Simonetti O, Laub G, Li D. Three-dimensional breathhold SSFP coronary MRA: a comparison between 1.5T and 3.0T. *J Magn Reson Imaging* 2005;22(2):206-212.
14. Sommer T, Hackenbroch M, Hofer U, et al. Coronary MR angiography at 3.0 T versus that at 1.5 T: initial results in patients suspected of having coronary artery disease. *Radiology* 2005;234(3):718-725.
15. Yang PC, Nguyen P, Shimakawa A, et al. Spiral magnetic resonance coronary angiography--direct comparison of 1.5 Tesla vs. 3 Tesla. *J Cardiovasc Magn Reson* 2004;6(4):877-884.
16. Stuber M, Botnar RM, Danias PG, Kissinger KV, Manning WJ. Submillimeter three-dimensional coronary MR angiography with real-time navigator correction: Comparison of navigator locations. *Radiology* 1999;212(2):579-587.

17. Botnar RM, Stuber M, Danias PG, Kissinger KV, Manning WJ. Improved coronary artery definition with T2-weighted, free-breathing, three-dimensional coronary MRA. *Circulation* 1999;99(24):3139-3148.
18. Bi X, Li D. Coronary arteries at 3.0 T: Contrast-enhanced magnetization-prepared three-dimensional breathhold MR angiography. *J Magn Reson Imaging* 2005;21(2):133-139.

Summary and conclusions

SUMMARY

The aim of this thesis was to evaluate MRI assessed end-organ damage, and the role of aortic pulse wave velocity in diabetes mellitus and hypertensive patients.

Increased aortic stiffness is an important risk factor for adverse cardiovascular outcome in various disease states including diabetes mellitus and hypertension. **Chapter 2** studies the independent and synergistic effect of type 1 diabetes mellitus and hypertension on MRI assessed aortic pulse wave velocity, as a marker of aortic stiffness. Aortic pulse wave velocity measurements were compared between 4 groups, all free from established cardiovascular disease and on treatment for diabetes (insulin use) respectively hypertension (antihypertensive medication): 20 type 1 diabetes mellitus patients, 31 hypertensive patients, 28 patients with type 1 diabetes mellitus and hypertension, 32 healthy controls. This study revealed that the independent effect of type 1 diabetes mellitus on aortic stiffness is minor, whereas hypertension in itself or hypertension in type 1 diabetes mellitus patients is a major determinant of increased aortic stiffness.

In **chapter 3** the influence of aortic pulse wave velocity on cardiac and cerebral end-organ damage is evaluated in hypertensive patients using a comprehensive MRI protocol. Fifty patients with hypertension underwent MR examination to assess aortic arch pulse wave velocity, left ventricular (LV) mass, LV systolic and diastolic function, lacunar brain infarcts and cerebral white matter hyperintensities. Aortic arch PWV was associated with LV mass and the presence of lacunar brain infarcts, independent of age, gender and hypertension duration, and not with diastolic and systolic LV function and white matter hyperintensities. The associations between aortic stiffness, LV mass and cerebral damage found in our study may be indirect through shared vascular risk factors or causative in nature due to aortic stiffness, increasing cardiac afterload and transmission of high pulsatile flow to the brain.

In **chapter 4** a similar MR evaluation of the effect of aortic pulse wave velocity on cardiac function and cerebral small vessel disease is assessed in eighty-six type 1 diabetes mellitus patients. Aortic PWV was associated with parameters of systolic LV function; LV ejection fraction, LV stroke volume, LV cardiac output, and with cerebral white matter hyperintensities after correction for age, gender, mean arterial pressure, heart rate, body mass index, smoking, diabetes mellitus disease duration and the presence of hypertension. In contrast to the results in hypertensive patients in the before mentioned chapter 2, no independent association was found between aortic pulse wave velocity and LV mass, lacunar brain infarcts or cerebral microbleeds in type 1 diabetes mellitus patients. These study results suggest that aortic stiffness is a marker or an independent risk factor for cardiac and cerebral end-organ damage, with different effects in type 1 diabetes mellitus and hypertension.

The study described in **chapter 5** aimed to explore the effect of type 1 diabetes mellitus on aortic stiffness, independent of the possible confounding effect of renal dysfunction that may aggravate reduction in vascular elasticity. Type 1 diabetes mellitus patients without microalbuminuria and with an estimated glomerular filtration rate > 60 ml/min/1.73m² showed slight increased MRI assessed aortic pulse wave velocity compared to age and renal function matched healthy controls. Furthermore, this study showed an inverse relationship between aortic pulse wave velocity and estimated glomerular filtration rate in normal range in type 1 diabetes mellitus patients as well as in healthy controls. Therefore, this study demonstrates interaction between aortic stiffness and renal function which is apparently physiological to some extent, and provides additional insight into the potential mechanism of aortic stiffening in renal failure. Diabetic nephropathy is one of the major complications of type 1 diabetes mellitus. Gradual progressive aortic stiffening, decreasing renal function and their interaction can accordingly be assumed in type 1 diabetes mellitus disease appearing before onset of clinically detectable renal failure.

In **chapter 6** we evaluated vascular mechanisms of brain atrophy in type 1 diabetes mellitus patients by investigating the relationship between brain volumes and cerebral perfusion and aortic stiffness using MRI. Type 1 diabetes mellitus patients with a mean diabetes disease duration of 23 years and without hypertension showed grey matter and white matter brain atrophy compared to age and gender matched healthy controls, with concomitant increased brain perfusion (expressed in ml/min/100ml brain tissue). Aortic pulse wave velocity was similar in type 1 diabetes mellitus and healthy controls. Total cerebral blood flow measured at the level of the internal carotid arteries and basilar artery and aortic pulse wave velocity both independently predicted white matter brain atrophy. The current findings suggest two separate vascular mechanisms operating on white matter brain atrophy. Also, the results of this study imply increased susceptibility of the brain of type 1 diabetes mellitus patients for relative small changes in aortic pulse wave velocity, even when aortic pulse wave velocity appears to be normal.

Chapter 7 reports accelerated progression of brain atrophy with cognitive consequences in type 2 diabetes mellitus patients in a population of non-demented elderly subjects, aged 70-82 years, with vascular disease or at increased vascular risk. Subjects were included for brain MRI scanning and cognitive function testing at baseline and re-examination after 3-years. Changes in brain atrophy, white matter hyperintensities, number of infarctions and cognitive function test results were determined in diabetes mellitus and non-diabetes mellitus subjects. Diabetes mellitus patients showed increased progression of brain atrophy and increased decline in cognitive performance on selective attention and recent memory after follow-up compared to control subjects. Furthermore, in diabetes mellitus patients, brain atrophy at baseline was a predictor for a decline in recent memory. These findings add fur-

ther evidence to the hypothesis that diabetes mellitus exerts deleterious effects on neuronal integrity by showing that non-demented elderly diabetes mellitus patients have accelerated progression of brain atrophy with significant consequences in cognition.

Chapter 8 evaluates the metabolic effect of diabetes mellitus on the skeletal muscle in patients carrying the mitochondrial Maternally Inherited Diabetes and Deafness (MIDD) mutation, present in approximately 1% of all diabetes mellitus patients, using the Phosphorus-31 MR spectroscopy technique. Phosphocreatine (PCr) and inorganic phosphate (Pi) were measured in the vastus medialis muscle immediately after exercise in 11 MIDD patients (six with diabetes mellitus and five non-diabetes mellitus) and eight healthy controls similar in age, height, and body weight. Half-time of PCr recovery after exercise was prolonged in MIDD patients compared to controls. No association of the presence of diabetes mellitus was found with PCr recovery half-time. Thus, subclinical mitochondrial dysfunction of the skeletal muscle in MIDD patients is demonstrated without additional effect of the presence of diabetes mellitus.

New developments in high magnetic field MRI, with the introduction of human 7 Tesla MRI scanners, potentially contribute to imaging of end-organ damage at early states of the disease. In the final two chapters of this thesis, implementation of coronary magnetic resonance angiography (MRA) at high field 7 Tesla MRI is described, relevant for studying coronary artery disease causing myocardial end-organ damage.

The use of higher magnetic field strengths for coronary MRA is attractive, with advantages arising from increases in signal-to-noise ratio, smaller voxel sizes, a higher temporal resolution, and/or shortened scanning times, likely to result in improved image quality for the noninvasive identification of significant proximal coronary artery disease. However, because of the large resonance frequency increase, the increase in magnetic field strength produces a series of challenges. In **chapter 9** we show feasibility of right coronary MRA at 7 Tesla by applying a home-built radiofrequency transmit and receive surface coil, vector electrocardiography hardware, navigator adaptations, specifically designed scout scanning procedures, segmented k-space gradient echo imaging and adiabatic inversion of the magnetization for fat suppression. With this methodology, the first human coronary MR images were successfully obtained at 7 Tesla.

Chapter 10 demonstrates a study comparing image quality of coronary MRA at 7 Tesla with lower field strength 3 Tesla. Ten healthy volunteers underwent navigator-gated 3 dimensional MRA of the right coronary artery at 7 Tesla and 3 Tesla using comparable imaging protocols. We found an improved contrast-to-noise ratio between the blood-pool and the epicardial fat, enhanced signal-to-noise ratio of the blood-pool, and increased vessel sharpness at 7 Tesla.

These findings may have important implications for the use of MRA images since vessel conspicuity and well-defined borders of the coronary arteries support improved identification of significant coronary artery stenoses. This study shows the benefits of imaging at higher magnetic field strengths.

CONCLUSIONS

Our studies have shown MRI assessed aortic stiffness to be an integrated marker of cardiac function, cerebral small vessel disease and atrophy, as well as of renal function in type 1 diabetes mellitus patients. Aortic stiffness already in normal range is related to end-organ damage in type 1 diabetes mellitus, suggesting increased organ-susceptibility for vascular alterations in diabetes mellitus. Structural changes in the brain as a manifestation of end-organ damage has shown to be clinical relevant to elderly with diabetes mellitus predicting accelerated cognitive decline.

Hypertension is a major contributor to increased aortic stiffness. There is a clear effect of aortic stiffness on cardiac and cerebral end-organ damage in hypertensive patients, which is different from type 1 diabetes mellitus.

The results of our cross-sectional studies suggest that MRI assessment of aortic pulse wave velocity could function as a marker or risk factor for generalized vascular disease and end-organ damage that might potentially be treated. Our findings may therefore have implications for cardiovascular risk stratification and optimization of therapy in diabetes mellitus and hypertensive patients beyond classical risk factors.

Finally, this thesis describes the technical implementation and benefits of right coronary artery MRA at high field 7 Tesla. This is a promising step towards improved MRI detection of coronary artery disease.

Samenvatting en conclusies

SAMENVATTING

In dit proefschrift worden MRI technieken beschreven om eind-orgaan schade te bestuderen, en wordt de relatie tussen eind-orgaan schade en de polsgolfsnelheid van de aorta beschreven bij patiënten met diabetes mellitus en hypertensie.

Verminderde elasticiteit van de aorta is een belangrijke risicofactor voor cardiovasculaire morbiditeit en mortaliteit bij verschillende ziekten zoals diabetes mellitus en hypertensie.

Hoofdstuk 2 beschrijft het onafhankelijke en synergistische effect van type 1 diabetes mellitus en hypertensie op de met MRI gemeten polsgolfsnelheid van de aorta, als een maat voor aorta-elasticiteit. De polsgolfsnelheid van de aorta werd vergeleken tussen 4 groepen: 20 type 1 diabetes mellitus patiënten, 31 hypertensie patiënten, 28 patiënten met type 1 diabetes mellitus en hypertensie, en 32 gezonde controles. Andere cardiovasculaire ziekten in deze groepen werden uitgesloten en de patiënten werden adequaat behandeld voor respectievelijk diabetes (insuline gebruik) of hypertensie (bloeddrukverlagende medicatie). De resultaten van deze studie lieten zien dat het onafhankelijke effect van type 1 diabetes mellitus op een verminderde aorta-elasticiteit klein is. Hypertensie blijkt een belangrijke factor te zijn bij type 1 diabetes mellitus patiënten, hetgeen tot uiting komt in een verminderde aorta-elasticiteit.

In **hoofdstuk 3** wordt door middel van MRI de relatie tussen polsgolfsnelheid van de aorta en cardiale en cerebrale eind-orgaan schade geëvalueerd bij hypertensie patiënten. Vijftig hypertensie patiënten ondergingen een MRI onderzoek voor het meten van de polsgolfsnelheid van de aortaboog, de cardiale linkerventrikel (LV) massa, de systolische en diastolische LV functie, lacunaire infarcten en wittestofafwijkingen in de hersenen. De polsgolfsnelheid van de aortaboog was geassocieerd met de LV massa en de aanwezigheid van lacunaire infarcten, onafhankelijk van leeftijd, geslacht en hypertensie ziekteduur. Er werden geen significante associaties gevonden tussen polsgolfsnelheid van de aortaboog en systolische en diastolische LV functie of cerebrale wittestofafwijkingen. De aangetoonde relaties in deze studie tussen aorta-elasticiteit, LV massa en cerebrale schade zouden indirect het gevolg kunnen zijn van gedeelde vasculaire risicofactoren, of causaal doordat een verminderde aorta-elasticiteit de afterload van het LV verhoogt en een drukgolf zich met hoge snelheid en verminderde demping naar de hersenen voortplant.

In **hoofdstuk 4** wordt een zelfde MRI protocol gebruikt om de relatie te bestuderen tussen de polsgolfsnelheid van de aorta en cardiale en cerebrale eind-orgaan schade bij 86 type 1 diabetes mellitus patiënten. Er werden significante relaties gevonden tussen de aorta-polsgolfsnelheid, systolische LV parameters (LV ejectiefraction, LV slagvolume, LV cardiac output) en cerebrale wittestofafwijkingen, onafhankelijk van leeftijd, geslacht, gemiddelde

arteriële polsdruk, hartslag, body mass index, roken, diabetes ziekteduur en de aanwezigheid van hypertensie. In tegenstelling tot de hierbovengenoemde resultaten van hoofdstuk 2 bij hypertensie patiënten werden er bij type 1 diabetes mellitus patiënten geen significante associaties gevonden tussen de aorta-polsgolfsnelheid en LV massa, cerebrale lacunaire infarcten of microbloedingen. De resultaten van deze studie suggereren dat aorta-elasticiteit een marker en/of een onafhankelijke risicofactor is voor cardiale en cerebrale eind-organ schade, met een verschillende werking bij type 1 diabetes mellitus en hypertensie.

Het doel van de studie beschreven in **hoofdstuk 5** was om het effect van type 1 diabetes mellitus op aorta-elasticiteit te evalueren onafhankelijk van nierfalen dat op zichzelf kan bijdragen aan een verminderde vasculaire elasticiteit. Type 1 diabetes mellitus patiënten zonder de aanwezigheid van microalbuminurie en met een nierklaring (eGFR) > 60 ml/min/1.73m² lieten een licht verhoogde aorta-polsgolfsnelheid zien ten opzichte van op leeftijd en nierfunctie gemaakte gezonde controles. Bovendien toonden we in deze studie aan dat er zowel bij type 1 diabetes mellitus patiënten als bij gezonde controles een omgekeerde relatie bestaat tussen de aorta-polsgolfsnelheid en de nierklaring (eGFR), in geval er sprake is van een normale nierfunctie bij zowel de patiënten als bij de vrijwilligers. Er is blijkbaar een fysiologische interactie tussen aorta-elasticiteit en de nierfunctie hetgeen kan bijdragen aan het begrip van de pathofysiologie van verminderde aorta-elasticiteit bij nierfalen. Diabetische nefropathie is een van de meest voorkomende complicaties bij type 1 diabetes mellitus. Het is denkbaar dat bij type 1 diabetes mellitus de geleidelijke vermindering van aorta-elasticiteit, nierschade en de interactie tussen beide reeds plaats vindt vóór de klinische manifestatie van nierfalen.

In **hoofdstuk 6** worden vasculaire mechanismen van hersenatrofie bij type 1 diabetes mellitus onderzocht. De relatie tussen hersenvolumina en cerebrale perfusie en aorta-elasticiteit wordt in dit hoofdstuk nader bestudeerd. Type 1 diabetes mellitus patiënten met een gemiddelde diabetes ziekteduur van 23 jaar en zonder hypertensie vertoonden atrofie van de grijze en witte stof en toegenomen cerebrale perfusie (uitgedrukt in ml/min/100ml hersenweefsel) in vergelijking met op leeftijd en geslacht gemaakte gezonde controles. De aorta-polsgolfsnelheid was niet significant verschillend tussen type 1 diabetes mellitus patiënten en gezonde controles. Onafhankelijke voorspellers voor hersenatrofie van de witte stof waren zowel de cerebrale perfusie (gemeten door middel van flow metingen in de arteria carotis interna beiderzijds en arteria basilaris), als de aorta-polsgolfsnelheid. De resultaten van deze studie geven aanwijzingen voor de aanwezigheid van twee verschillende vasculaire mechanismen voor hersenatrofie bij type 1 diabetes mellitus. Mogelijk speelt hierin ook een rol dat er een verhoogde gevoeligheid van het hersenweefsel voor fysiologische waarden van de aorta-polsgolfsnelheid bestaat.

Hoofdstuk 7 rapporteert een versnelde progressie van hersenatrofie bij type 2 diabetes mellitus patiënten met cognitieve achteruitgang. Een niet-demente oudere populatie in de leeftijd tussen 70-82 jaar met manifestaties van vasculaire ziekte of een verhoogd vasculair risico werd onderzocht. De deelnemers aan deze studie ondergingen bij start van de studie en na een follow-up duur van 3 jaar een MRI scan van de hersenen en cognitieve functietesten. Er werden veranderingen vastgesteld in hersenatrofie, wittestofafwijkingen, aantal infarcten en resultaten van de cognitieve functietest voor diabetes mellitus patiënten en voor deelnemers zonder diabetes mellitus (controles). De patiënten in de diabetes mellitus groep toonden versnelde progressie van hersenatrofie en een versnelde achteruitgang in cognitie in het gebied van selectieve aandacht en korte termijn geheugen ten opzichte van controles. Bovendien was de mate van hersenatrofie bij start van de studie een significante voorspeller van verslechtering in korte termijn geheugen in de diabetes mellitus groep.

Hoofdstuk 8 evalueert door middel van de Phosphor-31 MR spectroscopie techniek het metabole effect van diabetes mellitus op de skeletspier bij dragers van de mitochondriale 'Maternally Inherited Diabetes and Deafness' (MIDD) mutatie. Een groep van 11 MIDD patiënten (waarvan 6 met diabetes mellitus, en 5 zonder diabetes mellitus) werd op leeftijd, lengte en lichaamsgewicht gematched met een groep van 8 gezonde controles. Phosphocreatinine (PCr) en inorganisch fosfaat (Pi) werden direct na inspanning gemeten in de vastus medialis spier. De halfwaardetijd van PCr herstel na inspanning was toegenomen bij MIDD patiënten ten opzichte van controles. Er werd geen associatie gevonden met de aanwezigheid van diabetes mellitus en halfwaardetijd van PCr herstel. De aanwezigheid van subclinische mitochondriale dysfunctie in de skeletspier werd aangetoond bij MIDD patiënten, zonder dat een additioneel effect werd gezien tengevolge van de aanwezigheid van diabetes mellitus.

Nieuwe ontwikkelingen in hoge veldsterkte MRI, door de introductie van de 7 Tesla MRI scanners voor humane toepassingen, kunnen potentieel een bijdrage leveren aan het opsporen van eind-organ schade in een vroegtijdig stadium tijdens de manifestatie van de ziekte. De volgende twee hoofdstukken van dit proefschrift beschrijven de ontwikkelingen in magnetische resonantie angiografie (MRA) van de coronairen met hoge veldsterkte 7 Tesla MRI, hetgeen van belang is bij de bestudering van coronairziekten als oorzaak van eind-organ schade in het myocard.

Het gebruik van een hoge magnetische veldsterkte biedt potentiële voordelen voor het afbeelden van de coronairen met behulp van MRA vanwege de mogelijke toename in signaal-ruis-verhouding, het gebruik van kleinere voxels, een hogere temporele resolutie en/of kortere scantijden. Uiteindelijk kunnen deze verbeteringen bijdragen aan een verbeterde beeldkwaliteit voor het non-invasief identificeren van coronairziekten. De toename in magnetische veldsterkte gaat echter ook gepaard met technische uitdagingen. In **hoofdstuk 9**

beschrijven we de implementatie van MRA met 7 Tesla voor het afbeelden van de rechter coronair arterie door middel van de toepassing van in ons ziekenhuis ontwikkelde spoelen, vector electrocardiografie hardware, aanpassingen in de navigator technologie, speciaal ontwikkelde scout procedures, gesegmenteerde k-space gradient echo imaging en adiabatische inversie van de magnetisatie voor vet-suppressie. Door middel van deze ontwikkelde methodologie werden voor het eerst succesvol coronair MRA afbeeldingen met een 7 Tesla MRI verkregen bij gezonde vrijwilligers.

Hoofdstuk 10 beschrijft een studie waarin beeldkwaliteit van MRA van de rechter coronair arterie verkregen met 7 Tesla wordt vergeleken met 3 Tesla. Tien gezonde vrijwilligers ondergingen een 3D MRA van de rechter coronair arterie met 7 Tesla en met 3 Tesla gebruikmakend van vergelijkbare scan-protocollen. Met 7 Tesla werd een hogere contrast-ruis-verhouding tussen bloed en epicardiaal vet gemeten, een verhoogde signaal-ruis verhouding van bloed, en een scherpere definitie van het lumen van de rechter coronair arterie, ten opzichte van de 3 Tesla afbeeldingen. Deze bevindingen hebben belangrijke implicaties voor het gebruik van MRA beelden omdat een verbeterde signaal intensiteit van bloed in de beelden van de coronair arterie en een goede definitie van de vaatwand van belang zijn om vernauwingen in de coronair arterie nauwkeurig vast te kunnen stellen. De studie toont de potentiële voordelen van MRA technieken op hoge magnetische veldsterkte aan.

CONCLUSIES

De studies beschreven in dit proefschrift tonen aan dat met MRI gemeten aorta-elasticiteit een integrale marker is voor de hartfunctie, cerebrale 'small vessel disease' en atrofie, als ook voor de nierfunctie bij type 1 diabetes mellitus patiënten. Schommelingen reeds binnen normale waarden van aorta-elasticiteit zijn gerelateerd aan eind-orgaan schade bij type 1 diabetes mellitus, wat een toegenomen gevoeligheid voor arteriële (hemodynamische) veranderingen suggereert van de eind-organen, zoals het hart, de hersenen en de nieren. Het proefschrift toont aan dat structurele veranderingen in de hersenen een significante cognitieve verslechtering tot gevolg hebben bij oudere diabetes mellitus patiënten.

Hypertensie is een belangrijke oorzaak van een verslechterde aorta-elasticiteit. Er is een duidelijk effect van verminderde aorta-elasticiteit op cardiale en cerebrale eind-orgaanschade bij hypertensie patiënten.

De resultaten van onze observationele studies suggereren dat aorta-elasticiteit kan functioneren als marker en/of risicofactor voor algemene vasculaire ziekte en eind-orgaanschade. Onze bevindingen hebben potentieel implicaties voor de cardiovasculaire risico-screening en optimalisering van behandelingsstrategieën bij diabetes mellitus en hypertensie patiënten.

Ten slotte behandelt dit proefschrift de voordelen en technische implementatie van MRA van de rechter coronair arterie met gebruikmaking van MRI bij een veldsterkte van 7 Tesla. De studies beschreven in het proefschrift leggen de grondslag voor een verbeterde diagnostiek van coronairziekten met MRI.

List of publications

PAPERS

SGC van Elderen, JJM Westenberg, A Brandts, RW van der Meer, JA Romijn, JWA Smit, A de Roos. Increased aortic stiffness measured by magnetic resonance imaging in type 1 diabetes mellitus patients and the relationship with renal function. *American Journal of Roentgenology*, accepted 2010

SGC van Elderen, MJ Versluis, JJM Westenberg, H Agarwal, NB Smith, M Stuber, A de Roos, AG Webb. Right coronary magnetic resonance angiography at 7 Tesla: a direct quantitative comparison with 3 Tesla in young healthy volunteers. *Radiology*, 2010, Oct; 257(1):254-259

SGC van Elderen, A de Roos, AJM de Craen, RGJ Westendorp, GJ Blauw, JW Jukema, ELEM Bol-len, HAM Middelkoop, MA van Buchem, J van der Grond. Progression of brain atrophy and cognitive decline in diabetes mellitus, a 3 year follow-up. *Neurology*, 2010, Sept; 75(11):997-1002

SGC van Elderen, A Brandts, JJM Westenberg, MA van Buchem, J van der Grond, JT Tamsma, JA Romijn, LJM Kroft, JWA Smit, A de Roos. Aortic stiffness is associated with cardiac function and cerebral small vessel disease in patients with type 1 diabetes mellitus: assessment by magnetic resonance imaging. *European Radiology*, 2010 May; 20(5):1132-1138

SGC van Elderen, MJ Versluis, AG Webb, JJM Westenberg, J Doornbos, NB Smith, A de Roos, M Stuber. Initial results on in vivo human coronary magnetic resonance angiography at 7 Tesla. *Magnetic Resonance in Medicine*, 2009 Dec; 62(6):1379-1384

A Brandts, SGC van Elderen, JJM Westenberg, J van der Grond, MA van Buchem, MV Huisman, LJM Kroft, JT Tamsma, A de Roos. Association of aortic arch pulse wave velocity with left ventricular mass and lacunar brain infarcts in hypertensive patients: assessment with MR imaging. *Radiology*, 2009 Dec; 253(3):681-688

AH de Vries, MH Liedenbaum, S Bipat, R Truyen, IWO Serlie, RH Cohen, SGC van Elderen, A Heutink, O Kesselring, W de Mony , L te Strake, T Wiersma, J Stoker. Primary uncleaned 2D versus primary electronically cleansed 3D in limited bowel preparation CT-colonography. Is there a difference for novices and experienced readers? *European Radiology*, 2009 Aug; 19(8):1939-1950

SGC van Elderen, J Doornbos, EHR van Essen, HHPJ Lemkes, JA Maassen, JWA Smit, A de Roos. Phosphorus-31 magnetic resonance spectroscopy of skeletal muscle in maternally inherited diabetes and deafness A3243G mitochondrial mutation carriers. *Journal of Magnetic Resonance Imaging*, 2009 Jan; 29(1):127-131

HB Grotenhuis, LJM Kroft, SGC van Elderen, JJM Westenberg, J Doornbos, MG Hazekamp, HW Vliegen, J Ottenkamp, A de Roos. Right ventricular hypertrophy and diastolic dysfunction in arterial switch patients without pulmonary artery stenosis. *Heart*, 2007 Dec; 93(12):1604-1608

ORAL PRESENTATIONS

International Society for Magnetic Resonance in Medicine, Montréal, Canada, 2011
Topic: Magnetic resonance angiography, 3 Tesla and beyond; what is there to gain?

Society of Cardiovascular Magnetic Resonance – Euro CMR, Nice, France, 2011
Topic: Ultra-high field cardiac MR; 7 Tesla and beyond

Dutch Radiology days, Veldhoven, the Netherlands, 2010
Cerebral perfusion and aortic stiffness are independent predictors of white matter brain atrophy in type 1 diabetes mellitus patients, assessed with magnetic resonance imaging

International Society for Magnetic Resonance in Medicine, Stockholm, Sweden, 2010
Topic: 7 Tesla: Cardiovascular imaging, current status and future prospects

Ultrahigh Field MR-Symposium Berlin, Germany, 2010
Topic: Technical developments and role of 7 Tesla in cardiovascular MR

Society of Cardiovascular Magnetic Resonance, Phoenix, USA, 2010
Coronary magnetic resonance angiography at 7 Tesla: quantitative comparison with 3 Tesla

Dutch Radiology days, Amsterdam, the Netherlands, 2009
Stiffness of the descending aorta is independently related to renal function in type 1 diabetes mellitus patients without evident renal impairment

Society of Cardiovascular Magnetic Resonance, Orlando, USA, 2009
In vivo human coronary magnetic resonance angiography at 7 Tesla

Netherland Heart Days, Curacao, 2009
MRI assessment of cardiovascular and cerebral damage in diabetes mellitus patients, the role of aortic pulse wave velocity

Radiological Society of North America, Chicago, USA, 2008

MRI assessment of cardiovascular and cerebral damage in diabetes mellitus patients, the role of aortic pulse wave velocity

Dutch Radiology days, Rotterdam, the Netherlands, 2008

MRI assessment of cardiovascular and cerebral damage in diabetes mellitus patients, the role of aortic pulse wave velocity

POSTER PRESENTATIONS

International Society for Magnetic Resonance in Medicine, Stockholm, Sweden, 2010

Coronary magnetic resonance angiography at 7 Tesla: quantitative comparison with 3 Tesla

American Diabetes Association, New Orleans, Louisiana, USA, 2009

Stiffness of the descending aorta is independently related to renal function in type 1 diabetes mellitus patients without evident renal impairment

European Congress of Radiology, Vienna, Austria, 2009

Phosphorus: 31 magnetic resonance spectroscopy of skeletal muscle in maternally inherited diabetes and deafness A3243G mitochondrial mutation carriers

Society of Cardiovascular Magnetic Resonance, Orlando, USA, 2009

The role of aortic arch stiffening in cardiac and cerebral damage in type 1 diabetes mellitus patients, assessed by magnetic resonance imaging

European Society of Cardiology Congress, Stockholm, Sweden, 2005

Assessment with MRI of right ventricular function and pulmonary circulation in patients with transposition of the great vessels after arterial switch operation during long-term follow-up

Dankwoord

DANKWOORD

Graag wil ik alle collega's bedanken voor de fijne samenwerking tijdens mijn promotie-onderzoek. De artsen, secretaresses en verpleegkundige van de diabetes polikliniek wil ik hartelijk danken voor hun inzet omtrent de inclusie. Veel dank aan alle patiënten en vrijwilligers die bereid waren deel te nemen aan het MRI onderzoek. Alle geneeskunde studenten die me hebben geholpen met het scannen en de uitwerking daarvan, dankjulliewel. Graag wil ik mijn kamergenoten en lunch-collega's bedanken voor hun gezelligheid. Heyn, dank voor het zijn van een motiverende collega en vriend. Jos, bedankt voor je bijzondere toewijding. Jeroen, ik heb van je heldere aanpak geleerd. Joost, bedankt voor je hulpvaardigheid en MR fysica uitleg. Gerrit, bedankt voor jouw illustratieve hulp. De mannen van de technische ondersteuning radiologie veel dank voor het redden van mijn studie materiaal. Voor alle lieve familie en vrienden, dank!

Curriculum vitae

CURRICULUM VITAE

Saskia Gerdina Cornelia van Elderen werd geboren op 1 juli 1982 te Eindhoven. Na het behalen van het VWO-diploma aan het scholengemeenschap Durendael te Oisterwijk startte zij in 2000 met de opleiding Geneeskunde aan de Universiteit van Leiden. Gedurende haar doctoraalfase studeerde zij als keuze-vak Spaans aan de Universiteit van Valencia in Spanje. Haar afstudeeronderzoek aan het einde van de doctoraalfase Geneeskunde vond plaats op de afdeling Radiologie onder begeleiding van Dr. H.B. Grotenhuis en Prof. Dr. A. de Roos en beschreef een veranderde dynamiek van de pulmonaal arterie en het effect daarvan op de rechterhartkamerfunctie in arteriële switch operatie patiënten. In 2006 won zij voor haar scriptie de KNMG Dick Held Junior prijs. In de periode van 2005 tot 2007 liep zij co-assistentenschappen, waaronder een co-assistentenschap in het Diaconessenhuis in Paramaribo, Suriname. In 2007 slaagde zij voor haar arts-examen. Ze reisde gedurende 3 maanden door Canada, Noord-Amerika en Mexico. In hetzelfde jaar startte zij haar promotieonderzoek: 'MRI benadering van eind-orgaanschade bij Diabetes en Hypertensie' op de afdelingen Radiologie en Endocrinologie in het Leids Universitair Medisch Centrum onder begeleiding van Prof. Dr. A. de Roos en Prof. Dr. J.W.A. Smit, waarvan de onderzoeksresultaten staan beschreven in dit proefschrift. Zij verrichte gedurende 3 maanden onderzoek naar het effect van met MRI gemeten cerebrale schade op mortaliteit aan het Nationale Instituut voor de Gezondheidszorg (NIH) in Bethesda, Verenigde Staten, op de afdeling Epidemiologie, Veroudering (NIA) onder begeleiding van Prof. M.A. van Buchem en Dr. L.J. Launer. In december 2010 startte zij met de opleiding Radiologie in het Leids Universitair Medisch Centrum.